THEORETICAL STRENGTH OF SOLIDS

A Dissertation
Presented to
The Academic Faculty

by

Hao Wang

In Partial Fulfillment
of the Requirements for the Degree
Doctor of Philosophy in the
School of Physics

Georgia Institute of Technology
December 2010

THEORETICAL STRENGTH OF SOLIDS

Approved by:

Dr. Mo Li, Advisor
School of Materials Science and Engineering
Georgia Institute of Technology

Dr. Arash Yavari
School of Civill Engineering
Georgia Institute of Technology

Dr. Mei-Yin Chou
School of Physics
Georgia Institute of Technology

Dr. Dragomir Davidovic
School of Physics
Georgia Institute of Technology

Dr. Andrew Zangwill
School of Physics
Georgia Institute of Technology

Date Approved: [August 27, 2010]

To my wife

ACKNOWLEDGEMENTS

I am delighted to have this opportunity to say thank you to people who have helped me during my everyday life as a Ph.D. student.

First I am grateful to Professor Mo Li, my advisor. When I entered his group, I wasted quite some time complaining that there was no direction, no help, and how unfair it was. I assume most Ph.D. students have a similar experience, being in darkness and experiencing growing pains; some quit, most survive. Now I believe one can not make the transition to become an independent scientist without that type of experience. I appreciate that. I thank Professor Mo Li for his critiques and his patience with me. Besides that, he is a role model by showing me how to be a professional scientist. It was through him that I understood real physics is not only the principles in textbooks or popular legends of Newton and Einstein, but also it is a complex social activity that, in addition to working diligently to resolve physics problems, includes giving talks, presenting posters, writing articles, proposals, reports, rebutting referee comments, setting up a network of collaborators and interacting with colleagues. I saw the much broader landscape of physics through him.

I thank Professor Mo Li again for giving me the opportunity to work in such a wonderful group. Members with different backgrounds brought their various work styles and knowledge. They work in quite diversified research areas. I thank Dr. Mustafa Uludogan, Dr. Qikai Li, Dr. Xianming Bai, Dr. Huaming Li, Mr. Ken Beyerlein, Mr. Ming Zhao, Mr. Xueqiang Wang, Mr. Yuzheng Guo, Mr. Yongbo Guo, and Miss Jie Feng who inspired stimulating discussions and brought lots of fun to me.

Special thanks are due to Professor Mei-Yin Chou, Professor Andrew Zangwill, Professor Dragomir Davidovic, and Professor Arash Yavari for their service as my thesis committee members. I thank Mrs. Judy Melton for proofreading my thesis.

The love of my parents, my sister, as well as that of my good friends Dr. Donghua Xu, Dr. Xurong Chen, Dr. Xiya Liu, Dr. Haijing Tu, has been of great comfort to me.

Finally I wish to say thanks to my wife, Ao Yang, who has been with me during the past six years. She taught me to swim, reminded me to improve my everyday behaviors, and trained me, a nerd, to be a nerdless, decent cook, and cat fancier.

TABLE OF CONTENTS

LIST OF TABLES

LIST OF FIGURES

SUMMARY

Theoretical strength of solids is defined as the ultimate strength beyond which plastic deformation, fracture, or decohesion would occur. Understanding the microscopic origin from quantum mechanics and thermoelastic formulation is of great importance to mechanical properties and engineering design of various solids. While quite a few theory models have been made in the past century by several generations of scientists, including Frankel and Born, a general and convincing framework has not been fully established. In this thesis, we study this issue from two respects: (1) Unify various elastic stability criteria for solids that determine an upper bound of theoretical strength; (2) propose a nonlinear theoretical formulation of stability criterion. As an analytic method, this scheme is quite simple, in the mean time, it saves computation resource.

Studies of theoretical strength based on electronic structure calculation, so called *ab initio* (or first-principles) method, have appeared since 1980. Density functional theory is a basis of those calculations. The problem of many interacting electrons is transformed into the study of the motion of a single electron in an effective potential, as described by the Kohn-Sham equation. It should be noted most *ab initio* calculations of the theoretical strength analyzed only the position of the inflexion point in the total energy vs. deformation curve. In some cases, another elastic stability condition may be violated prior to that inflexion point, which is called stability bifurcation.

We begin by developing a homogeneous deformation scheme to calculation the high order elastic constants with *ab initio* method. So, we may obtain high order elastic

constants to test the nonlinear theoretical formulation of elastic stability criterion. In addition, we derive a nonlinear stress-strain equation for solids under arbitrary initial configurations. After that, we try to unify the elastic stability criteria of solids, and with *ab initio* method, we test the elastic stability conditions of crystal Au. The phenomenon of bifurcation is observed: under hydrostatic expansion, the rhombohedral modulus reaches zero first of all; while under uniaxial tensile stress, the tetragonal shear modulus reaches zero first.

In the next part, we develop the nonlinear theoretical formulation of elastic stability criterion and test it with both experimental values and our calculated ones of high order elastic constants. The results are compared with the ones from our previous *ab initio* simulation work. At last, we extend this nonlinear theoretical formulation to isotropic materials. We use metallic glass $Zr_{52.5}Ti_5Cu_{17.9}Ni_{14.6}Al_{10}$ as a sample to test it.

CHAPTER ONE

INTRODUCTION

A primary objective of materials research is to understand, design, and control the mechanical properties of materials. It is well known that the strength of a usual material is dominated by the behavior of dislocations or microcracks. If such defects were not present, the material under loading would fail only if the theoretical strength, also called ideal strength, were reached. As an intrinsic property of materials, the theoretical strength has drawn considerable attention theoretically and experimentally.

1.1 Traditional methods to predict theoretical strength

Scientists have developed quite a few theoretical models to explain the ideal strength of materials. Some of models displayed enormous differences with the actual strength of materials, like Frenkel's[1] and Orowan's[2] models (those divergences were explained with the postulation of dislocations). Some of the theoretical models are widely accepted nowadays.

When a material breaks under an external stress and the fracture direction is perpendicular to the applied stress, it is said to cleave. This process involves the separation of the atoms along the applied stress. Orowan[2-3] proposed a simple method to obtain the theoretical tensile strength of a crystal. The stress required to separate two planes can be regarded as a function of the distance between these planes. Given the

distance initially equal to a_0, the stress $\sigma = 0$ for $a = a_0$. In Orowan's model, the stress-strain curve is assumed to be a sine function, and the area under the curve is the work required to cleave the solid. This work can not be less than the energy of the two new surfaces created by the cleavage. Given that the surface energy per unit area is γ_0, the maximum value of σ is equal to the theoretical cleavage stress, $\sigma_{\max} = \sqrt{E\gamma_0 / a_0}$, where E is the Young's modulus along the deformation path.

Instability in tension also was explained with the necking criterion proposed by Considère[3]. An ideal plastic material in which no strain hardening happens would become unstable in tension and begin to neck when yielding takes place. However, a real metal undergoes strain hardening, the load-carrying capacity of the specimen increases as the deformation increases. Necking or localized deformation generally starts at maximum load of a ductile metal, where the increase in stress, due to decrease in the cross-sectional area of the specimen, becomes greater than the increase in the load-carrying ability of the metal due to strain hardening. The necking criterion can be expressed as $d\sigma / d\varepsilon = \sigma$, where σ and ε represent the tensile stress and strain, respectively. This idea was generalized for rate sensitive and pressure dependent materials under adiabatic conditions of deformation by Argon[4].

Frenkel[1] developed a simple calculation method of the theoretical shear strength of crystals by considering two adjacent and parallel lines of atoms subjected to a shear stress. Assume a is the separation between the adjacent planes and b is the interatomic distance, due to the periodic properties of crystals, the stress varies cyclically with a period b. Frenkel proposed a sine function of shear stress τ with respect to deformation, and then obtained the maximum value of shear stress $\tau_{\max} = Gb / 2\pi a$, where G is the

shear modulus. For face-centered cubic (FCC) metals with $b = a_0/\sqrt{2}$, $a = a_0\sqrt{3/8}$, then $\tau_{\max} \simeq G/5.4$.

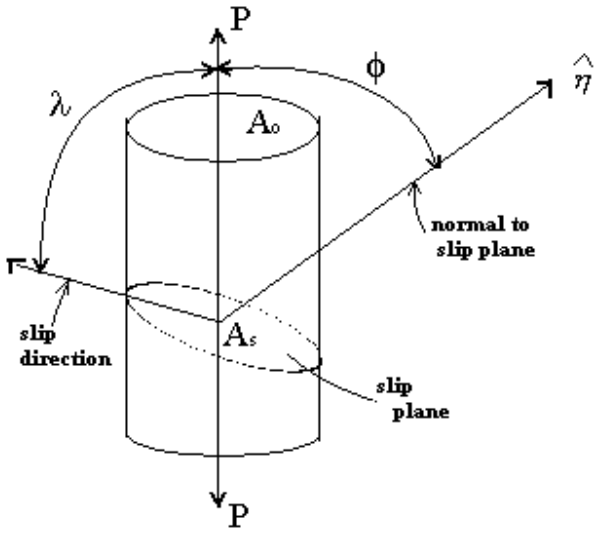

Figure 1.1 A model is shown for the critical resolved shear stress in a single-crystal specimen. P is an applied force, A_0 the cross-sectional area of the specimen, ϕ the angle between the slip plane normal and the tension direction, and λ the angle between the slip direction and the tension axis.

The value of the shear stress required to initiate slip in a pure and perfect single crystal is also known as the critical resolved shear stress, σ_{CR}, which is a constant for a given slip system. This rule, known as Schmid's Law, has been confirmed experimentally for a large number of single crystals. As shown in figure 1.1, let ϕ be the angle between the slip plane normal and the tension direction, and λ be the angle between the slip direction and the tension axis, then the critical resolved shear stress is $\sigma_{CR} = \tau \cos\phi \cos\lambda$, where τ is the applied tensile stress, $\tau = P/A_0$.

1.2 Elastic stability and bifurcation

The elastic stability limit is formulated traditionally following Born's original idea[5-6] that a crystal should remain stable when the change of the elastic energy with respect to the spontaneous strain exhibits convexity; otherwise, instability would occur consequentially. The condition of convexity leads to the stability criteria in the form of a set of relations involving elastic constants appropriate to the crystal symmetry. However, Born's theory is formulated for systems without external load. For systems under external load, it was shown[7-17] that the elastic stiffness coefficients B_{ijkl} rather than elastic constants C_{ijkl} should be used in formulating the stability criteria.

The stability criterion based on the elastic stiffness constants[14-16] certainly provides a convenient and powerful recipe to measure stability limit. As done in those previous works, one follows a standard recipe. First calculate the elastic constants; then construct the elastic stiffness coefficients as a function of the applied stress to a system that is usually under some specific loading modes such as hydrostatic, uniaxial tensile or compressive, or shear strain; and finally obtain the stability limit at the strain where a principal minor of the elastic stiffness constant matrix first becomes non-positive, or $\det\left|B_{ijkl}\right| \le 0$. Along some simple loading paths such as uniaxial tension, the stability limit is found to relate to some shear strain modes[18-19]. Under hydrostatic loading, it is observed that the stability is dominated by the rhombohedral shear modulus[20]. Born[5-6] and Hill[7-11] argue that some perturbations, fluctuations, as well as sample loading conditions would make the deformation path astray from the primary loading path, causing a measured stability limit different from that intended originally. This

phenomenon, called “stability bifurcation”, plays an important role in determining the theoretical strength of a crystal lattice.

The research work performed here in this thesis is solely based on the elastic stability theory. As known, it is possible that some phonon instabilities may appear along the deformation path. Recent studies on elastic[18] and phonon[21] instabilities of aluminum suggests that this scenario may likely occur in FCC metals, specially at elevated temperatures. Other types of instability such as that caused by magnetic perturbation also might occur and determine the theoretical strength, although those problems are beyond the research objective in this thesis.

1.3 Nonlinear elastic and transcription theory

Suppose a material point in configuration X under stress $\sigma_{ij}(X)$ is undergoing a small displacement, i.e., with a strain η, to a new state x with a corresponding stress $\sigma_{ij}(x)$, then, we assume, without loss of generality, that the displacement could be arbitrary and infinitesimal as needed. The corresponding change of the Helmholtz free energy $F(x,T)=F(\eta,T)$ at state x from $F(X,T)=F(0,T)$ at sate X can be expressed as [22-23],

$$F(\eta,T)=F(0,T)+\left.\frac{\partial F}{\partial \eta}\right|_{X,\eta'}\eta+\frac{1}{2!}\left.\frac{\partial^2 F}{\partial\eta\partial\eta}\right|_{X,\eta'}\eta\eta+\frac{1}{3!}\left.\frac{\partial^3 F}{\partial\eta\partial\eta\partial\eta}\right|_{X,\eta'}\eta\eta\eta+\frac{1}{4!}\left.\frac{\partial^4 F}{\partial\eta\partial\eta\partial\eta\partial\eta}\right|_{X,\eta'}\eta\eta\eta\eta+\ldots, \tag{1.1}$$

correct to the fourth power of η with the understanding that all derivatives appearing in Eq. (1.1) are done at state X with all other strain components η' held constants. The

corresponding stress, the second and third order isothermal elastic constants at state X, are then

$$\tau(X)=\frac{1}{V(X)}\frac{\partial F}{\partial \eta}\bigg|_{X,\eta'}, \tag{1.2a}$$

$$C(X)=\frac{1}{V(X)}\frac{\partial^2 F}{\partial \eta\partial \eta}\bigg|_{X,\eta'}, \tag{1.2b}$$

$$c(X)=\frac{1}{V(X)}\frac{\partial^3 F}{\partial \eta\partial \eta\partial \eta}\bigg|_{X,\eta'}, \tag{1.2c}$$

$$\tilde{c}(X)=\frac{1}{V(X)}\frac{\partial^4 F}{\partial \eta\partial \eta\partial \eta\partial \eta}\bigg|_{X,\eta'}, \tag{1.2d}$$

where $V(X)$ is the volume of the system at X. To avoid overcrowded notations, we shall not use indices for vectors and tensors unless necessary. Summation convention is assumed automatically. Following the same scheme, we can obtain the corresponding stress, the second and third order isothermal elastic constants at state x,

$$\tau(x)=\frac{1}{V(x)}\frac{\partial F}{\partial \xi}\bigg|_{x,\xi'}, \tag{1.3a}$$

$$C(x)=\frac{1}{V(x)}\frac{\partial^2 F}{\partial \xi\partial \xi}\bigg|_{x,\xi'}, \tag{1.3b}$$

$$c(x)=\frac{1}{V(x)}\frac{\partial^3 F}{\partial \xi\partial \xi\partial \xi}\bigg|_{x,\xi'}, \tag{1.3c}$$

where $V(x)$ is the volume of the system at state x and ξ is a Lagrangian strain from state x to state y. Therefore, we can simply take a derivative of Eq. (1.1) with respect to ξ at state x, so after dividing it by $V(x)$ on both sides, we have,

$$\tau(x)=\frac{1}{V(x)}\frac{\partial F}{\partial \xi}\bigg|_{x,\eta'}=\frac{V(X)}{V(x)}\frac{\partial \eta}{\partial \xi}\left[\tau(X)+C(X)\eta+\frac{1}{2!}c(X)\eta\eta+\frac{1}{3!}\tilde{c}(X)\eta\eta\eta+...\right]. \quad (1.4a)$$

Following the same scheme, we can systematically obtain the second and higher order elastic constants at state x in relation to those at state X,

$$C(x)=\frac{1}{V(x)}\frac{\partial^2 F}{\partial \xi\partial \xi}\bigg|_{x,\eta'}=\frac{V(X)}{V(x)}\frac{\partial \eta}{\partial \xi}\left[C(X)+c(X)\eta+\frac{1}{2!}\tilde{c}(X)\eta\eta+...\right], \quad (1.4b)$$

$$c(x)=\frac{1}{V(x)}\frac{\partial^3 F}{\partial \xi\partial \xi\partial \xi}\bigg|_{x,\eta'}=\frac{V(X)}{V(x)}\frac{\partial \eta}{\partial \xi}\left[c(X)+\tilde{c}(X)\eta+...\right], \quad (1.4c)$$

and so forth and so on.

Realizing the relations expressed explicitly in Eqs. (1.4) between the stress and elastic constants at any deformed state x and those at a reference state X, one can significantly simplify the procedure for acquiring the elastic stability criterion by using the reference at zero stress state or natural state as it is often called in mechanics where $\tau(X)=0$. We could express stress and elastic constants at any arbitrary stressed state x as the function of the deformation strain and the stress and elastic constants at the natural state. Krenn *et al*[24] applied the above transcription theory to investigate the nonlinear elastic behavior and ideal shear strength of face-centered cubic crystals Al and Cu, and to explain the different structural relaxation modes of the crystals Al and Cu under shear loading. As shown in this thesis, the relations in Eqs. (1.4) can enable us to formulate the nonlinear theoretical formulation of elastic stability criterion.

1.4 State-of-the-art calculations of theoretical strength

A large number of numerical simulations have been performed to investigate the theoretical strength associated with phase transition, ideal strength, crystal defect

formation, etc. Continuum models with finite element method[25], atomistic simulation with empirical[26] or semiempirical potentials[27-28], and *ab initio* quantum mechanical calculations[18-20, 29-32] have been employed extensively in various situations. However, all these models require tremendous amount of computational resources, the largest fraction of which is on calculation of the second order elastic constants C_{ijkl}'s in each deformed state. For *ab initio* calculation, the total energy needs to be calculated and used later to obtain C_{ijkl}'s ; for atomistic simulation, C_{ijkl}'s can be obtained using either analytical expression or fluctuation formula. For the latter case, large amounts of computation resources are needed to guarantee the convergence of fluctuations so that reliable results can be acquired[33-34]. In addition, the elastic stability criterion, though simple, often encapsulates the physical mechanisms underlying the stability limit. For example, anharmonic effects present in a crystal under applied stress play an important role in softening the material, leading to elastic instability. By focusing only on the second order elastic constants C_{ijkl}'s , this and other effects often manifested in higher order elastic constants are often masked.

Besides *ab initio* quantum mechanical calculations, we present a general theoretical framework of elastic stability criterion using higher order elastic constants. In finite deformation theory, both the stress and the second order elastic constants in a stressed state can be expressed in a series expansion in terms of the deformation strain with the expansion coefficients being the elastic constants of higher orders from a reference state. Choosing the reference state as the zero stress state, we test the stability conditions in terms of the second and higher order elastic constants at zero stress states. Many of these zero stress elastic constants are now available either from experiments or

theoretical calculations, making it extremely desirable, and possible, to use the nonlinear formulation analytically to predict stability and ideal strength of crystalline materials without resorting to extensive computation.

1.5 Organization

The thesis is organized as follows. In chapter two, the method of first-principles calculation based on density functional theory is introduced. In chapter three, we test the first-principles calculation to obtain elastic constants of metallic crystals. We propose a homogeneous deformation scheme to get second-, third-, and fourth-order elastic constants. In chapter four, we derive a nonlinear stress-strain equation for crystal solids with arbitrary initial configurations, and test it to crystal Au with first-principles calculation. In chapter five, we first show a proof to unify the elastic stability criteria of solids; then in section 5.2, we use first-principles calculation to test the stability conditions of face-centered cubic crystal Au under hydrostatic stress; and finally in section 5.3, we use the same method to study the elastic stability of face-centered cubic crystal Au under uniaxial stress along [100] direction. In chapter six, we present a nonlinear theoretical formulation to the elastic stability criterion and show the results obtained from several crystal systems whose higher order elastic constants are available. In chapter seven, we extend this nonlinear theoretical formulation to isotropic solids, and use metallic glass $Zr_{52.5}Ti_5Cu_{17.9}Ni_{14.6}Al_{10}$ as a sample to test it.

CHAPTER TWO

FIRST-PRINCIPLES CALCULATION METHOD

This chapter describes the first-principles calculation method employed in my thesis work. Determining the total energy and electronic structure of a solid system requires solving the quantum-mechanical Schrödinger equation. This procedure can be performed only if a large number of simplifications and approximations are used. This chapter is organized as follows. In section 2.1, the Born-Oppenheimer approximation is introduced in order to reduce the many-body problem to the solution of the dynamics of the electrons in some frozen-in configuration of the nuclei. In section 2.2, the Hohenberg-Kohn theorem is shown, and the Kohn-Sham equation is derived under the local density functional approximation (LDA). With the help of the Kohn-Sham equation, the interacting many-electron system is mapped onto a system of noninteracting electrons moving in an effective potential due to all the other electrons. In section 2.3, a brief review of numerical methods for solution of the Kohn-Sham equation is given. Bloch theorem states that the electronic wave functions at each k point can be expanded in terms of a discrete plane-wave basis set. Because a very large number of plane waves are needed to expand the tightly bound core orbitals, the pseudopotential approximation is desired to expect a much smaller number of plane-wave basis states. The ultrasoft pseudopotential (US-PP) and the projector augmented wave approach (PAW) are also introduced. The PAW approach is analogous to the pseudopotential approach but retains information about the core states without significant additional computation.

2.1 Born-Oppenheimer approximation

To obtain the electronic structure of a solid system, we can write the nonrelativistic time-independent Schrödinger equation as,

$$H\Psi(r,R) = E^{H}\Psi(r,R), \tag{2.1}$$

where r represents the set of electronic coordinates $\{\vec{r}_i\}$; R represents the set of nuclear coordinates $\{\vec{R}_j\}$. If there are no other external fields acting on this system, the Hamiltonian operator is,

$$H = H_e + H_N + H_{e-N}, \tag{2.2}$$

where

$$H_e(r) = T_e(r) + V_e(r) = -\sum_i \frac{1}{2m}\nabla_{r_i}^2 + \sum_{i<i'} \frac{1}{|r_i - r_{i'}|}. \tag{2.3}$$

The first term is the kinetic energy of electrons, the second term represents electron-electron Coulomb interaction (atomic units used), and m the mass of electrons. So far we do not take the exchange and correlation effects into account. And,

$$H_N(R) = T_N(R) + V_N(R) = -\sum_j \frac{1}{2M_j}\nabla_{R_j}^2 + \sum_{j<j'} V_N(R_j - R_{j'}), \tag{2.4}$$

where the first term is the kinetic energy of nuclei, the second term the Coulomb interaction among nuclei, M nuclear mass. The electron-nucleus interaction is,

$$H_{e-N}(r,R) = -\sum_{i,j} V_{e-N}(r_i - R_j). \tag{2.5}$$

Unfortunately, the V_{e-N} term prevents us from separating H into nuclear and electronic parts, which would allow us to write the wave function as a product of nuclear and electronic terms.

The Born-Oppenheimer approximation[35] is based on the fact that the nuclei are much more massive than the electrons, which means that the nuclei are nearly fixed with respect to electron motion. The solution for the Eq. (2.1) can be given as,

$$\Psi_n(r,R) = \sum_n x_n(R)\Phi_n(r,R). \tag{2.6}$$

Here $\Phi_n(r,R)$ is solution to the so-called "clamped-nuclei" Schrödinger equation,

$$H_0(r,R)\Phi_n(r,R) = E_n(R)\Phi_n(r,R), \tag{2.7}$$

where $H_0(r,R)$ is Hamiltonian of the many-electron system,

$$H_0(r,R) = H_e(r) + V_N(R) + H_{e-N}(r,R). \tag{2.8}$$

In the Eq. (2.7), R is just a parameter; $V_N(R)$ is a constant and shifts the eigenvalues by only some constant amount. To represent the perturbative effect of the operator $T_N(R)$ to the many-electron system Hamiltonian H_0, we introduce a parameter κ:

$$\kappa = (m/M_0)^{1/4}. \tag{2.9}$$

M_0 is the average mass of nuclei. And, we use $\kappa u = R - R^0$ to represent the displacement of the nuclei, so that we may rewrite the nuclei kinetic operator $T_N(R) = -\sum_j (1/2M_j)\nabla^2_{R_j}$ as

$$T_N(R) = -\kappa^2 \sum_j (M_0/M_j)(1/2m)\nabla^2_{u_j}. \tag{2.10}$$

And expand the wave function $\Phi_n(r,R)$ as a series of u,

$$\Phi_n(r,R) = \Phi_n(r,R^0+\kappa u) = \Phi_n^{(0)} + \kappa\Phi_n^{(1)} + \kappa^2\Phi_n^{(2)} + \kappa^3\Phi_n^{(3)} + \cdots, \tag{2.11}$$

where $\Phi_n^{(\nu)}$ is the ν order derivative of $\Phi_n(r,R)$ with respect to u.

To obtain $\chi_n(R)$, Eq. (2.6) is inserted into Eq. (2.1); then Eq. (2.1) is left multiplied with $\Phi_{n'}(r,R)$, and integrated with respect to r to yield

$$\left[T_N(R)+E_n(R)+C_n(u)\right]\chi_n(R)+\sum_{n'(\neq n)}C_{nn'}(u)\chi_{n'}(R)=E^H\chi_n(R), \qquad (2.12)$$

where

$$C_{nn'}(u)=-\kappa^2\sum_i(M_0/M_i)(1/2m)\int dr\Phi_n^*(r,u)\left[\nabla_{u_i}\Phi_{n'}(r,u)\nabla_{u_i}+\nabla_{u_i}^2\Phi_{n'}(r,u)\right], \qquad (2.13)$$

$$C_n(u)=-\kappa^2\sum_i(M_0/M_i)(1/2m)\int dr\Phi_n^*(r,u)\nabla_{u_i}^2\Phi_n(r,u). \qquad (2.14)$$

The first term of $C_{nn'}(u)$ is $\sim O(\kappa^3)$; the second term and $C_n(u)$ are $\sim O(\kappa^4)$. $T_N(R)$ is $\sim O(\kappa^2)$. In most cases, the coupling terms $C_{nn'}(u)\chi_{n'}(R)$ in the Eq. (2.12) are small. If they can be safely neglected, we will have the following equation,

$$\left[T_N(R)+E_n(R)+C_n(u)\right]\chi_{n\mu}(R)=E_{n\mu}^H\chi_{n\mu}(R). \qquad (2.15)$$

Here μ represents the vibration quantum number. This equation clearly shows that, when the off-diagonal couplings can be ignored, the nuclei move in a potential field set up by the electrons. The potential energy at each point is given primarily by $E_n(R)$ (the expectation value of the electronic energy) with a small correction factor $C_n(u)$. As $m/M_0\sim 1/1000$, $C_n(u)$ is expected to be small, and it is usually dropped (however, to achieve very high accuracy, this term must be retained). The whole system wave function is thereafter,

$$\Psi_{n\mu}(r,R)=\chi_{n\mu}(R)\Phi_n(r,R). \qquad (2.16)$$

This is the so-called adiabatic approximation: the first factor $\chi_{n\mu}(R)$ describes the nuclei behavior, which depends on the potential field set up by the electrons; the second factor

$\Phi_n(r,R)$ describes the movement of electrons, which is independent of the nuclei kinetic operator; $C_{nn'}(u)$ is a nonadiabatic operator.

2.2 Density functional theory

Born-Oppenheimer approximation enables one to separate the nuclei and electronic wave functions. To obtain the electronic structure of a many-electron system with a fixed-nuclei configuration $\left\{\vec{R}_j\right\}$, we need to solve Eq. (2.7). A simplification is to transform the many-electron problem to a single-electron problem. Non-interacting approximation and Hartree-Fock approximation are two basic independent-electron approaches, assuming that electrons are uncorrelated except that they obey the exclusion rule. Some effect of the real interaction is incorporated in the effective potentials of those theories, but there is no interaction term included explicitly in the effective Hamiltonian. Another independent-electron approach, density functional theory (DFT), which incorporates the exchange-correlation effects approximately into an effective single-particle Hamiltonian and has become the primary tool for calculation of electronic structures in condensed matter. The key postulate of density functional theory is that any ground-state property of a system of many interacting particles can be expressed as a functional of the ground state density $n_0\left(\vec{r}\right)$, which is a scalar function of position.

2.2.1 Hohenberg-Kohn theorems

The density functional theory can be tracked back to the original method proposed by Thomas[36] and Fermi[37] in 1920's, and it was formulated based on two theorems proved by Hohenberg and Kohn[38]. Here we reproduce the proof.

Considering a system of inhomogeneous interacting electron gas, the Hamiltonian is

$$H = T + U + V \,, \tag{2.17}$$

where T is the kinetic energy, U the interaction energy between electrons, and V is the potential energy of the electrons in the external field $\upsilon\left(\vec{r}\right)$. Given that there is another external field $\upsilon'\left(\vec{r}\right)$ and the two external fields lead to two different Hamiltonians, H and H', which have different ground state wave functions, $\left|\Psi\right\rangle$ and $\left|\Psi\right\rangle'$, if those two wave functions give the same density $n_0\left(\vec{r}\right)$, there would be an inconsistency. Since $\left|\Psi\right\rangle'$ is the ground state for H', the ground state energy is,

$$E' = \left\langle \Psi' \middle| H' \middle| \Psi' \right\rangle < \left\langle \Psi \middle| H' \middle| \Psi \right\rangle = \left\langle \Psi \middle| H - V + V' \middle| \Psi \right\rangle, \tag{2.18}$$

and then

$$E' < E + \int \left[\upsilon'\left(\vec{r}\right) - \upsilon\left(\vec{r}\right) \right] n_0\left(\vec{r}\right) d\vec{r} \,. \tag{2.19}$$

In the same way we may find that

$$E < E' + \int \left[\upsilon\left(\vec{r}\right) - \upsilon'\left(\vec{r}\right) \right] n_0\left(\vec{r}\right) dr \,. \tag{2.20}$$

If we add Eq. (2.19) and (2.20), we get $E + E' < E' + E$. This inconsistency shows that $\left|\Psi\right\rangle$ and $\left|\Psi\right\rangle'$ lead to different ground state particle density, which means the external potential $\upsilon\left(\vec{r}\right)$ is a unique functional of $n_0\left(\vec{r}\right)$.

Then we define a universal functional with the form

$$F\left[n_0\left(\vec{r}\right) \right] \equiv \left\langle \Phi \middle| T + U \middle| \Phi \right\rangle, \tag{2.21}$$

where $F\left[n_0\left(\vec{r}\right)\right]$ is valid for any number of particles and any external fields. Given a specific external potential $\upsilon\left(\vec{r}\right)$, the system energy functional is written as

$$E_\upsilon\left[n_0\left(\vec{r}\right)\right] \equiv \int \upsilon\left(\vec{r}\right) n_0\left(\vec{r}\right) d\vec{r} + F\left[n_0\left(\vec{r}\right)\right]. \tag{2.22}$$

Assuming that the particle number is constant, $N = \int n_0\left(\vec{r}\right) d\vec{r}$, then this energy functional $E_\upsilon\left[n_0\left(\vec{r}\right)\right]$ is equal to the ground-state energy for the correct $n_0\left(\vec{r}\right)$ and has a minimum value.

When the electronic spin and the relativistic effect are taken into account, the extension of Hohenberg-Kohn theorem can be referred in the review article by Callaway and March[39].

2.2.2 Kohn-Sham Equation

Based on Hohenberg-Kohn theorem, the system properties at ground state can be determined once we know the exact form of the universal functional $F\left[n_0\left(\vec{r}\right)\right]$. Kohn and Sham[40] published their work on this issue in 1965: the many-particle variational problem is replaced by an independent-particle equation with all the many-particle effects covered in the exchange-correlation term, and then a self-consistent procedure is provided to solve the ground state of the system. A brief introduction of their work is given below.

Kohn and Sham proposed that the system energy is

$$E = \int \upsilon\left(\vec{r}\right) n_0\left(\vec{r}\right) d\vec{r} + \frac{1}{2}\int\int \frac{n_0\left(\vec{r}\right) n_0\left(\vec{r'}\right)}{\left|\vec{r} - \vec{r'}\right|} d\vec{r} d\vec{r'} + G\left[n_0\left(\vec{r}\right)\right], \tag{2.23}$$

where $G\left[n_0\left(\vec{r}\right)\right]$ is a universal functional of particle density at ground state,

$$G\left[n_0\left(\vec{r}\right)\right] \equiv T\left[n_0\left(\vec{r}\right)\right] + E_{xc}\left[n_0\left(\vec{r}\right)\right]. \tag{2.24}$$

Here $T\left[n_0\left(\vec{r}\right)\right]$ is the kinetic energy of an artificial non-interacting electron gas with the same ground state density, and $E_{xc}\left[n_0\left(\vec{r}\right)\right]$ is the exchange-correlation energy. The exchange-correlation energy contains all the many-particle interaction information except that in Hartree term. Given a slowly varying $n_0\left(\vec{r}\right)$, the exchange-correlation energy is assumed to have a localized form that is called the local density functional approximation (LDA). If $\varepsilon_{xc}\left[n_0\left(\vec{r}\right)\right]$ is the exchange-correlation energy per electron of a uniform electron gas with density $n_0\left(\vec{r}\right)$, then

$$E_{xc} = \int n_0\left(\vec{r}\right)\varepsilon_{xc}\left[n_0\left(\vec{r}\right)\right]d\vec{r}\,. \tag{2.25}$$

Here the exchange-correlation energy is determined by $\varepsilon_{xc}\left[n_0\left(\vec{r}\right)\right]$, which comes from a homogeneous electron gas.

With the constraint that the number of electrons being a constant, we have the following variational form,

$$\int \delta n_0\left(\vec{r}\right)\left\{\varphi\left(\vec{r}\right) + \frac{\delta T\left[n_0\left(\vec{r}\right)\right]}{\delta n_0\left(\vec{r}\right)} + \mu_{xc}\left[n_0\left(\vec{r}\right)\right]\right\}d\vec{r} = 0\,, \tag{2.26}$$

where

$$\varphi\left(\vec{r}\right) = \upsilon\left(\vec{r}\right) + \int \frac{n_0\left(\vec{r'}\right)}{\left|\vec{r} - \vec{r'}\right|}d\vec{r'}\,, \tag{2.27}$$

$$\mu_{xc}\left[n_0\left(\vec{r}\right)\right]=\frac{d\left(n_0\varepsilon_{xc}(n_0)\right)}{dn_0}. \tag{2.28}$$

The variation form of the Eq. (2.26) leads to a single-particle Schrödinger-like equation as the following,

$$\left\{-\frac{1}{2m}\nabla^2+\left[\varphi\left(\vec{r}\right)+\mu_{xc}\left(n_0\left(\vec{r}\right)\right)\right]\right\}\psi_i\left(\vec{r}\right)=E_i\psi_i\left(\vec{r}\right). \tag{2.29}$$

E_i and $\psi_i\left(\vec{r}\right)$ are eigenvalues and eigenstates of this equation. The relation between the electron density and wave functions at ground state is

$$n_0\left(\vec{r}\right)=\sum_{i=1}^{N}\left|\psi_i\left(\vec{r}\right)\right|^2. \tag{2.30}$$

Eq. (2.29) is called the Kohn-Sham equation, which represents a mapping of the interacting many-particle system onto a system of noninteracting electrons moving in an effective potential due to all the other electrons. The Eqs. (2.29) and (2.30) consist of the self-consistent procedure in practical calculations, so that the occupied electronic states generate a charge density that produces the electronic potential that was used to construct the equations. The sum of the single-particle Kohn-Sham eigenvalues does not give the total electronic energy because this overcounts the effects of the electron-electron interaction in the Hartree energy and in the exchange-correlation energy. The actual total energy is

$$E=\sum_{i=1}^{N}E_i-\frac{1}{2}\int\int\frac{n_0\left(\vec{r}\right)n_0\left(\vec{r'}\right)}{\left|\vec{r}-\vec{r'}\right|}d\vec{r}d\vec{r'}+\int n_0\left(\vec{r}\right)\left\{\varepsilon_{xc}\left[n_0\left(\vec{r}\right)\right]-\mu_{xc}\left[n_0\left(\vec{r}\right)\right]\right\}d\vec{r}. \tag{2.31}$$

The functional $\varepsilon_{xc}\left[n_0\left(\vec{r}\right)\right]$ can be further divided into the exchange and the correlation terms as

$$\varepsilon_{xc}\left[n_0\left(\vec{r}\right)\right]=\varepsilon_x\left[n_0\left(\vec{r}\right)\right]+\varepsilon_c\left[n_0\left(\vec{r}\right)\right], \tag{2-32}$$

where the exchange term $\varepsilon_x\left(n_0\right)$ is obtained either from the Dirac exchange energy functional,

$$\varepsilon_x\left(n_0\right)=-\frac{3}{4}\left(\frac{3}{\pi}\right)^{1/3} n_0^{1/3}, \tag{2.33}$$

or from a Hartree-Fork style calculation. The correlation term, $\varepsilon_c\left(n_0\right)$, can be obtained through other methods such as the Quantum Monte Carlo (QMC).

The success of LDA has made it widely accepted, even in very inhomogeneous cases, and has stimulated ideas for constructing improved functional, such as those from generalized gradient approximation (GGA). The basic idea of GGA is that E_{xc} is a functional of the local electron density and its gradient,

$$E_{xc}=E_{xc}\left[n_0;\nabla n_0\right].$$

There are quite a few GGA functionals that are used for different requirements, such as Lee-Yang-Parr (LYP)[41] and Perdew-Wang-91[42]. One of the most important characteristics of present GGAs is to result in the reduction of binding energy, correcting the LDA overbinding.

The Kohn-Sham scheme powerfully handles the many-particle problem. For instance, the structural properties of materials such as the lattice constant, the elastic modulus, and the cohesive energy are determined to within a few percent of the experimental values. Band gap values are underestimated by Kohn-Sham theory, because the Kohn-Sham equation gives the eigenvalues of the Kohn-Sham particles, a collection of fictitious particles, not the eigenvalues of real electrons. In most cases, Kohn-Sham

scheme is used to give a first-hand estimation of the band structures. Some people try to find an appropriate exchange-correlation functional to handle this issue. However, Green's function method and GW approximation are proposed to improve the band gap values.

2.3 Solving Kohn-Sham equation numerically

In the preceding section it is demonstrated that a many-body problem can be mapped into a noninteracting single-particle problem with an effective potential containing all the interaction information. While the task to handle an infinite number of electrons moving in the static potential of an infinite number of nuclei is still formidable, Bloch's theorem overcomes this difficulty.

Bloch's theorem states that the electronic wave functions in a periodic solid can be written as a product of two parts[43],

$$\psi_i\left(\vec{r}\right) = e^{i\vec{k}\cdot\vec{r}} f_i\left(\vec{r}\right), \tag{2.34}$$

where $f_i\left(\vec{r}\right)$ can be expanded with a discrete set of plane waves whose wave vectors are reciprocal lattice vectors of the crystal,

$$f_i\left(\vec{r}\right) = \sum_{\vec{G}} c_{i,\vec{G}} \exp[i\vec{G}\cdot\vec{r}]. \tag{2.35}$$

Here the reciprocal lattice vector $\vec{G}$ is defined by $\vec{G}\cdot\vec{l} = 2\pi m$ where l is a lattice vector of the crystal and m is an integer. And then each electronic wave function is a sum of plane waves,

$$\psi_i\left(\vec{r}\right) = \sum_{\vec{G}} c_{i,\vec{k}+\vec{G}} \exp[i\left(\vec{k}+\vec{G}\right)\cdot\vec{r}]. \tag{2.36}$$

In principle, an infinite plane-wave basis set is desired to expand the electronic wave function. But the coefficient $c_{i,\vec{k}+\vec{G}}$ with a small kinetic energy $(1/2m)\left|\vec{k}+\vec{G}\right|^2$ is more important than that with large kinetic energy. Normally the basis set can be truncated so that only those plane waves with kinetic energy less than a certain value E_{cutoff} are retained. When a plane-wave basis set is used to express the electronic wave function, the Kohn-Sham equation becomes a particularly simple form. Insert into Eq. (2.29) the sum from Eq. (2.36), and integration over $\vec{r}$ gives a secular equation,

$$\sum_{\vec{G}'}\left[\left(\frac{1}{2m}\right)\left|\vec{k}+\vec{G}\right|^2\delta_{\vec{G}\vec{G}'}+\varphi\left(\vec{G}-\vec{G}'\right)+\mu_{xc}\left(\vec{G}-\vec{G}'\right)\right]c_{i,\vec{k}+\vec{G}'}=E_i c_{i,\vec{k}+\vec{G}}. \qquad (2.37)$$

To find the solution of Eq. (2.37), we must diagonalize the Hamiltonian matrix with element $H_{\vec{k}+\vec{G},\vec{k}+\vec{G}'}$ given by the materials in the bracket above. The size of the matrix is decided by the cutoff energy $(1/2m)\left|\vec{k}+\vec{G}_c\right|^2$.

Because the electronic wave functions have complicated nodal structure near the ion cores, if all the valence electrons and core electrons of the system are taken into account, the size of this Hamiltonian matrix might be intractably large. A convenient solution for this trouble is to use the pseudopotential approximation.

2.3.1 Pseudopotential Approximation

We know most physical properties of solids depend on the valence electrons to a much greater extent than on the core electrons. When we use Bloch's theorem to solve the Kohn-Sham equation, one critical issue is that a large number of plane-waves are required to expand the core orbitals and to follow the rapid oscillations of the wave functions of the valence electrons in the core region. The pseudopotential approximation

removes the core electrons and replaces them and the strong ionic potential with a weaker pseudopotential acting on a set of pseudo wave functions rather than the true wave functions. The true valence wave functions oscillate rapidly in the core region because of the strong potential of the nuclei and core electrons. This oscillation ensures the orthogonality between core wave functions and valence wave functions as required by the exclusion principle. An ionic potential, valence wave function and the corresponding pseudopotential, and pseudo wave function are illustrated in figure 2.1[44]. The pseudopotential is designed ideally so that its scattering properties or phase shifts for the pseudo wave functions are identical to the scattering properties of the ion and the core electrons for the valence wave functions, but in such way that the pseudo wave functions have no radial nodes in the core region. Pseudopotential approximation scheme allows the pseudo wave functions to be expanded with a much less plane-wave basis states.

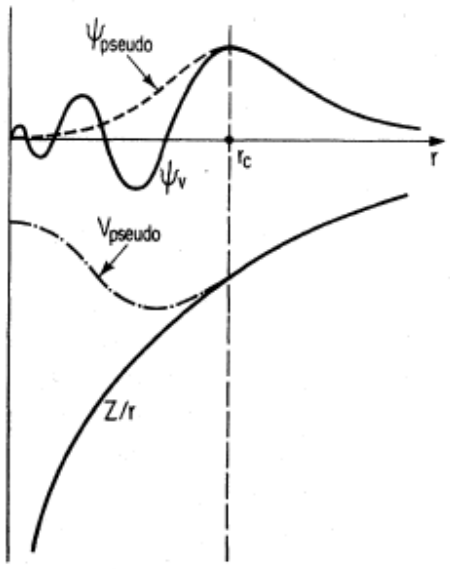

Figure 2.1 Schematic illustration of all-electron (solid lines) and pseudoelectron (dashed lines) potentials and their corresponding wave functions. The radius at which all-electron and pseudoelectron values match is designated r_c [44].

There are two types of pseudopotentials: empirical[45-46] and *ab initio.* The parameters of the empirical pseudopotentials are obtained from the experimental data fitting of a specific material. Its accuracy depends on the fitting procedure, and therefore its utility is limited to the material from which the parameters come. The *ab initio* pseudopotential is obtained from the core electronic states of atoms of a certain element, independent of the chemical environment outside of core region. The *ab initio* pseudopotential has better transferability and nowadays is widely used in first-principles calculations.

The basic idea of the *ab initio* pseudopotential approximation is demonstrated in the orthogonalized-plane-wave (OPW) calculations, which were first introduced by Herring in 1940[47-48]. A major part of the large negative potential energy inside the atomic core region and the large positive kinetic energy of the valence electrons in the same region cancel out. OPW method gives a pseudopotential with pseudo wave functions that is still "hard core". The pseudo wave functions are proportional, but not equal, to the real wave functions outside of the core region. Norm-conservation condition[49] was thereafter proposed to make improvement. Then pseudopotentials constructed following the norm-conservation requirement are referred to as norm-conserving pseudopotentials. However, norm-conserving pseudopotentials are not reliable to handle first-row and transition-metal atoms, because the highly localized p and d orbitals which are nodeless cannot be represented efficiently.

2.3.2 Ultrasoft pseudopotential

In 1990 Vanderbilt[50-51] first proposed the ultrasoft pseudopotential model in 1990. The potentials have a separable form well suited for plane-wave solid-state calculations

and show reliability for application to first-row and transition-metal systems. The pseudopotential itself becomes charge-state dependent, the usual norm-conservation constraint does not apply while the transferability is allowed to be improved systematically with holding the cutoff radius fixed.

Considering an all-electron wave function $\psi_i\left(\vec{r}\right)$ of definite angular momentum lm, which is a solution of the Schrödinger equation at an arbitrary energy ε_i, we have

$$\left[T+V_{AE}\left(\vec{r}\right)\right]\psi_i\left(\vec{r}\right)=\varepsilon_i\psi_i\left(\vec{r}\right). \tag{2.38}$$

Here $i=\left\{\varepsilon_i lm\right\}$ is a composite index, $T=-\frac{1}{2}\nabla^2$, V_{AE} is the original reference screened all-electron potential. Cutoff radii r_{cl} and r_c^{loc} are chosen for the wave functions and local pseudopotentials, respectively. And a diagnostic radius R is chosen so that all pseudo- and all-electron quantities agree beyond R. Now a pseudo-wave-function ϕ_i is constructed with two constraints so that it joins smoothly to $\psi_i\left(\vec{r}\right)$ at r_{cl} and it satisfies the norm-conserving condition $\left\langle\phi_i\middle|\phi_i\right\rangle_R=\left\langle\psi_i\middle|\psi_i\right\rangle_R$. Then a local wave function is defined as the following,

$$\left|\chi_i\right\rangle=\left(\varepsilon_i-T-V_{loc}\right)\left|\phi_i\right\rangle, \tag{2.39}$$

which vanishes at and beyond R where $V_{AE}=V_{loc}$ and $\phi_i=\psi_i$. The nonlocal pseudopotential operator is defined as

$$V_{NL}=\frac{\left|\chi_i\right\rangle\left\langle\chi_i\right|}{\left\langle\chi_i\middle|\phi_i\right\rangle}. \tag{2.40}$$

It is straightforward to verify that $|\phi_i\rangle$ is an eigenvector of $T+V_{loc}+V_{NL}$, and the scattering properties and their energy derivatives are correct at ε_i.

The second stage is to generalize the procedure above to the case of two or more energy ε_i. The set of pseudo wave functions $\phi_i's$ is constructed from the all-electron wave functions $\psi_i's$ as before, except that they have to satisfy the generalized norm-conserving condition

$$Q_{ij} \equiv \langle \psi_i | \psi_j \rangle_R - \langle \phi_i | \phi_j \rangle_R = 0. \tag{2.41}$$

Forming the matrix $B_{ij} \equiv \langle \phi_i | \chi_j \rangle$ and defining a set of local wave functions

$$|\beta_i\rangle = \sum_j \left(B^{-1}\right)_{ji} |\chi_j\rangle, \tag{2.42}$$

which are dual to the $|\phi_i\rangle$, the nonlocal pseudopotential operator can be chosen as

$$V_{NL} = \sum_{i,j} B_{ij} |\beta_i\rangle\langle\beta_j|. \tag{2.43}$$

Then it can be verified that

$$\left(T+V_{loc}+V_{NL}-\varepsilon_i\right)|\phi_i\rangle = 0, \tag{2.44}$$

and that B_{ij} and V_{NL} are Hermitian when $Q_{ij}=0$.

The third stage is to show that the constraint $Q_{ij}=0$ is unnecessary, if one is willing to adopt a generalized eigenvalue formalism in which an overlap operator appears. The nonlocal overlap operator is defined as,

$$S = 1 + \sum_{i,j} Q_{ij} |\beta_i\rangle\langle\beta_j|, \tag{2.45}$$

and then redefine the nonlocal potential operator to be

$$V_{NL} = \sum_{i,j} D_{ij} \left|\beta_i\right\rangle \left\langle\beta_j\right|, \tag{2.46}$$

where

$$D_{ij} = B_{ij} + \varepsilon_i Q_{ij}, \tag{2.47}$$

and $Q_{ij} = \left\langle\psi_i \middle| \psi_j\right\rangle_R - \left\langle\phi_i \middle| \phi_j\right\rangle_R$. Following these definitions, we have

$$\left\langle\phi_i \middle| S \middle| \phi_j\right\rangle_R = \left\langle\psi_i \middle| \psi_j\right\rangle_R, \tag{2.48}$$

and the pseudo wave function $\left|\phi_i\right\rangle$ is the solution of the generalized eigenvalue problem $\left(H - \varepsilon_i S\right)\left|\phi_i\right\rangle = 0$, where $H = T + V_{loc} + V_{NL}$ and S are Hermitian. When we make derivative of the equation $\left(H - \varepsilon S\right)\left|\phi_\varepsilon\right\rangle = 0$ with respect to ε, we may find that the logarithmic derivatives of all-electron and pseudo wave functions match in the usual way. The deficit of valence charge in the core region associated with a pseudo wave function needs to be restored. The solution of the generalized eigenvalue problem should be normalized according to

$$\left\langle\phi_{n\vec{k}} \middle| S \middle| \phi_{n'\vec{k}}\right\rangle = \delta_{n'n}. \tag{2.49}$$

To make up the deficit of the charge, the valence charge density is defined as

$$n_v\left(\vec{r}\right) = \sum_{n,\vec{k}} \phi^*_{n\vec{k}}\left(\vec{r}\right)\phi_{n\vec{k}}\left(\vec{r}\right) + \sum_{i,j} \rho_{ij} Q_{ji}\left(\vec{r}\right), \tag{2.50}$$

where

$$\rho_{ij} = \sum_{n,\vec{k}} \left\langle\beta_i \middle| \phi_{n\vec{k}}\right\rangle \left\langle\phi_{n\vec{k}} \middle| \beta_j\right\rangle, \tag{2.51}$$

$$Q_{ij}\left(\vec{r}\right) = \psi^*_i\left(\vec{r}\right)\psi_j\left(\vec{r}\right) - \phi^*_i\left(\vec{r}\right)\phi_j\left(\vec{r}\right). \tag{2.52}$$

Following Eq. (2.45) and Eq. (2.49), we have $\int n_v\left(\vec{r}\right)d^3r = N_v$ exactly, where N_v is the number of valence electrons in the unit cell.

2.3.3 Projected augmented wave method

Pseudopotential approximation permits accurate calculations with a smaller set of plane-wave basis states. The price to pay is that all information on the charge density and wave function near the nuclei is lost. That loss causes the transferability problem: for instance, pseudopotentials constructed from an isolated atom might not be guaranteed to be accurate for a molecule. The projected augmented wave (PAW) method[52] is a combination of augmented wave method and the pseudopotential approach. Without sacrificing efficiency, the projected augmented wave method avoids transferability problems of the pseudopotential approach, and the PAW method has been valuable to predict properties that depend on the all-election wave function, such as full charge and spin density.

Considering a transformation operator T that connects the real valence wave functions $|\Psi\rangle$ and that of a set of smooth pseudo wave functions $|\widetilde{\Psi}\rangle$:

$$|\Psi\rangle = T|\widetilde{\Psi}\rangle = \left(1+\sum_R S_R\right)|\widetilde{\Psi}\rangle. \tag{2.53}$$

Here each S_R adds the difference between the true and the auxiliary wave function. The index R is a label for an atomic site Ω_R which encloses one atom. All-electron and pseudo wave functions coincide outside this augmentation region. Within Ω_R we have

$$|\phi_i\rangle = \left(1+S_R\right)|\tilde{\phi}_i\rangle, \tag{2.54}$$

where $|\phi_i\rangle$ and $|\tilde{\phi}_i\rangle$ are the all-electron and pseudo partial wave functions of valence states, respectively, and $i=\{R,nlm\}$ is a composite index. The pseudo wave functions are smooth and complete inside Ω_R, and identical to the all-electron partial wave functions outside Ω_R. The all-electron and pseudo wave functions can be expanded in terms of the pseudo partial waves

$$|\tilde{\Psi}\rangle=\sum_i|\tilde{\phi}_i\rangle c_i\,, \tag{2.55}$$

$$|\Psi\rangle=T|\tilde{\Psi}\rangle=\sum_i|\phi_i\rangle c_i\,, \tag{2.56}$$

so we have

$$|\Psi\rangle=|\tilde{\Psi}\rangle-\sum_i|\tilde{\phi}_i\rangle c_i+\sum_i|\phi_i\rangle c_i\,. \tag{2.57}$$

Then we write the coefficient c_i as

$$c_i=\langle\tilde{p}_i|\tilde{\Psi}\rangle, \tag{2.58}$$

which defines the projector function $|\tilde{p}_i\rangle$. $|\tilde{p}_i\rangle$ probes the local character of the auxiliary wave function in the atomic region, with

$$\sum_i|\tilde{\phi}_i\rangle\langle\tilde{p}_i|=1\,, \tag{2.59}$$

$$\langle\tilde{p}_i|\tilde{\phi}_i\rangle=\delta_{ij}\,. \tag{2.60}$$

Eq. (2.57) thereafter can be written as

$$|\Psi\rangle=T|\tilde{\Psi}\rangle=\left(1+\sum_i\left(|\phi_i\rangle-|\tilde{\phi}_i\rangle\right)\langle\tilde{p}_i|\right)|\tilde{\Psi}\rangle. \tag{2.61}$$

This expression for the true wave function can be understood in this way. Consider two regions: (1) Far from the atoms, $|\phi_i\rangle = |\tilde{\phi}_i\rangle$, so that $|\Psi\rangle = |\tilde{\Psi}\rangle$; (2) Close to an atom, because $\sum_i |\tilde{\phi}_i\rangle\langle\tilde{p}_i| = 1$; then we have $|\Psi\rangle = \sum_i |\phi_i\rangle\langle\tilde{p}_i|\tilde{\Psi}\rangle$. It is constructed from the partial waves that contain the proper nodal structure.

The core states are decomposed in a similar way,

$$|\Psi^c\rangle = |\tilde{\Psi}^c\rangle + |\phi^c\rangle - |\tilde{\phi}^c\rangle. \tag{2.62}$$

Here the projector function is simplified into the unity operator.

The expectation value of an operator A can be expressed in terms of either the true or the auxiliary wave functions,

$$\begin{aligned}\langle A\rangle &= \sum_n f_n \langle\Psi_n|A|\Psi_n\rangle + \sum_{n=1}^{N_c}\langle\phi_n^c|A|\phi_n^c\rangle \\ &= \sum_n f_n \langle\tilde{\Psi}_n|T^\dagger A T|\tilde{\Psi}_n\rangle + \sum_{n=1}^{N_c}\langle\phi_n^c|A|\phi_n^c\rangle,\end{aligned} \tag{2.63}$$

where f_n are the occupations of the valence states, and N_c is the number of core states. The first sum runs over the valence states and the second over the core states. Following the Eq. (2.63), the physical quantities such as charge density $n(\vec{r})$ and total energy E can be obtained accordingly.

CHAPTER THREE

AB INITIO CALCULATIONS OF SECOND-, THIRD-, AND FOURTH-ORDER ELASTIC CONSTANTS FOR SINGLE CRYSTALS

3.1 Introduction

In the theory of linear elasticity, infinitesimal deformation strains are assumed. As a result, the second-order elastic constants (SOECs) are sufficient to describe the elastic stress-strain response and wave propagation in solids[6, 22]. In case of finite strains, the theory of nonlinear elasticity is required[53-57]. It is well known that third-order elastic constants (TOECs) are important quantities to describe nonlinear mechanical effects. In many occasions, even higher order elastic constants such as the fourth-order ones may be needed to describe the nonlinear effect. As shown by Ghate[58], for a crystal with cubic symmetry subject to a simple shear with a finite shear strain, e.g., η_{12}, the elastic energy expanded in Taylor series to the third order in terms of the strain parameter gives $E = E_0 + \psi_2 + \psi_3$, where E_0 is the energy of the undeformed sample, $\psi_2 = C_{44}\eta_{12}^2 / 2$, and $\psi_3 = 0$. The last result shows that nonlinear effect, if there is any, would not be present in this case. To reach higher order accuracy, one would expect to add the fourth order term, $\psi_4 = \frac{2}{3} C_{4444}\eta_{12}^4$, in which the C_{4444} is the fourth order elastic constant (FOEC). In many real applications beyond this simple example, there are plenty of cases where the high order elastic constants are needed that are not merely limited in

the area of mechanics. For example, TOECs, FOECs, and higher order elastic constants have been used to interpret anharmonic phenomena in solid-state physics, such as phonon-phonon interaction, Grűneisen parameters[59], etc. They also have appeared in the development of ion-electron pseudopotentials[60-61], or empirical interatomic potentials[61]. Recently, the nonlinear effects in elastic[62-64] and piezoelectric properties[65-66] have drawn many interests in nanoscale materials where nonlinear effects become significant. Of particular interest are those activities that involve the fourth-order elastic constants in the description of nonlinear phenomena such as intermodulation in thickness-shear and trapped-energy resonators[67-68], the generation of third harmonics in finite-amplitude waves[69], the description of shock-compression stress-strain curves[70-71], and in the nonlinear constitutive equations for thermo-electroelastic materials[72].

Many experiments have been performed to determine the SOECs and high order elastic constants[73]. However, for crystals with low symmetry or with low yield stress, to obtain a complete set of TOECs is still not a simple task. For FOECs the difficult becomes more acute. As a result, there are few experimental values for the FOECs available so far. A feasible alternative is theoretical calculations. In the past two decades, several theoretical methods have been developed to calculate higher order elastic constants for single crystals. For the TOECs, there are quite a few methods available, including empirical interatomic force-constant model[74-75], molecular dynamics simulation using fluctuation formula[76-77], the methods of homogeneous deformation based on empirical or the first-principles total-energy methods[78], and other quantum calculations[79-81]. The approaches used in the TOEC calculations, in principle, could be extended in the calculations of the FOECs, except that certain care must be exercised due to the

increasing complexity of the formulations and the demand for high accuracies needed in the computation.

In this chapter, we shall employ the method similar to that practiced earlier by Nielsen and Martin[79-80]. In this approach, the homogeneous deformation strain is applied to the system, and usually simple deformation modes are used such as uniaxial tension or compression, simple or pure shear, and other combinations of homogeneous strains. The total elastic energies of the system subject to these deformations are calculated using *ab initio* methods employing the density-functional theory (DFT). The internal energy-strain curves under the various strains, which are often far beyond those of the linear elastic limit, are numerically fitted using polynomials. Because of the deliberate selection of the homogeneous deformation modes, the coefficients in the internal energy polynomial functions are simple combinations of the second-, third-, or fourth-order elastic constants. Through the numerical fitting, we can obtain the elastic constants straightforwardly. Recently, the same method was used in the first-principles quantum mechanics calculations of the third-order order elastic constants by Zhao *et al*[82] and Łopuszyński and Majeski[83] in single crystals with covalent bond. Their results show good agreement with experiments. In this paper, we extend this method to calculating the fourth-order elastic constants, which to the best of our knowledge, has not been systematically performed and tested.

This chapter is organized as follows. In section 3.2, we give a general introduction of nonlinear elasticity with a particular attention paid to the relation of the higher order elastic constants with the internal energy. In section 3.3, we present the methods of applying homogeneous deformation strains to the system and *ab initio* calculation to

obtain the internal energy-strain relations. In section 3.4, we give the results for the calculated fourth-order elastic constants for the four FCC metals: Cu, Al, Au, and Ag, along with the second- and third-order ones. Available results from experiments and other theoretical methods are also shown for comparison. In section 3.5, we draw conclusions from this work.

3.2 Theory of nonlinear elasticity

For a solid body subject to a finite deformation, the configuration of a material point in the system after deformation is represented as $x = x(a)$, where a is the initial configuration at the equilibrium state. The deformation gradient is defined by

$$J_{ij} = \frac{\partial x_i}{\partial a_j}, \tag{3.1}$$

where i and j (=1,2,3) represent the Cartesian coordinates. Then the Lagrangian strain tensor is defined as

$$\eta = \frac{1}{2}(J^T J - I), \tag{3.2}$$

where I is the unit matrix.

The internal energy and the free energy are related to the Lagrangian strain tensor in the theory of nonlinear elasticity through Taylor series expansion in terms of the strain tensor[22, 53-54],

$$U(a,\eta_{ij},S) = U(a,S) + (1/2!)V\sum_{ijkl} C^S_{ijkl}\eta_{ij}\eta_{kl} + (1/3!)V\sum_{ijklmn} C^s_{ijklmn}\eta_{ij}\eta_{kl}\eta_{mn} + (1/4!)V\sum_{ijklmnpq} C^s_{ijklmnpq}\eta_{ij}\eta_{kl}\eta_{mn}\eta_{pq} + \ldots, \tag{3.3}$$

$$F(a,\eta_{ij},T) = F(a,T) + (1/2!)V\sum_{ijkl} C^T_{ijkl}\eta_{ij}\eta_{kl} + (1/3!)V\sum_{ijklmn} C^T_{ijklmn}\eta_{ij}\eta_{kl}\eta_{mn} + (1/4!)V\sum_{ijklmnpq} C^T_{ijklmnpq}\eta_{ij}\eta_{kl}\eta_{mn}\eta_{pq} + \ldots, \quad (3.4)$$

where $U(a,\eta_{ij},S)$ is the internal energy, $F(a,\eta_{ij},S)$ is the Helmholtz free energy, T is the temperature, S is the entropy, and V is the volume of the system.

The elastic constants of second, third, fourth, and higher order are defined as the second-, third-, fourth-, and higher order derivatives of the above functions with respect to the strain, respectively. The adiabatic elastic constants of second-, third-, and fourth-order are

$$C^S_{ijkl} = V^{-1}(\partial^2 U/\partial\eta_{ij}\partial\eta_{kl})_{S\eta}, \quad (3.5)$$

$$C^S_{ijklmn} = V^{-1}(\partial^2 U/\partial\eta_{ij}\partial\eta_{kl}\partial\eta_{mn})_{S\eta}, \quad (3.6)$$

$$C^S_{ijklmnpq} = V^{-1}(\partial^2 U/\partial\eta_{ij}\partial\eta_{kl}\partial\eta_{mn}\partial\eta_{pq})_{S\eta}. \quad (3.7)$$

And the isothermal elastic constants are

$$C^T_{ijkl} = V^{-1}(\partial^2 F/\partial\eta_{ij}\partial\eta_{kl})_{T\eta}, \quad (3.8)$$

$$C^T_{ijklmn} = V^{-1}(\partial^2 F/\partial\eta_{ij}\partial\eta_{kl}\partial\eta_{mn})_{T\eta}, \quad (3.9)$$

$$C^T_{ijklmnpq} = V^{-1}(\partial^2 F/\partial\eta_{ij}\partial\eta_{kl}\partial\eta_{mn}\partial\eta_{pq})_{T\eta}. \quad (3.10)$$

These elastic constants are defined at the initial configuration a, where η_{ij} are measured from a. The initial state as represented by a is in fact arbitrary but must be in equilibrium. In this work, we have the initial state a at $\eta = 0$, a undeformed state. Since our *ab initio* calculations are performed at 0 K. $F = U - TS = U$, so $C^S = C^T$. We will not distinguish those two types of elastic constants in the following.

We can simplify the notations in the tensors by using the Voigt notation ($11 \to 1$, $22 \to 2$, $33 \to 3$, $23 \to 4$, $31 \to 5$, and $12 \to 6$). We have therefore for the strain tensors, $\eta_{11} \to \eta_1$, $\eta_{22} \to \eta_2$, $\eta_{33} \to \eta_3$, $\eta_{23} \to \eta_4/2$, $\eta_{31} \to \eta_5/2$, and $\eta_{12} \to \eta_6/2$. Equations (3.3) and (3.4) now can be written as

$$V^{-1}[U(a,\eta)-U(a,0)] = \frac{1}{2!}\sum_{i,j=1,6} c_{ij}\eta_i\eta_j + \frac{1}{3!}\sum_{i,j,k=1,6} c_{ijk}\eta_i\eta_j\eta_k + \frac{1}{4!}\sum_{i,j,k,l=1,6} c_{ijkl}\eta_i\eta_j\eta_k\eta_l + \ldots. \tag{3.11}$$

For single crystals with cubic symmetry, we can express Eq. (3.11) in the second-, third- and fourth-order terms of the strain tensor,

$$V^{-1}[U(a,\eta)-U(a,0)] = \psi_2 + \psi_3 + \psi_4 \ldots, \tag{3.12}$$

where

$$\psi_2 = \frac{1}{2}c_{11}(\eta_1^2+\eta_2^2+\eta_3^2) + c_{12}(\eta_1\eta_2+\eta_2\eta_3+\eta_3\eta_1) + \frac{1}{2}c_{44}(\eta_4^2+\eta_5^2+\eta_6^2), \tag{3.13}$$

$$\begin{aligned}\psi_3 = {} & \frac{1}{6}c_{111}(\eta_1^3+\eta_2^3+\eta_3^3) + \frac{1}{2}c_{112}(\eta_2\eta_1^2+\eta_3\eta_1^2+\eta_1\eta_2^2+\eta_1\eta_3^2+\eta_2\eta_3^2+\eta_3\eta_2^2) \\ & + c_{123}\eta_1\eta_2\eta_3 + \frac{1}{2}c_{144}(\eta_1\eta_4^2+\eta_2\eta_5^2+\eta_3\eta_6^2) + \\ & \frac{1}{2}c_{155}(\eta_2\eta_4^2+\eta_3\eta_4^2+\eta_1\eta_5^2+\eta_3\eta_5^2+\eta_1\eta_6^2+\eta_2\eta_6^2) + c_{456}\eta_4\eta_5\eta_6,\end{aligned} \tag{3.14}$$

and[58],

$$\psi_4 = \frac{1}{24}C_{1111}(\eta_1^4+\eta_2^4+\eta_3^4)+\frac{1}{6}C_{1112}[\eta_1^3(\eta_2+\eta_3)+\eta_2^3(\eta_3+\eta_1)+\eta_3^3(\eta_1+\eta_2)]$$
$$+\frac{1}{4}C_{1122}(\eta_1^2\eta_2^2+\eta_2^2\eta_3^2+\eta_3^2\eta_1^2)+\frac{1}{2}C_{1123}(\eta_1^2\eta_2\eta_3+\eta_2^2\eta_3\eta_1+\eta_3^2\eta_1\eta_2)$$
$$+\frac{1}{4}C_{1144}(\eta_1^2\eta_4^2+\eta_2^2\eta_5^2+\eta_3^2\eta_6^2)+\frac{1}{4}C_{1155}[\eta_1^2(\eta_5^2+\eta_6^2)+\eta_2^2(\eta_4^2+\eta_6^2)+\eta_3^2(\eta_4^2+\eta_5^2)]$$
$$+\frac{1}{2}C_{1255}[\eta_1\eta_2(\eta_4^2+\eta_5^2)+\eta_2\eta_3(\eta_5^2+\eta_6^2)+\eta_1\eta_3(\eta_4^2+\eta_6^2)]$$
$$+\frac{1}{2}C_{1266}(\eta_1\eta_2\eta_6^2+\eta_2\eta_3\eta_4^2+\eta_1\eta_3\eta_5^2)+C_{1456}[\eta_4\eta_5\eta_6(\eta_1+\eta_2+\eta_3)]$$
$$+\frac{1}{24}C_{4444}(\eta_4^4+\eta_5^4+\eta_6^4)+\frac{1}{4}C_{4455}(\eta_4^2\eta_5^2+\eta_5^2\eta_6^2+\eta_6^2\eta_4^2). \quad (3.15)$$

As shown above, there are three independent SOECs (c_{11}, c_{12}, and c_{44}), six TOECs ($c_{111}, c_{112}, c_{123}, c_{144}, c_{155}$, and c_{456}), and 11 FOECs (c_{1111}, c_{1112}, c_{1122}, c_{1123}, c_{1144}, c_{1155}, c_{1255}, c_{1266}, c_{1456}, c_{4444}, and c_{4455}). As shown below, these elastic constants can be obtained in the theoretical calculations by subjecting the system to various simple deformation strains, provided also that the system does not have any polymorphic phase transition and internal deformation under these strains.

The Lagrangian stress is defined as the first order derivative of the internal energy or Helmholtz free energy with respect to the strain tensor,

$$\sigma_{ij} = V^{-1}\left(\partial U/\partial\eta_{ij}\right) = V^{-1}\left(\partial F/\partial\eta_{ij}\right), \quad (3.16)$$

which can also be used also to evaluate the elastic constants[79-80].

3.3 Methods of homogeneous deformation and ab initio computation

Table 3.1 For each type of strain modes, $\eta_\alpha(\xi)$, $\alpha = A, B, ..., K$, the internal energy is expressed as a polynomial function of ξ. The coefficients P_2, P_3, P_4 in Eq. (3.17) are shown as the linear combinations of the second-, third-, and fourth-order elastic constants, respectively.

Strain type	P2	P3	P4
$\eta_A = (\xi,0,0,0,0,0)$	$\frac{1}{2}C_{11}$	$\frac{1}{6}C_{111}$	$\frac{1}{24}C_{1111}$
$\eta_B = (\xi,\xi,0,0,0,0)$	$C_{11}+C_{12}$	$\frac{1}{3}C_{111}+C_{112}$	$\frac{1}{12}C_{1111}+\frac{1}{3}C_{1112}+\frac{1}{4}C_{1122}$
$\eta_C = (\xi,-\xi,0,0,0,0)$	$C_{11}-C_{12}$	0	$\frac{1}{12}C_{1111}-\frac{1}{3}C_{1112}+\frac{1}{4}C_{1122}$
$\eta_D = (\xi,0,0,2\xi,0,0)$	$\frac{1}{2}C_{11}+2C_{44}$	$\frac{1}{6}C_{111}+2C_{144}$	$\frac{1}{24}C_{1111}+C_{1144}+\frac{2}{3}C_{4444}$
$\eta_E = (\xi,0,0,0,0,2\xi)$	$\frac{1}{2}C_{11}+2C_{44}$	$\frac{1}{6}C_{111}+2C_{155}$	$\frac{1}{24}C_{1111}+C_{1155}+\frac{2}{3}C_{4444}$
$\eta_F = (0,0,0,2\xi,2\xi,2\xi)$	$6C_{44}$	$8C_{456}$	$2C_{4444}+12C_{4455}$
$\eta_G = (0,0,0,2\xi,0,0)$	$2C_{44}$	0	$\frac{2}{3}C_{4444}$
$\eta_H = (\xi,\xi,0,0,0,2\xi)$	$C_{11}+C_{12}+2C_{44}$	$\frac{1}{3}C_{111}+C_{112}+4C_{155}$	$\frac{1}{12}C_{1111}+\frac{1}{3}C_{1112}+\frac{1}{4}C_{1122}+2C_{1155}+2C_{1266}+\frac{2}{3}C_{4444}$
$\eta_I = (\xi,\xi,0,2\xi,0,0)$	$C_{11}+C_{12}+2C_{44}$	$\frac{1}{3}C_{111}+C_{112}+2C_{144}+2C_{155}$	$\frac{1}{12}C_{1111}+\frac{1}{3}C_{1112}+\frac{1}{4}C_{1122}+C_{1144}+C_{1155}+2C_{1255}+\frac{2}{3}C_{4444}$
$\eta_J = (\xi,0,0,2\xi,2\xi,2\xi)$	$\frac{1}{2}C_{11}+3C_{44}$	$\frac{1}{6}C_{111}+2C_{144}+4C_{155}+8C_{456}$	$\frac{1}{24}C_{1111}+C_{1144}+2C_{1155}+8C_{1456}+2C_{4444}+12C_{4455}$
$\eta_K = (\xi,\xi,\xi,0,0,0)$	$\frac{3}{2}C_{11}+3C_{12}$	$\frac{1}{2}C_{111}+3C_{112}+C_{123}$	$\frac{1}{8}C_{1111}+C_{1112}+\frac{3}{4}C_{1122}+\frac{3}{2}C_{1123}$

Eq. (3.11) and Eqs. (3.13-3.15) suggest that we can treat the internal energy difference as a polynomial function of the strain parameter η_{ij}. Since there are six strain

components in the strain tensor η_{ij} when the system is rotation-free, one must select specific deformation modes to reduce the number of the strain components that will appear in the internal energy function. To make this feasible, we can select certain simple deformation or loading modes such that the strain tensor η_{ij} only has one or a few components. As a result, the coefficients in the polynomial are simple combinations of the elastic constants. For example, if we choose to subject the system with a uniaxial tension along the *x* direction (or *i, j*=1), the tensile strain, $\eta_1 = \xi$, and the rest of the strain components are all zero, that is, $\eta = (\xi,0,0,0,0,0)$. From Eqs. (3.13-3.15), we can see that this selection of the deformation mode results in an internal energy that can be expressed as a polynomial of the strain parameter ξ, that is, $V^{-1}\left[U(0,\xi)-U(0,0)\right]=1/2c_{11}\xi^2+1/6c_{111}\xi^3+1/24c_{1111}\xi^4$. To simplify the matter further, we can use only one scalar parameter ξ for all non-zero strain components. The selection of the different deformation modes leads to different strains used in this work, which are labeled as η_α, $\alpha = A,B,...,K$ and listed in table 3.1. There are total of eleven independent deformation modes we use in this work. Therefore, each time we apply a certain type of deformation mode to the crystal system, we use a specific strain parameter η_α in which there is only one strain parameter ξ that we can vary. That is, when we substitute a particular type of strain to Eqs. (3.11-3.16), we will have the polynomial functions for the internal energy function and the stress,

$$V^{-1}[U(a,\xi)-U(a,0)] = f_\alpha[\eta_\alpha(\xi)] = P_2\xi^2 + P_3\xi^3 + P_4\xi^4 + O(\xi^5). \tag{3.17}$$

$$V^{-1}(\partial U/\partial\eta_i) = \sigma_\alpha[\eta_\alpha(\xi)] = Q_1\xi + Q_2\xi^2 + Q_3\xi^3 + O(\xi^4), \tag{3.18}$$

where $\alpha = A, B, ..., K$ and the coefficients, P_2, P_3, P_4, Q_1, Q_2, and Q_3, are related to the elastic constants. As mentioned earlier, we have eleven of those functions for the internal energies and stresses corresponding to the different strains that are needed to fit 11 of the FOECs (see table 3.1).

To implement the different deformation modes in our calculation, we need to have the deformation gradient matrix J. As mentioned at Eq. (3.2), J is related to the strain η. Inversion of Eq. (3.2) gives

$$J_{ij} = \delta_{ij} + \eta_{ij} - \frac{1}{2}\sum_k \eta_{ki}\eta_{kj} + ..., \quad . \tag{3.19}$$

For a given strain η, in general, J is not unique, but this is not a problem since the Lagrange strain brings rotational invariance of total energy. Furthermore, for the system without rotation Eq. (3.19) provides a unique relation. We then apply the deformation gradient J to each of the crystal lattice vector r_i, where i is the lattice index. The deformed, or strained crystal is obtained then from $R_i = J_{ij} r_j$.

For each specific deformation mode in our calculation labeled as $\alpha = A, B, ..., K$, we change the value of ξ from $-|\xi_{\max}|$ to $+|\xi_{\max}|$ with a finite step size $\Delta\xi$, where $\xi_{\max}$ is the maximum value for the strain parameter chosen for each deformation calculation. As we show below, the values for both $\xi_{\max}$ and $\Delta\xi$ are important to obtaining high quality data, which are needed for the calculations of the higher order elastic constants. For each value of ξ, the total energy and stress tensor of the deformed crystal are calculated by *ab initio* method. Therefore, in our case, the 11 internal energy polynomial curves are calculated separately.

To obtain the coefficients in Eqs. (3.17-3.18) we fit the polynomial curves, $f(\xi)$ and $\sigma(\xi)$. Using nonlinear least-squares fitting, we first obtain the values for the coefficients $P_2, P_3, P_4,$ and Q_1, Q_2, Q_3. Each of these coefficients is a linear combination of the second-, third-, or fourth-order elastic constants; P_i is given in table 3.1. Then from the relations between the coefficients and the elastic constants, we can obtain the later.

In this paper, we will use FCC single crystal as examples because first, they do not possess internal deformation related to the absence of inversion symmetry. Secondly, as compared with other types of crystals, these FCC metals have the complete set of the third- and fourth-order elastic constants available from experiments or theoretical calculations, so we have those reference data to compare. Third, since we propose to use DFT to compute the FOECs, our goal is more on testing the feasibility than on general utility of this technique which may be extended later to other systems with more industrial and commercial relevance, which includes some covalent crystals that have the FOECs available from experiments[73].

For the cubic crystals, there are 11 independent fourth-order elastic constants, so we need at least 11 types of homogeneous deformation strain parameter, since for each deformation mode, we can only identify one coefficient as a linear combination of a certain number of the fourth-order elastic constants. We should mention that from the stress-strain relation (Eq. (3.16)) we could in principle obtain the fourth-order elastic constants as originally shown by Nielsen and Martin [79-80]. In this work, however, we shall focus on the method based on the internal energy-strain relation (Eqs. (3.11-3.15)).

To obtain the internal energy, or strain energy at T=0 and with only external force exerted by applying strain, we performed the *ab initio* calculations using the Vienna *ab initio* Simulation package (VASP) developed by the Hafner Research Group at the University of Vienna[84]. VASP uses pseudopotentials or the projector-augmented wave method (PAW) and a plane wave basis set. To obtain lattice parameters that are in better agreement with experimental values, we used the exchange-correlation energy evaluated by local-density approximation (LDA) for Ag and Au; for Al we used generalized gradient approximation (GGA) of PW91 type. Ultrasoft pseudopotentials[50] were employed to describe the electron-ion interactions for Al, Ag and Au, while projector-augmented wave method was employed for Cu, with Perdew-Burke-Ernzerhof GGA functional. Since high accuracy is needed to evaluate the FOECs, we used the k-point mesh ranging from $24\times24\times24$ to $30\times30\times30$ in our calculations following the Monkhost-Pack scheme. As our experience shows, it is sufficient to reach the desired convergence for the total energy, as well as for the fourth order elastic constants. We took the cutoff energy set at $E_{cutoff}^{Ag} = 500$ eV, $E_{cutoff}^{Cu} = 490$ eV, $E_{cutoff}^{Al} = 500$ eV, and $E_{cutoff}^{Au} =$ 450 eV, which as our experience shows are sufficiently large for the total energy to converge to the equilibrium state, and particularly for the fourth order elastic constants to converge well.

Take Cu as an example. Figure 3.1(a) shows the internal energy convergence with the k-points grid size. Starting from $14\times14\times14$ k-points grid, the internal energy is well converged. Figure 3.1(b) is a zoom-in picture of Figure 3.1(a), it shows at the k-point grid size we used of $30\times30\times30$, the internal energy convergence at meV level. Figure 3.2 shows how the selection of the cut-off energy affects the internal energy

convergence. As shown, E_{cutoff}^{Cu} = 490 eV is sufficient. The calculated lattice constant of the FCC Cu at the equilibrium state is shown in Figure 3.3; so we use 3.64 Å as the equilibrium lattice parameter to construct our supercell in the simulation work later on.

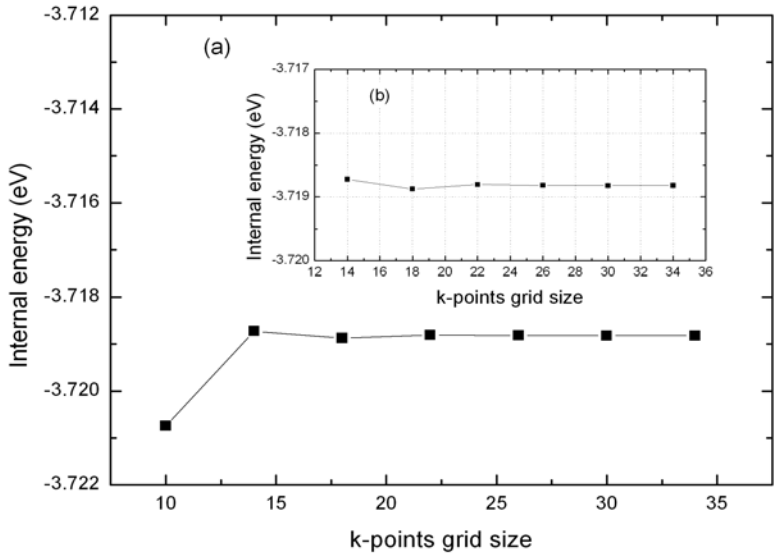

Figure 3.1 (a) The dependence of the first-principles results of internal energy of Cu on the k-points mesh size. The energy converges well when the k-point mesh size goes beyond $14\times14\times14$. **(b)** The inset is the zoom-in picture of the internal energy variation with the k-point mesh size. It shows that the energy converges to meV level at the choice of the k-point mesh size.

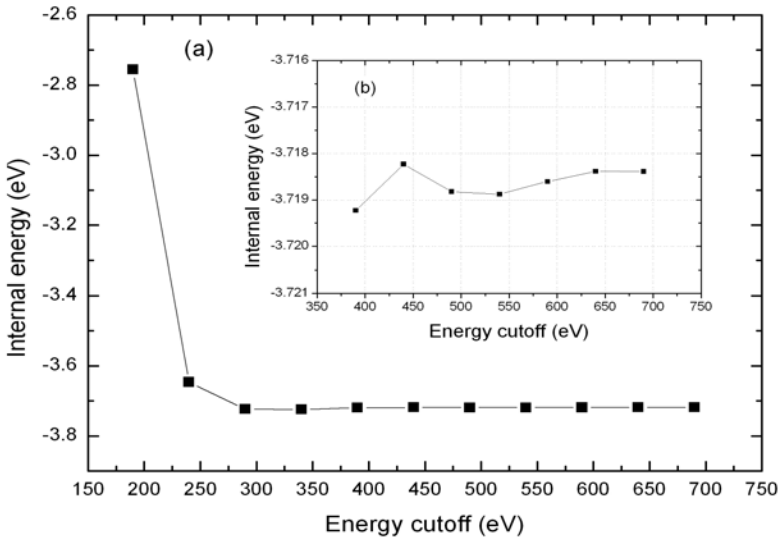

Figure 3.2 (a) The calculated internal energy of Cu as a function of the cutoff energy. **(b)** The inset is the zoom-in picture of the energy that converges within meV level when the cutoff energy is beyond 340 eV. In our calculation, we chose $E_{cutoff}^{Cu} = 490$ eV.

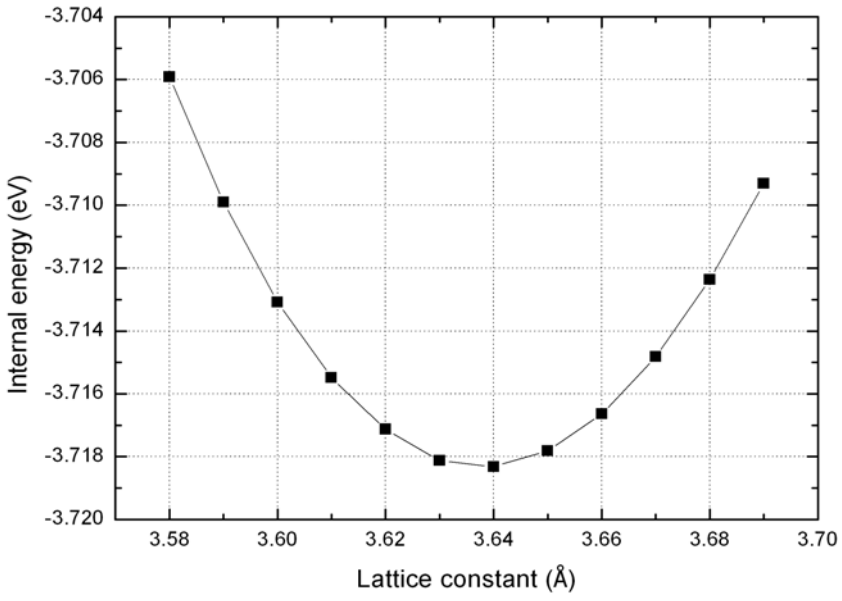

Figure 3.3 In the calculated internal energy of Cu as a function of lattice constant, the equilibrium lattice parameter is found to be 3.64 Å, which is determined from the corresponding minimum value of the internal energy.

The convergence test for the calculated elastic constants of Cu is presented in figure 3.4 and figure 3.5. Those results show us a stronger dependence of the fourth-order elastic constants $C_{1111}, C_{1112}, C_{4444}, C_{1155}$ on the cutoff energy and Monkhost-Pack k-point mesh size as compared with the total energy. From the four samples, it is clear that the FOECs converge rapidly after the k-point mesh size reaches $24\times24\times24$. For the selected parameters ($E_{cutoff}^{Cu} = 490$ eV and $30\times30\times30$ k-point mesh size), the relative difference between the FOECs obtained with this mesh size and with the smaller mesh size of $28\times28\times28$ is less than 1%. This difference is less than the standard error when we perform polynomial fitting. Therefore, we adopt the following criterion in our selection of the k-point mesh size: in the converging region, if the difference of FOECs calculated with two successive k-point mesh sizes are within 1%, we shall pick the later as our choice. The same principle applies to cutoff energy selection. This approach allows us to save considerable amount of computing time.

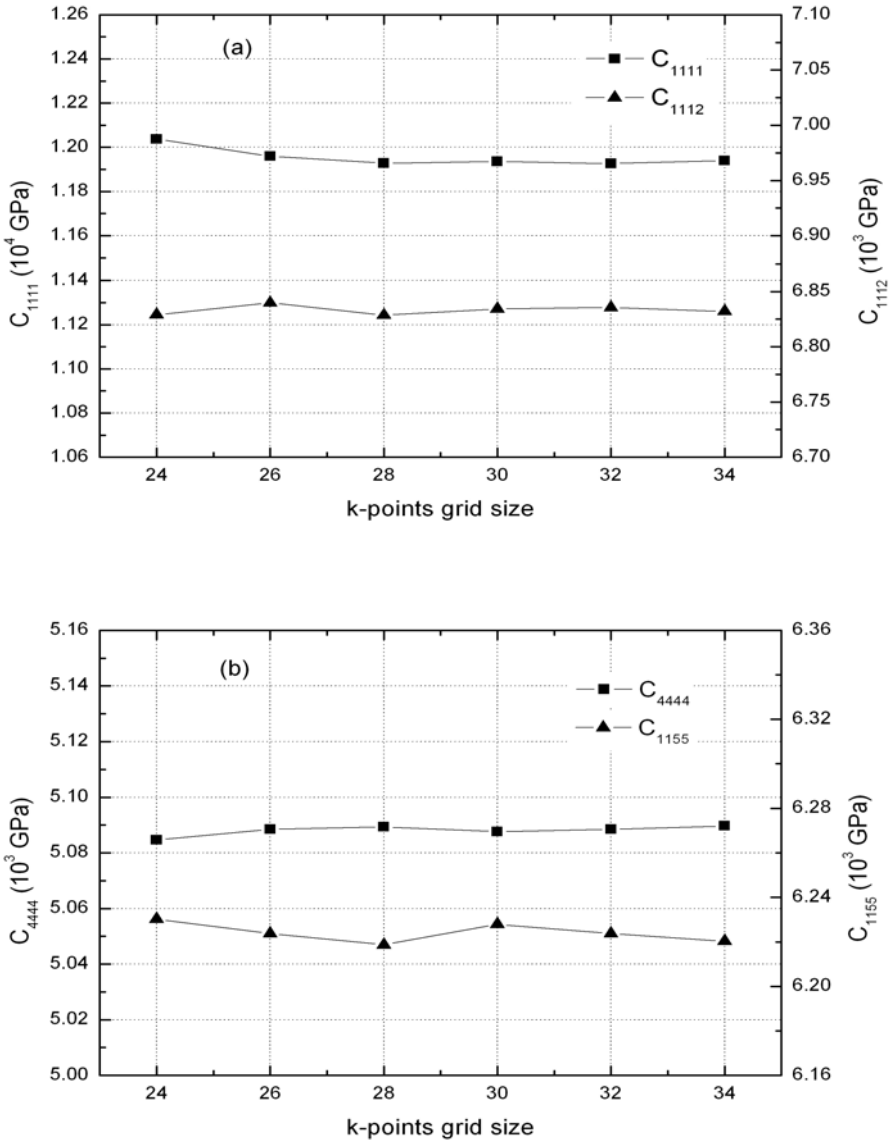

Figure 3.4 The dependence of four fourth-order elastic constants $C_{1111}, C_{1112}, C_{4444}, C_{1155}$ on the Monkhost-Pack k-point mesh size. With $E_{cutoff}^{Cu} = 490$ eV applied to all points, the relative difference between two successive values of examined constants in our test after $24 \times 24 \times 24$ is lower than 1%.

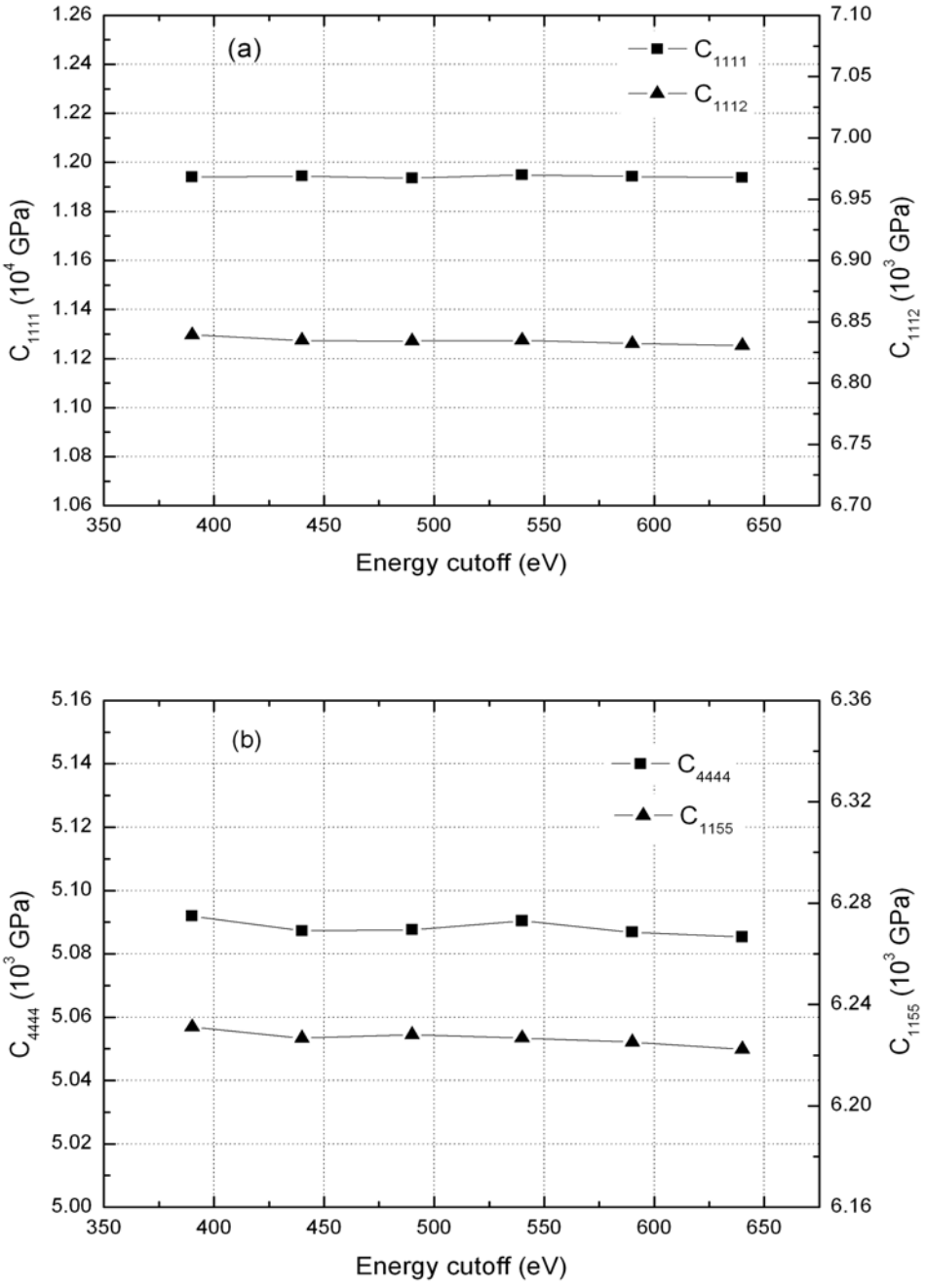

Figure 3.5 The dependence of four fourth-order elastic constants $C_{1111}, C_{1112}, C_{4444}, C_{1155}$ on the cutoff energy. With $30\times30\times30$ k-point mesh size applied to all points, the relative difference between two successive values of examined constants in our test is lower than 1%.

Table 3.2 The calculated and experimentally determined lattice constants for Cu, Al, Au, and Ag. The unit is Å.

	This work	Experiment
Cu	3.64	3.62 [a]
Al	4.04	4.05 [b]
Au	4.07	4.08 [a]
Ag	4.02	4.09 [a]

[a] Ref. 85 (T=25 ℃).
[b] Ref. 85 (T=24.8 ℃).

The lattice constants we obtained for Cu, Au, Al, and Ag are very close to the experimental measurements[85], the results are listed in table 3.2. Ag has a relatively larger deviation as compared with other metals in this group. As seen below, this larger error for Ag in the lattice constant may also be the reason that the elastic constants calculated show larger differences as compared with the reference data. In addition, we would like to mention that since our calculation is performed at 0 K and the experimental values are measured at room temperature, certain differences in the lattice constants and elastic

constants should be anticipated. Based on those calculated lattice constants, we prepared supercells to calculate energy-strain curves. The deformation is implemented for each supercell using the deformation gradient from Eq. (3.19) in the incremental fashion governed by the two parameters $\xi_{\max}$ and $\Delta\xi$.

3.4 Results

Table 3.3 shows all elastic constants up to the fourth-order ones calculated using the above methods. By inspecting the data in table 3.3(a), it becomes obvious that the values of the SOECs (c_{11}, c_{12}, and c_{44} in table 3.3(a)) are the best in agreement with the experimental ones. The differences are well within 5% for Cu, Au, and Al, but a large deviation around 20% is found for all three SOECs for Ag, which may share the same origin as that in the lattice constant calculated. Nevertheless, the excellent overall agreement of the SOECs provides the support for the approaches used in this work, which appears more feasible as compared with other *ab initio* calculations[86].

As compared with the SOECs, the TOECs are much difficult to measure experimentally. As a result, only a small number of FCC metals have a full set of TOECs available that include Cu, Au, Al, and Ag[73, 87-90]. By inspecting the data in table 3.3(b), we see that the overall agreement between our calculated TOECs for all FCC metals listed and the existing experimental values is very good. For Cu and Al, we tabulated three sets of experimental data, one at 4.2 K for Cu, one at 80 K for Al, and two at RT for both metals. We see that our *ab initio* calculation captures both the signs and the magnitude of the TOECs very well. A small positive C_{456} for Cu and C_{123} for Al are reproduced well; and both C_{111} and C_{112} agree with experimental values very well,

especially for Al. For Au, the opposite sign was found for C_{456}, which we suspect is caused by the temperature effects, as seen for Cu, since the experimental value is at RT while our calculation is at 0 K. A set of TOECs for Cu from a total energy calculation by Soma and Hiki is listed also in table 3.3 for comparison.

The discrepancies found in the TOECs could be originated from many sources in experiments as well as in our calculations. For experimental measurement, as noted by Hiki and Granato[91], dislocations could be easily generated when the samples are under external loading during measurement since pure single crystals have relatively low yield stress. The dislocations would cause interference in the ultrasound waves, leading to errors. For this reason, those higher order elastic constants (C_{144}, C_{155}, C_{456}, etc.) that involves shear would have much larger uncertainties. In *ab initio* calculation, as noted in the work of Zhao *et al.*,[32] the strain range $\xi_{\max}$ is an important parameter affecting the accuracy of the elastic constants. This is understandable as the nonlinear elastic constants become significant only when the strains are larger. Another parameter is the strain incremental value, $\Delta\xi$. Too large a value could lead to systematic errors.

For the above reasons, the FOECs are much difficult to obtain in our calculations. To get converging values for them, besides the large k-point mesh size and energy cutoffs, we need a larger strain range $\xi_{\max}$. As for Cu, for example, C_{1111} converges only after $\xi_{\max} \sim 0.15$ (see figure 3.6). The reason comes from that, at small strain range, ψ_4 is much less than ψ_2 and ψ_3 as well. Thus, if the magnitude of $\xi_{\max}$ is not sufficiently large, large fitting errors will appear, resulting mainly from the fitted coefficient of ψ_4. This situation will be improved when those errors are not comparable with the value of

ψ_4 with a larger strain. From different testing runs, we found that $\xi_{\max} \sim 0.15$ is a best choice that was used in all our calculations of the internal energy function $f_A(\xi)$. With this choice, we select a series of values for ξ within [-0.15, +0.15] at each strain increment $\Delta\xi$=0.0025 and then calculate the internal energy E at a given strain ξ. The small value for $\Delta\xi$ may prolong the calculations but gives better results.

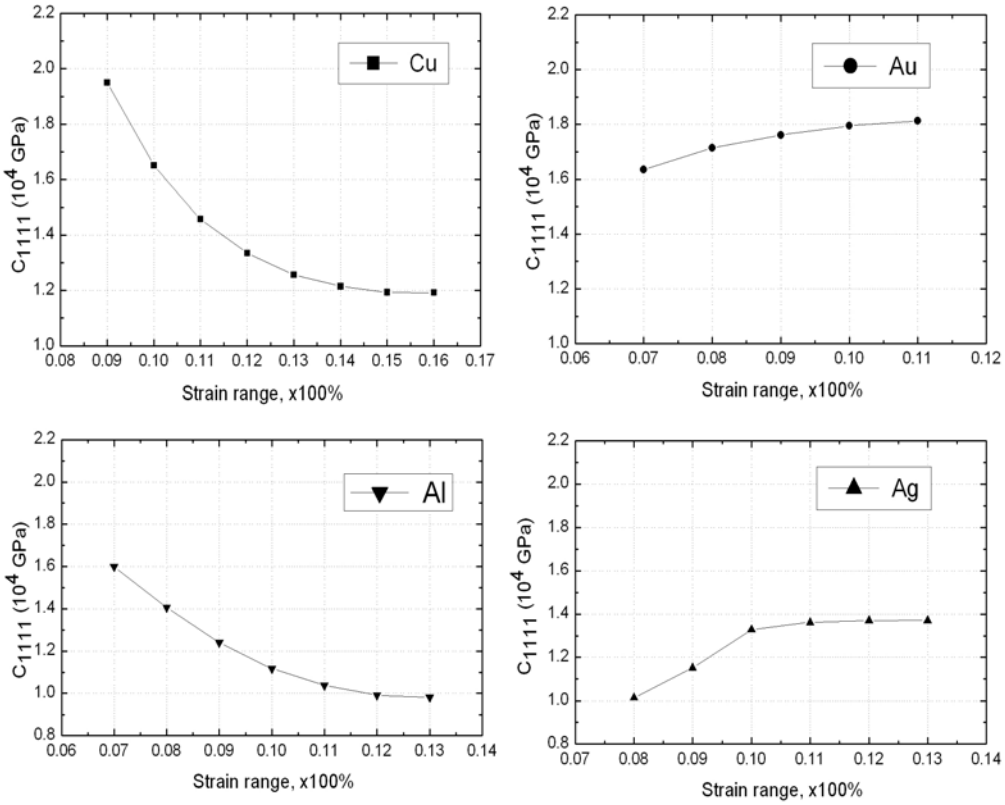

Figure 3.6 (a) Cu, **(b)** Au, **(c)** Al, and **(d)** Ag, the fourth-order elastic constants C_{1111} vs the strain range $\xi_{\max}$. Only at large enough strain range do those elastic constants become convergent. For Cu, Au, Al and Ag, we selected a strain range of 0.15, 0.10, 0.12, and 0.12 respectively.

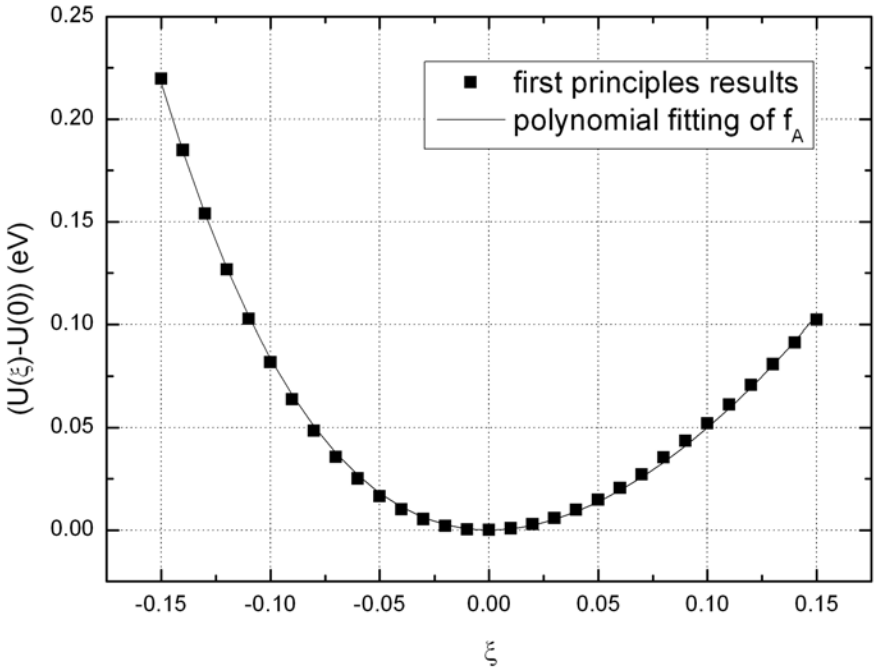

Figure 3.7 The calculated change in internal energy as a function of strain for the strain tensor defined in table 3.1, η_A, and fitted by a fourth-order polynomial function.

The $E-\xi$ curves of $f_A(\xi)$ are shown in figure 3.7. The relations between E and ξ are fitted with a fourth-order polynomial and the coefficients in the polynomials are obtained numerically. Using relations in table 3.1, we obtain the elastic constants. The calculated FOECs are shown in table 3.3(c). Since there is no single set of FOECs known experimentally so far, the accuracy of the FOECs is difficult to judge without a reference. The values listed in table 3.3(c) are from other theoretical calculations[88-90]. For this reason, we shall treat our calculation as an attempt to predict the FOECs from *ab initio* calculations. Cu is the only case where we have a complete set of FOECs from Hiki and Soma[88] who calculated all 11 independent FOECs from an approximate scheme of total energy and the homogeneous deformation method. For other FCC metals, various

approximations including using empirical pair potentials and Cauchy relations were made in the calculations. As a result, the independent FOECs are further reduced. We listed some of these results in table 3.3(c) for comparison.

Table 3.3 The calculated **(a)** second-, **(b)** third-, and **(c)** fourth-order elastic constants of Cu, Ag, Au, and Al. Experimental results and other theoretical calculations are also shown. The unit is in GPa.

(a)

	C_{11}	C_{12}	C_{44}
Cu	167.8 [a]	113.5 [a]	74.5 [a]
	169 [b]	122 [b]	75.3 [b]
Al	110.4 [a]	54.5 [a]	31.3 [a]
	108 [c]	62 [c]	28.3 [c]
Au	202.1 [b]	174.2 [b]	37.9 [b]
	191 [d]	162 [d]	42.2 [d]
Ag	161.2 [a]	119.1 [a]	58.1 [a]
	122 [e]	92 [e]	45.5 [e]

[a] This work.
[b,c,d,e] Ref. 73.

(b)

	C_{111}	C_{112}	C_{123}	C_{144}	C_{155}	C_{456}
Cu	-1 507 [a]	-965 [a]	-71 [a]	-7 [a]	-901 [a]	45 [a]
	-1 271 [b]	-814 [b]	-50 [b]	-3 [b]	-780 [b]	-95 [b]
	-1 500 [c]	-850 [c]	-250 [c]	-135 [c]	-645 [c]	-16 [c]
	-2 000 [d]	-1 220 [d]	-500 [d]	-132 [d]	-705 [d]	25 [d]
	-1 190 [e]	-646 [e]	219 [e]	17 [e]	-800 [e]	1 [e]
Al	-1 253 [a]	-426 [a]	153 [a]	-12 [a]	-493 [a]	-21 [a]
	-1 080 [f]	-315 [f]	36 [f]	-23 [f]	-340 [f]	-30 [f]
	-1 224 [g]	-373 [g]	25 [g]	-64 [g]	-368 [g]	-27 [g]
	-1 427 [h]	-408 [h]	32 [h]	-85 [h]	-396 [h]	-42 [h]
Au	-2 023 [a]	-1266 [a]	-263 [a]	-63 [a]	-930 [a]	54 [a]
	-1 730 [b]	-922 [b]	-233 [b]	-13 [b]	-648 [b]	-12 [b]
Ag	-1 012 [a]	-975 [a]	162 [a]	80 [a]	-759 [a]	53 [a]
	-843 [b]	-529 [b]	189 [b]	56 [b]	-637 [b]	83 [b]

[a] This work.

[b,c] At 290 and 300K from Ref. 73, 87, 88.

[d] At 4.2 K from Ref. 87.

[e] From a total energy calculation, Ref. 88.

[f,g] At 300K and 298K from Ref. 73, 89.

[h] At 80K from Ref. 73.

(c)

	C_{1111}	C_{1112}	C_{1122}	C_{1123}	C_{1144}	C_{1155}	C_{1244}	C_{1266}	C_{1456}	C_{4444}	C_{4455}
Cu	11 936 [a]	6 834 [a]	6 602 [a]	-98 [a]	135 [a]	6 628 [a]	-308 [a]	5 736 [a]	-417 [a]	5 088 [a]	-191 [a]
	9 587 [b]	6 052 [b]	6 623 [b]	56 [b]	-287 [b]	8 701 [b]	-390 [b]	4 100 [b]	-43 [b]	6 527 [b]	-404 [b]
	7 449 [c]	4 233 [c]	4 756 [c]	-262 [c]	-262 [c]	4 233 [c]	-262 [c]	4 756 [c]	-262 [c]	4 756 [c]	-262 [c]
	10 100 [d]	5 050 [d]	5 050 [d]	0 [d]	0 [d]	5 050 [d]	0 [d]	5 050 [d]	0 [d]	5 050 [d]	0 [d]
Al	9 916 [a]	2 656 [a]	3 708 [a]	-1 000 [a]	-578 [a]	3 554 [a]	-91 [a]	4 309 [a]	148 [a]	3 329 [a]	127 [a]
	3 900 [c]	2 173 [c]	2 471 [c]	-146 [c]	-146 [c]	2 173 [c]	-146 [c]	2 471 [c]	-146 [c]	2 471 [c]	-146 [c]
Au	17 951 [a]	8 729 [a]	9 033 [a]	416 [a]	691 [a]	7 774 [a]	-752 [a]	9 402 [a]	-170 [a]	8 352 [a]	15 [a]
	10 300 [d]	5 150 [d]	5 150 [d]	0 [d]	0 [d]	5 150 [d]	0 [d]	5 150 [d]	0 [d]	5 150 [d]	0 [d]
Ag	13 694 [a]	7 115 [a]	6 652 [a]	-387 [a]	-154 [a]	5 295 [a]	3 [a]	6 718 [a]	-196 [a]	5 416 [a]	-75 [a]
	5 780 [c]	3 495 [c]	3 818 [c]	-172 [c]	-172 [c]	3 495 [c]	-172 [c]	3 818 [c]	-172 [c]	3 818 [c]	-172 [c]
	8 000 [d]	4 000 [d]	4 000 [d]	0 [d]	0 [d]	4 000 [d]	0 [d]	4 000 [d]	0 [d]	4 000 [d]	0 [d]

[a] This work.

[b] Ref. 88.

[c] Ref. 89, assuming the validity of Eq. (3.21).

[d] Ref. 90, assuming the validity of Eq. (3.22).

From the observation of the elastic constants measured from their experiment, Hiki and Granato pointed out that while the SOECs deviate from the so-called Cauchy relations much more, the TOECs follow them more closely,

$$\begin{aligned} &C_{111} = 2C_{112} = 2C_{155}, \\ &C_{123} = C_{456} = C_{144} = 0. \end{aligned} \tag{3.20}$$

In fact, our results show that indeed the SOECs are far from the Cauchy relation but the TOECs are closer.

Hiki and Granato further expected that the higher order elastic constants would follow the relation even more closely based on the argument that as the deformation strains become larger, the close shell interactions between atoms become stronger. For Al, Rose[89] used the Cauchy relationship to estimate the FOECs,

$$\begin{aligned} &C_{1112} = C_{1155}, \\ &C_{1123} = C_{1144} = C_{1255} = C_{1456} = C_{4455}, \\ &C_{1122} = C_{1266} = C_{4444}. \end{aligned} \tag{3.21}$$

As a result, only 4 independent fourth-order elastic constants are left (see table 3.3(c)). Those four independent elastic constants were then obtained using an empirical pair interaction. As for Au and Ag, Hiki *et al*[90] utilized the generalized Cauchy relationship to obtain the following relations among some of the FOECs,

$$\begin{aligned} &C_{1111} = 2C_{1112} = 2C_{1122} = 2C_{1155} = 2C_{1266} = 2C_{4444}, \\ &C_{1123} = C_{1144} = C_{1255} = C_{1456} = C_{4455} = 0, \end{aligned} \tag{3.22}$$

which obviously leads to even more reduction in the number of FOECs.

Our results for both the TOECs and FOECs show that indeed, the Cauchy relations are followed, more for FOECs than TOECs, given the possible errors in our calculations. For example, for the FOECs for Cu, we have $C_{1111}/C_{1112}=1.75$, which is very close to the ratios for C_{1111}/C_{1122} and C_{1111}/C_{1155}. And C_{1111}/C_{1266} and C_{1111}/C_{4444} are close to 2.0. The values of C_{1123}, C_{1144}, C_{1255} C_{1456}, and C_{4455} are very small as compared with the rest of the FOECs. The same trend can be found for the rest of FCC metals.

3.5 Conclusions

In this work, we represented a systematic scheme to compute the second- and high-order elastic constants for four FCC metals using the DFT and homogeneous deformation method. In principle, this scheme can apply to single crystalline systems with arbitrary symmetry. Our theoretical results are in excellent agreement with experimental results for the SOECs which are available from many measurements. For the TOECs, the agreement with the available experimental data is very well considering the sparsity of the experimental data and also the errors resulting from the difficulties in the measurements. Built on the results from the SOECs and TOECs, we took a further step forward to calculate the FOECs. While the experimental data are still not available for those metals, our results are quite well inline with other theoretical calculations and estimates. Our results in the higher order elastic constants also provide support for Hiki and Granato's expectation that as the atomic repulsion becomes stronger at large deformation strain, the higher order elastic constants would follow more closely the Cauchy relations. Since there are fewer experimental data available for TOECs and none

for FOECs even to date, we would like to treat our results of the FOECs as the first predicted values from *ab initio* calculations, which may serve as a valuable guide or reference for experimenters who would someday perform a measurement. On the other hand, we are quite encouraged by the overall results as a proof of the applicability of the DFT calculation for such highly sensitive quantities as the TOECs and the FOECs.

CHAPTER FOUR

NONLINEAR STRESS-STRAIN RELATIONS OF CRYSTAL SOLIDS WITH ARBITRARY INITIAL CONFIGURATIONS

4.1 Introduction

Stress-strain response curves are a fundamental description of a material's mechanic properties. In the linear elastic theory of crystal[22], the second-order elastic stiffness tensors $B_{ijkl}'s$ are employed to describe the stress-strain relations when infinitesimal deformation strains are assumed. For example, given a face-centered cubic crystal under external pressure P, when a shear strain η_4 is applied to the crystal, the stress-strain relation is: $\tau_4 = B_{44}\eta_4 = (C_{44} - P)\eta_4$. Here C_{44} is an elastic constant of the crystal under pressure P, and Voigt notation is used. In case of finite strains, nonlinear relations are required to describe the response of stress with respect to strain. As shown by Barsch[92], for crystals with the $A15$ structure under uniaxial compression along the c-axis, the nonlinear stress-strain relation was derived using second-, third-, and fourth-order elastic constants, and then the results were compared with the experimental data; fair agreement was observed. In that work, the crystal sample V_3Si was initialized at a stress-free state. They used elastic constants, $C_{ijkl}'s$, $C_{ijklmn}'s$, and $C_{ijklmnpq}'s$. However, generally speaking, for crystal solids with arbitrary initial states, its nonlinear stress-strain relations are more complicated. We need second-order and higher order elastic stiffness tensors. This problem is still open in both experimental and theoretical fields.

In this chapter, we present an analytic derivation of nonlinear stress-strain formula for crystal solids with arbitrary initial configurations, and then test it to face-centered cubic gold under hydrostatic stress with *ab initio* calculations. Our derivation is involved with second-, third-, and fourth-order elastic stiffness tensors. Previously we developed a general scheme to calculate second-, third-, and fourth-order elastic constants for single crystals[93]. This method enables us to obtain the nonlinear stress-strain relations numerically.

This chapter is organized as follows. In Sec. 4.2, we review the formulation of the linear stress-strain relations, as well as elastic stiffness tensor. In Sec. 4.3, we present our derivation of nonlinear stress-strain relations. In Sec. 4.4, we test the nonlinear relations to a face-centered cubic crystal Au under hydrostatic stress. We shall elaborate on the method we use to obtain the shear stress-strain curves with both theoretical derivation and *ab initio* calculation. In Sec. 4.5, we show and discuss the results. In Sec. 4.6, we draw conclusions from our work.

4.2 Linear stress-strain relations

Given a crystal solid, $\overline{X}$ and X represent its two configurations. There is only symmetric strain, i.e., no rotations, from $\overline{X}$ to X . The transformation coefficients from $\overline{X}$ to X are given as a_{ij} [22],

$$a_{ij} = a_{ji} = (\partial X_i / \partial \overline{X}_j), \tag{4.1}$$

and the corresponding Lagrangian strain parameters are n_{ij} ,

$$n_{ij} = \frac{1}{2}(\sum_k a_{ki} a_{kj} - \delta_{ij}). \tag{4.2}$$

Inversion of Eq. (4.2) as a power series in n_{ij} gives

$$a_{ij} = \delta_{ij} + n_{ij} - \frac{1}{2}\sum_k n_{ki} n_{kj} + \cdots. \tag{4.3}$$

The ratio of the crystal volumes in the two configurations is,

$$V / \overline{V} = \det[a_{ij}] = 1 + \sum_i n_{ii} + \cdots. \tag{4.4}$$

Let the Lagrangian strains from $\overline{X}$ to an arbitrary final configuration x be $\overline{\eta}_{ij}$, and those from X to x be η_{ij}, it follows that,

$$(\partial \overline{\eta}_{ij} / \partial \eta_{rs})_{\eta'} = a_{ri} a_{sj}. \tag{4.5}$$

Here the subscript η' means that all other η_{kl} are to be held constant while differentiating with respect to η_{rs}. The state functions *U* and *F* may be expanded in powers of the strains,

$$U(X, \eta_{ij}, S) = U(X, 0, S) + V\sum_{ij} \tau_{ij}\eta_{ij} + (1/2!)V\sum_{ijkl} C^S_{ijkl}\eta_{ij}\eta_{kl} + \cdots, \tag{4.6}$$

$$F(X, \eta_{ij}, T) = F(X, 0, T) + V\sum_{ij} \tau_{ij}\eta_{ij} + (1/2!)V\sum_{ijkl} C^T_{ijkl}\eta_{ij}\eta_{kl} + \cdots. \tag{4.7}$$

Suppose the strain from $\overline{X}$ to X is carried out adiabatically, $\tau_{ij} - \overline{\tau}_{ij}$ may be calculated as follows,

$$\tau_{ij} = V^{-1}(\partial U / \partial \eta_{ij})_{S\eta'}, \text{ at } X; \tag{4.8}$$

and then,

$$\tau_{ij} = \overline{V}^{-1}(\overline{V}/V)\sum_{kl} (\partial U / \partial \overline{\eta}_{kl})_{S\overline{\eta}'} (\partial \overline{\eta}_{kl} / \partial \eta_{ij})_{\eta'}, \tag{4.9}$$

and from the strain expansion of U, Eq. (4.6), and Eq. (4.5) for $(\partial\bar{\eta}_{kl}/\partial\eta_{ij})_{\eta'}$,

$$\tau_{ij} = (\bar{V}/V)\sum_{kl} a_{ik}a_{jl}\left\{\bar{\tau}_{kl} + \sum_{mn}\bar{C}^{S}_{klmn}n_{mn} + \cdots\right\}, \tag{4.10}$$

where the strain n_{mn} is a result of evaluation at configuration X. With Eq. (4.4) for $V/\bar{V}$ and Eq. (4.3) for a_{ij}, Eq. (4.10) may evolve to first order in the strain n_{ij} from $\bar{X}$ to X,

$$\tau_{ij} = \bar{\tau}_{ij} + \sum_{kl} n_{kl}[-\bar{\tau}_{ij}\delta_{kl} + \bar{\tau}_{il}\delta_{jk} + \bar{\tau}_{jk}\delta_{il} + \bar{C}^{S}_{ijkl}]. \tag{4.11}$$

Eq. (4.11) is the expected linear relation between the variation of stress and strain, to first order in the strains and for adiabatic processes. The results can be summarized in terms of the stress-strain coefficients B_{ijkl}'s. For adiabatic strains,

$$\tau_{ij}(x,S) = \tau_{ij}(X,S) + \sum_{kl} B^{S}_{ijkl}\eta_{kl} + \cdots, \tag{4.12}$$

and for isothermal strains

$$\tau_{ij}(x,T) = \tau_{ij}(X,T) + \sum_{kl} B^{T}_{ijkl}\eta_{kl} + \cdots, \tag{4.13}$$

where

$$B^{S}_{ijkl} = C^{S}_{ijkl} + (1/2)(\delta_{ik}\tau_{jl} + \delta_{jk}\tau_{il} + \delta_{il}\tau_{jk} + \delta_{jl}\tau_{ik} - 2\delta_{kl}\tau_{ij}), \tag{4.14}$$

$$B^{T}_{ijkl} = C^{T}_{ijkl} + (1/2)(\delta_{ik}\tau_{jl} + \delta_{jk}\tau_{il} + \delta_{il}\tau_{jk} + \delta_{jl}\tau_{ik} - 2\delta_{kl}\tau_{ij}). \tag{4.15}$$

In Eqs. (4.12-4.13) the B_{ijkl}'s are evaluated at X. Since k and l are summed in Eq. (4.11), k and l are interchanged in the quantity in brackets in Eq. (4.11) to obtain the symmetric forms shown in Eqs. (4.14-4.15).

4.3 Derivation of nonlinear stress-strain relations

In order to obtain the stress-strain relations beyond linear equations (4.14-4.15), First we will prepare some useful equations. Eq. (4.3) is developed to be,

$$a_{ij} = \delta_{ij} + n_{ij} - \frac{1}{2}\sum_{k} n_{ki}n_{kj} + \frac{1}{2}\sum_{mn} n_{im}n_{mn}n_{nj} + \cdots. \tag{4.16}$$

And Eq. (4.4) is replaced by,

$$V/\overline{V} = 1 + n_{\alpha\alpha} + \frac{1}{2}(\delta_{\alpha\beta}\delta_{\sigma\tau} - \delta_{\alpha\sigma}\delta_{\beta\tau} - \delta_{\alpha\tau}\delta_{\beta\sigma})n_{\alpha\beta}n_{\sigma\tau} + \cdots. \tag{4.17}$$

where we use the Einstein summation convention, implying a sum over repeated indices. Or we may use another type of relation,

$$V/\overline{V} = (1 + 2I_1 + 4I_2 + 8I_3)^{1/2}, \tag{4.18}$$

where I_1, I_2, and I_3 are the three invariants of the Lagrangian strain tensor,

$$\begin{aligned} I_1 &= n_{ii}, \\ I_2 &= \frac{1}{2}(n_{ii}n_{jj} - n_{ij}n_{ij}), \\ I_3 &= \frac{1}{6}(n_{ii}n_{jj}n_{kk} - 3n_{ij}n_{ij}n_{kk} + 2n_{ij}n_{jk}n_{ki}). \end{aligned} \tag{4.19}$$

Eq. (4.6) is re-written as,

$$\begin{aligned} U(X,\eta_{ij},S) = U(X,0,S) + V\sum_{ij}\tau_{ij}\eta_{ij} + (1/2!)V\sum_{ijkl}C^{S}_{ijkl}\eta_{ij}\eta_{kl} + \\ (1/3!)V\sum_{ijklmn}C^{S}_{ijklmn}\eta_{ij}\eta_{kl}\eta_{mn} + (1/4!)V\sum_{ijklmnpq}C^{S}_{ijklmnpq}\eta_{ij}\eta_{kl}\eta_{mn}\eta_{pq} + \cdots. \end{aligned} \tag{4.20}$$

In the following we do not distinguish C^S and C^T. With the help of Eq. (4.20), Eq. (4.10) becomes,

$$\tau_{ij} = (\overline{V}/V)\sum_{kl} a_{ik}a_{jl}\left\{\begin{array}{l} \overline{\tau}_{kl} + \sum_{mn}\overline{C}_{klmn}n_{mn} + (1/2)V\sum_{mnpq}\overline{C}_{klmnpq}n_{mn}n_{pq} + \\ (1/3)V\sum_{mnpqrs}\overline{C}_{mnpqrs}n_{mn}n_{pq}n_{rs} + \cdots \end{array}\right\}, \tag{4.21}$$

and then when we use Eq. (4.16) for a_{ij} and Eq. (4.18-4.19) for $V/\overline{V}$, Eq. (4.21) will evolve into,

$$\tau_{ij} = \bar{\tau}_{ij} + \psi_1 + \psi_2 + \psi_3 + ..., \tag{4.22}$$

where

$$\psi_1 = \sum_{kl} n_{kl}[-\bar{\tau}_{ij}\delta_{kl} + \bar{\tau}_{il}\delta_{jk} + \bar{\tau}_{jk}\delta_{il} + \overline{C}_{ijkl}], \tag{4.23}$$

$$\begin{aligned}\psi_2 = & \sum_{klmn} n_{kl}n_{mn}\left(\delta_{jn}\delta_{il}\bar{\tau}_{km} - \delta_{mn}\delta_{kj}\bar{\tau}_{il} - \delta_{mn}\delta_{il}\bar{\tau}_{kj} + \overline{C}_{ilmn}\delta_{jk} + \overline{C}_{kjmn}\delta_{il} - \overline{C}_{klmn}\delta_{kl} + \overline{C}_{ijklmn}\right) \\ & + \sum_{kr}\left(-\frac{1}{2}n_{ri}n_{rk}\right)\bar{\tau}_{jk} + \sum_{ls}\left(-\frac{1}{2}n_{sj}n_{sl}\right)\bar{\tau}_{il} + \left(\frac{3}{2}I_1^2 - 2I_2\right)\bar{\tau}_{ij},\end{aligned} \tag{4.24}$$

$$\begin{aligned}\psi_3 = & \left(6I_1I_2 - 4I_3 - \frac{5}{2}I_1^3\right)\bar{\tau}_{ij} + \sum_{klmn}\frac{1}{2}\left(n_{im}n_{mn}n_{nk}\delta_{jl} + n_{jm}n_{mn}n_{nl}\delta_{ik}\right)\bar{\tau}_{kl} \\ & + \frac{1}{6}\sum_{mnpqrs}\overline{C}_{ijmnpqrs}n_{mn}n_{pq}n_{rs} + \left(\frac{3}{2}I_1^2 - 2I_2\right)\left[\sum_{kl}\left(n_{ik}\delta_{jl} + n_{jl}\delta_{ik}\right)\bar{\tau}_{kl} + \sum_{mn}\overline{C}_{ijmn}n_{mn}\right] \\ & + \sum_{klr}\left(-\frac{1}{2}n_{ri}n_{rk}\right)\left(-I_1\delta_{jl}\bar{\tau}_{kl} + n_{jl}\bar{\tau}_{kl} + \delta_{jl}\sum_{mn}\overline{C}_{klmn}n_{mn}\right) \\ & + \sum_{kls}\left(-\frac{1}{2}n_{sj}n_{sl}\right)\left(-I_1\delta_{ik}\bar{\tau}_{kl} + n_{ik}\bar{\tau}_{kl} + \delta_{ik}\sum_{mn}\overline{C}_{klmn}n_{mn}\right) \\ & + \frac{1}{2}\sum_{klmnpq}\overline{C}_{klmnpq}n_{mn}n_{pq}\left(-I_1\delta_{ik}\delta_{jl} + \delta_{ik}n_{jl} + \delta_{jl}n_{ik}\right) \\ & - I_1\left(\sum_{kl}n_{ik}n_{jl}\bar{\tau}_{kl} + \sum_{klmn}\delta_{ik}n_{jl}n_{mn}\overline{C}_{klmn} + \sum_{klmn}\delta_{jl}n_{ik}n_{mn}\overline{C}_{klmn}\right) \\ & + \sum_{klmn}n_{ik}n_{jl}n_{mn}\overline{C}_{klmn}.\end{aligned} \tag{4.25}$$

Considering Eq. (4.23-4.25), for those terms where subscripts k and l, m and n are summed, a symmetric form needs to be derived further in the same way we obtain Eq. (4.15).

4.4 Test the nonlinear stress-strain relations to gold

4.4.1 Nonlinear shear stress-strain equations of gold under hydrostatic stress

Face-centered cubic gold under hydrostatic stress is a good example to test the nonlinear stress-strain equations we derive in section 4.3. We name the initial state configuration $\overline{X}$, and we have, $\bar{\tau}_1 = \bar{\tau}_2 = \bar{\tau}_3$, $\bar{\tau}_4 = \bar{\tau}_5 = \bar{\tau}_6 = 0$. Here we simplify the subscript in the tensor by using the Voigt notation ($11 \to 1$, $22 \to 2$, $33 \to 3$, $23 \to 4$, $31 \to 5$, and $12 \to 6$). When a rhombohedral shear strain is applied to the system, $\eta_1' = \eta_2' = \eta_3' = 0$, $\eta_4' = \eta_5' = \eta_6' = 2\zeta$, or

$$\delta\eta' = \begin{pmatrix} 0 & \zeta & \zeta \\ \zeta & 0 & \zeta \\ \zeta & \zeta & 0 \end{pmatrix},$$

using Eqs. (4.22-4.25) with their symmetric forms, we will have,

$$\tau_4 = \psi_1 + \psi_2 + \psi_3 + ..., \tag{4.26}$$

$$\psi_1 = (\overline{C}_{44} - P)\eta_4', \tag{4.27}$$

$$\psi_2 = (\overline{C}_{456} + \overline{C}_{44})\eta_4'^2, \tag{4.28}$$

$$\psi_3 = (\frac{1}{6}\overline{C}_{4444} + \overline{C}_{4455} + \frac{1}{2}\overline{C}_{456} + \frac{3}{2}\overline{C}_{44} - \frac{3}{2}P)\eta_4'^3, \tag{4.29}$$

where $P = -\bar{\tau}_1$, following the convention that the inward pressure is positive while outward stress is negative (i.e., $P < 0$ for tension). When we use Eq. (4.20), we have,

$$\delta U = \overline{C}_{44}\eta_4'^2 + \overline{C}_{456}\eta_4'^3 + (\overline{C}_{4444}/6 + \overline{C}_{4455})\eta_4'^4 + \cdots. \tag{4.30}$$

To identify the nonlinear Eq. (4.26), we need to obtain the values of $\overline{C}_{44}$, $\overline{C}_{456}$, and $\overline{C}_{4444}/6 + \overline{C}_{4455}$ through the relation (4.30) and *ab initio* calculations.

4.4.2 An *ab initio* calculation of the rhombohedral shear stress-strain curves

To perform *ab initio* simulation, we first calculate the properties (total energy and equilibrium lattice parameter) of a single crystal Au in the ground state. We perform the *ab initio* DFT calculations using the Vienna *ab initio* simulation package (VASP) developed by the Hafner Research Group at the University of Vienna. VASP uses pseudopotentials or the projector-augmented wave method and a plane wave basis set. To obtain a lattice parameter that is in better agreement with experimental value, we use the exchange-correlation energy evaluated with the local density approximation (LDA). Ultrasoft pseudopotentials are always employed to describe the electron-ion interactions. We use $24\times24\times24$ k-point mesh in our calculations following the Monkhost-Pack scheme that, as our experience shows, is sufficient to reach the desired convergence of the total energy and elastic constants. We take the cutoff energy set at E_{cutoff}^{Au} = 450 eV, which is sufficiently large for the total energy to converge to the stable equilibrium state. For Au, the ground state has a face-centered cubic structure with the lattice parameter a_0=4.07 Å, very close to experimental measurement 4.08 Å at room temperature. We thus use 4.07 Å as the lattice parameter in our supercell that is a face-centered cubic cell containing 4 atoms to perform the following simulation work. The benefit of using such a supercell is that we can easily apply specific strains to the supercell and read the values of the six components of stress tensor directly from VASP output files.

In the next step, we apply hydrostatic deformation to the crystal supercell via a strain, $\eta_{11}=\eta_{22}=\eta_{33}=\xi$, $\eta_{ij}=0$ for $i\neq j$. We select four different values of ξ: -0.04, -0.02, 0.0, and 0.02. This operation changes the lattice parameter homogeneously. Let a be the lattice constant of the deformed crystal and obviously $a/a_0=\sqrt{1+2\xi}$ from Eqs. (4.1-4.2). This type of deformation amounts to the application of a hydrostatic stress or

pressure. The values of those pressures are obtained from *ab initio* calculation and listed in table 4.1.

Table 4.1 For each crystal configuration of gold with various hydrostatic deformations, $\xi = $ -0.04, -0.02, 0.0, and 0.02, respectively, we have the hydrostatic pressure P, and those elastic constants by *ab initio* calculation and polynomial fitting.

ξ	P (GPa)	$\overline{C}_{44}$ (GPa)	$\overline{C}_{456}$ (GPa)	$\frac{1}{6}\overline{C}_{4444}+\overline{C}_{4455}$ (GPa)
-0.04	32.49	122.3	84	2087
-0.02	13.07	73.1	69	1714
0.0	0	37.9	54	1407
0.02	-9.53	11.5	45	1144

For supercells with various hydrostatic deformations, to explore the rhombohedral stress-strain relations, we apply an additional shear deformation to the supercell,

$$\delta\eta' = \begin{pmatrix} 0 & \zeta & \zeta \\ \zeta & 0 & \zeta \\ \zeta & \zeta & 0 \end{pmatrix},$$

where ζ is the magnitude of the shear strain. We vary the value of ζ from 0 to 0.15 with a finite step size $\Delta\zeta = 0.005$. For each value of ζ, we calculate the total energy and the Hellmann-Feynman stress of the supercell with VASP. The results are shown at figures 4.1 and 4.2.

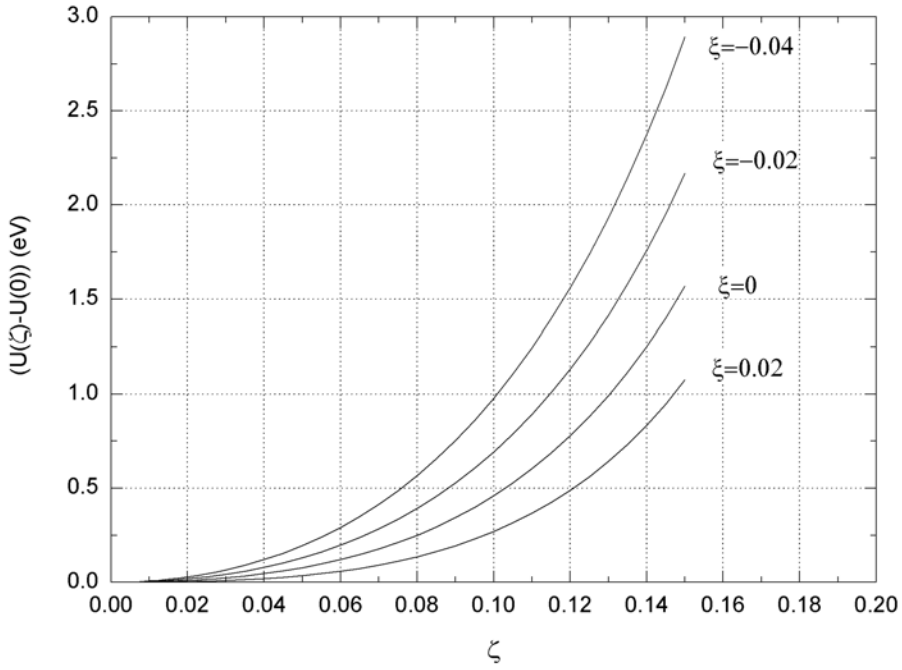

Figure 4.1 For each supercell with various hydrostatic deformations, ξ = -0.04, -0.02, 0.0, and 0.02, respectively, we apply a rhombohedral shear deformation, ζ, to the supercell, and then obtain the variations of total energy with respect to the shear strains.

4.5 Results and discussion

We develop a general scheme to calculate second-, third-, and fourth-order elastic constants for single crystals[93]. We follow that scheme, using Eq. (4.30) and the $\delta U - \zeta$ curves in figure 4.1, where $\zeta = \eta_4^{'} / 2$, and get elastic constants listed at table 4.1 by

polynomial fitting. Then we are able to plot the rhombohedral shear stress-strain curves with Eq. (4.26) and compare them with those in figure 4.2.

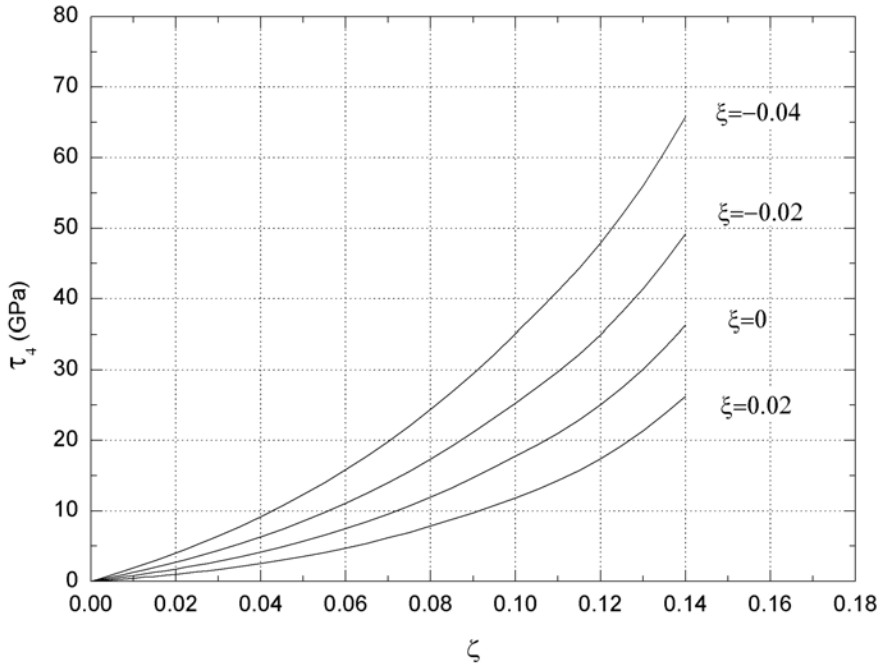

Figure 4.2 For each supercell with various hydrostatic deformations, ξ = -0.04, -0.02, 0.0, and 0.02, respectively, we apply a rhombohedral shear deformation, ζ, to the supercell, and then obtain the variations of shear stress with respect to the shear strains.

We plot the $\tau_4 - \zeta$ curves up to the third power of ζ, marked with A at figure 4.3, where lines marked with B are those curves already shown in figure 4.2, representing the calculated Hellmann-Feynman stresses by VASP. At linear elastic region, with strain up to 2% or 3%, line A and line B agree fairly. At finite strain range, the discrepancy between line A and line B becomes substantial: $\delta\tau_4 / \tau_4 > 10\%$, when the strain is beyond 8%. The discrepancy may be attributed to the polynomial fitting error of

the $\delta U - \zeta$ curves, and also may come from the truncation error in the stress-strain Eq. (4.26).

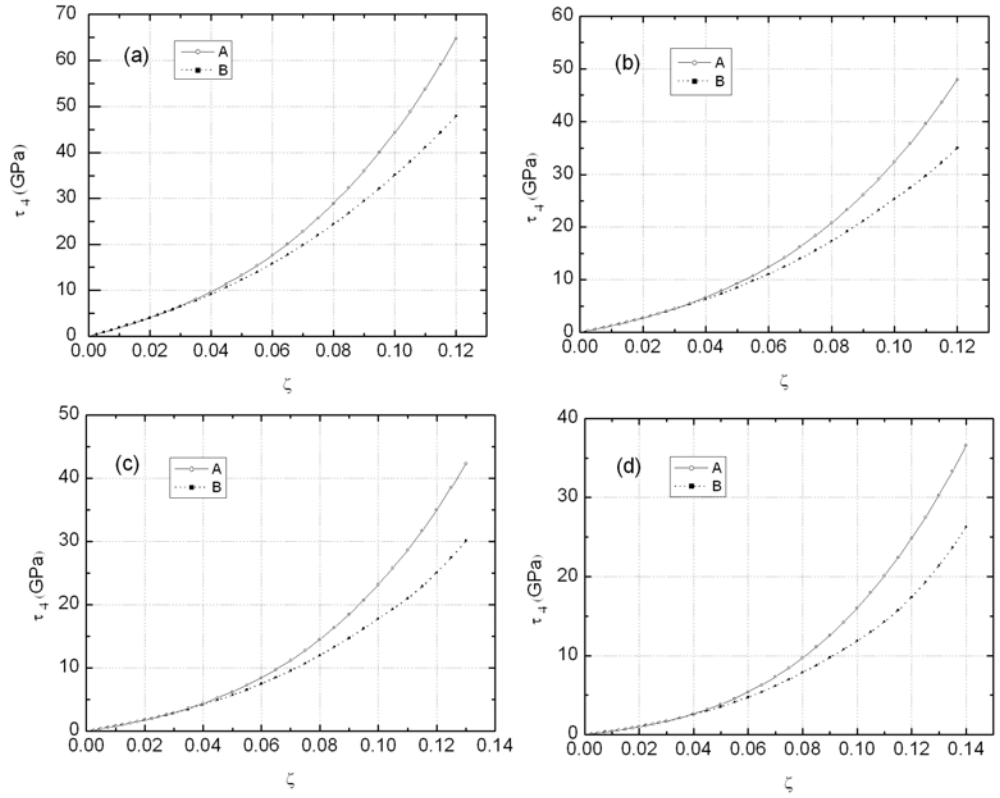

Figure 4.3 For each supercell with various hydrostatic deformation strain ξ's: (a) -0.04, (b) -0.02, (c) 0.0, and (d) 0.02, the Hellmann-Feynman stress-strain curves (marked with B) compared with the ones from our analytic results Eqs. (4.26-4.29) (marked with A).

4.6 Conclusions

In the linear elastic theory of crystal, the elastic stiffness tensors B_{ijkl}'s are defined to be coefficients of the linear stress-strain relations for crystal solids with arbitrary initial states. In this chapter, we derive the general stress-strain relations further to the nonlinear region involved with third-, and fourth-order elastic constants. We test

the derived relations to the face-centered cubic crystal Au. Using the scheme we developed before, we obtain the second-, third-, and fourth-order elastic constants of crystal Au under hydrostatic deformations. Then the nonlinear stress-strain relations from our analytic work are plotted and compared with those Hellmann-Feynman stress-strain curves directly from VASP. Satisfactory results are obtained.

CHAPTER FIVE

THEORETICAL AND COMPUTATIONAL STUDY OF ELASTIC STABILITY CRITERIA

5.1 Unifying the criteria of elastic stability in solids

The concept of elastic stability of a solid phase was introduced by Born in considering a crystal heated toward melting[5, 94]. The crystal would lose its rigidity, or "stability", and become a liquid when a shear modulus becomes zero. For a crystal with arbitrary symmetry, Born criterion becomes

$$|C| > 0, \tag{5.1}$$

where C is the elastic constant tensor. Eq. (5.1) ensures that all principal minors of the elastic constant matrix are positive definite. For a cubic lattice, the criterion is equivalent to $(C_{11} + 2C_{12})/2 > 0$, $C_{44} > 0$ and $(C_{11} - C_{12})/2 > 0$. The criterion is the condition of convexity of the free energy F of a crystal under any infinitesimal strain fluctuation such as that caused by lattice vibration during melting. Here C is related to the second order derivative of F, $C_{\alpha\beta} = \rho_0 \partial^2 F / \partial\varepsilon_\alpha \partial\varepsilon_\beta$, where ε is strain and ρ_0 is the density of the crystal. As pointed out by Furth[95], the Born criterion also sets the limit of the strength of a perfect crystal subject to external stress that causes displacement strains. Thus $|C| \to 0$ would set the elastic stability condition at temperature below melting point when the crystal without defects becomes unstable, either breaking or plastically deforming[95-96] or transforming into other crystalline phases[97]. The theory is normally referred to as the

elastic instability theory in materials physics and mechanics community. Eq. (5.1) is problematic for predicting elastic stability of a crystal under external loading since the Born criterion was formulated at zero stress state. Under external loading, the elastic constants are dependent on applied stress[54]. Born criterion thus needs to be developed further with the stress-dependent elastic constants, B, called elastic stiffness constants that were derived by Wallace in the context of formulating equations of elastic wave propagation in stressed crystals[22]. Then, the Born stability criterion should remain valid, that is,

$$|B| > 0 . \tag{5.2}$$

Following a different path, Polanyi, Frenkel and later Orowan[1-2, 98] proposed a scheme to estimate the ideal strength of perfect crystals subject to tension or shear stress. The Frenkel-Orowan model assumes that if the internal stress follows the same translational symmetry of the crystals, say, a simple sinusoidal function $\tau = \tau_{\max} \sin(2\pi\delta u / a_0) = \tau_{\max} \sin(2\pi\alpha\varepsilon)$, where δu is the displacement caused by external stress, a_0 is the periodicity of the crystal along the deformation path, ε is the deformation strain, and α is a parameter related to the geometry of the crystal lattice, the requirement of the crystal to remain stable is

$$\tau(\varepsilon + \Delta\varepsilon) - \tau(\varepsilon) > 0 , \tag{5.3a}$$

where $\Delta\varepsilon$ is an increment of strain from the state marked by the deformation strain ε. The limit of stability is reached when the maximum stress $\tau_{\max}$ is approached:

$$d\tau / d\varepsilon = 0 . \tag{5.3b}$$

This stress is called ideal strength of a crystal.

Concerned about the coordinate invariance and thermodynamics of deformed crystals, Hill[7] and later Hill and Milstein[8] proposed that the elastic stability condition should be expressed as the difference between the free energy, δF, and the work done to the system, δW, by the external loading, or

$$\delta F - \delta W > 0 . \tag{5.4}$$

In other words, for a stable crystal at thermodynamic equilibrium at a given temperature, the input work done by the external stress counts as only part of the total free energy; otherwise, it becomes unstable since the second law of thermodynamics is violated. When expanding Eq. (5.4) to second order derivative with respect to Langrangian strain, η, Hill and Milstein showed that $\frac{\partial^2 F}{\partial \eta_\alpha \partial \eta_\beta} - \frac{\partial^2 W}{\partial \eta_\alpha \partial \eta_\beta}$ is a quantity invariant of the choice of coordinates.

Eqs. (5.1-5.4) have been used extensively in dealing with a wide range of problems related to phase transitions[97], ideal strength of perfect crystals[20, 31], and crystal defect formation in various calculations using quantum and atomistic methods[31, 97, 99]. However, their relations with each other have not been connected formally, although in various numerical calculations they have been identified[20, 100-101]. In this paper, using a unified scheme in virtual displacement in finite deformation theory, we show that the different formulations of the criteria are in fact the same.

For a solid, including a crystal, under applied external stress, one general free energy can be expressed as

$$f = F - W . \tag{5.5}$$

If the system in any arbitrary deformed state X, or initial state that includes the natural state at undeformed condition with zero external stress, is subject to a perturbation, it is

moved from state X to state x with a Lagrangian strain η. We assume, without loss of generality, that the displacement could be arbitrary and infinitesimal as needed. The corresponding change of the Helmholtz free energy $F(x,T)=F(\eta,T)$ at state x from $F(X,T)=F(0,T)$ at state X is expressed as

$$F(\eta,T)=F(0,T)+\left.\frac{\partial F}{\partial \eta}\right|_{X,\eta'}\eta+\frac{1}{2!}\left.\frac{\partial^2 F}{\partial\eta\partial\eta}\right|_{X,\eta'}\eta\eta+\frac{1}{3!}\left.\frac{\partial^3 F}{\partial\eta\partial\eta\partial\eta}\right|_{X,\eta'}\eta\eta\eta+\frac{1}{4!}\left.\frac{\partial^4 F}{\partial\eta\partial\eta\partial\eta\partial\eta}\right|_{X,\eta'}\eta\eta\eta\eta+\ldots, \tag{5.6}$$

correct to the fourth power in η with the understanding that all derivatives appearing in Eq. (5.6) are done at state X with all other strains η' held constant. The corresponding stress, the second and third order isothermal elastic constants at state X, are

$$\tau(X)=\frac{1}{V(X)}\left.\frac{\partial F}{\partial \eta}\right|_{X,\eta'}, \tag{5.7a}$$

$$C(X)=\frac{1}{V(X)}\left.\frac{\partial^2 F}{\partial\eta\partial\eta}\right|_{X,\eta'}, \tag{5.7b}$$

$$c(X)=\frac{1}{V(X)}\left.\frac{\partial^3 F}{\partial\eta\partial\eta\partial\eta}\right|_{X,\eta'}, \tag{5.7c}$$

$$\tilde{c}(X)=\frac{1}{V(X)}\left.\frac{\partial^4 F}{\partial\eta\partial\eta\partial\eta\partial\eta}\right|_{X,\eta'}, \tag{5.7d}$$

where $V(X)$ is the volume of the system at X. Note that to avoid overcrowded notations, we shall not use indices for vectors and tensors unless necessary. Summation convention is automatically assumed.

Now let us consider giving another perturbation to move the system from state x to state y with a Lagrangian strain ξ following the same scheme as above. We can

obtain the corresponding stress, the second, the third, and the fourth order isothermal elastic constants at state x,

$$\tau(x) = \frac{1}{V(x)} \frac{\partial F}{\partial \xi}\bigg|_{x,\xi'}, \tag{5.8a}$$

$$C(x) = \frac{1}{V(x)} \frac{\partial^2 F}{\partial \xi \partial \xi}\bigg|_{x,\xi'}, \tag{5.8b}$$

$$c(x) = \frac{1}{V(x)} \frac{\partial^3 F}{\partial \xi \partial \xi \partial \xi}\bigg|_{x,\xi'}, \tag{5.8c}$$

$$\tilde{c}(x) = \frac{1}{V(x)} \frac{\partial^4 F}{\partial \xi \partial \xi \partial \xi \partial \xi}\bigg|_{x,\xi'}, \tag{5.8d}$$

where $V(x)$ is the volume of the system at state x. The two-step virtual displacement scheme suggests that we can take a derivative of Eq. (5.6) with respect to ξ at state x, so, after dividing by $V(x)$ on both sides, we have,

$$\tau(x) = \frac{1}{V(x)} \frac{\partial F}{\partial \xi}\bigg|_{x,\eta'} = \frac{V(X)}{V(x)} \frac{\partial \eta}{\partial \xi}\left[\tau(X) + C(X)\eta + \frac{1}{2!}c(X)\eta\eta + \frac{1}{3!}\tilde{c}(X)\eta\eta\eta + \ldots\right]. \tag{5.9}$$

Since state y is arbitrary and infinitesimally close to x, we have

$$\frac{\partial \eta}{\partial \xi} = a^T a, \tag{5.10}$$

where a is the deformation gradient matrix, $a = \partial x / \partial X$ if we let $y \to x$. Using the relations,

$$J = \det|a| = \frac{V(x)}{V(X)} \approx 1 + \eta_{ii} + \ldots \tag{5.11}$$

and

$$a_{ij} \approx \delta_{ij} + \eta_{ij} - \frac{1}{2}\eta_{ki}\eta_{kj} + \ldots, \tag{5.12}$$

correct to $O[(\eta)^2]$, Eq. (5.9) becomes

$$\tau_{ij}(x) = \tau_{ij}(X) + B_{ijkl}\eta_{kl} + O[(\eta)^2], \tag{5.13}$$

correct to the second power of Lagrangian strain η from the state X to state x with

$$B_{ijkl} = C_{ijkl} + (1/2)(\delta_{ik}\tau_{jl} + \delta_{jk}\tau_{il} + \delta_{il}\tau_{jk} + \delta_{jl}\tau_{ik} - 2\delta_{kl}\tau_{ij}), \tag{5.14}$$

where τ is the applied stress if the system is in equilibrium, and C_{ijkl} is the elastic constants in any deformed state X where τ is applied. Eq. (5.13) is formally the relation in Frenkel-Orowan model (Eq. (5.3a)) with the proportional coefficient identified as B_{ijkl}.

Following the same scheme, we can systematically obtain the second and higher order elastic constants at state x in relation to those at state X,

$$C(x) = \frac{1}{V(x)}\frac{\partial^2 F}{\partial\xi\partial\xi}\bigg|_{x,\eta'} = \frac{V(X)}{V(x)}\frac{\partial\eta}{\partial\xi}\left[C(X) + c(X)\eta + ...\right], \tag{5.15}$$

$$c(x) = \frac{1}{V(x)}\frac{\partial^3 F}{\partial\xi\partial\xi\partial\xi}\bigg|_{x,\eta'} = \frac{V(X)}{V(x)}\frac{\partial\eta}{\partial\xi}\left[c(X) + \tilde{c}(X)\eta + ...\right], \tag{5.16}$$

and so forth and so on. For example, after using Eqs. (5.10-5.12), the second order elastic constants in Eq. (5.15) become

$$\begin{aligned} C_{ijkl}(x) &= C_{ijkl}(X) + c_{ijklmn}(X)\eta_{mn} \\ &+ \left[-C_{ijkl}(X)\eta_{mm} + C_{ijkm}(X)\eta_{lm} + C_{ijml}(X)\eta_{km} + C_{imkl}(X)\eta_{jm} + C_{mjkl}(X)\eta_{im}\right]. \end{aligned} \tag{5.17}$$

Now we use the approach outlined above to prove that Eqs. (5.2-5.4) are the same. In other words, one can derive one from another directly from the free energy $f = F - W$ (Eq. (5.5)). The change of the free energy f from state X to x is

$$\delta f = \delta F - \delta W. \tag{5.18}$$

$$\delta W = Ja^{-1}\tau(X)(a^{-1})^T V(X)\eta. \tag{5.19}$$

Using the change of the free energy, $\delta F = F(x,T) - F(X,T)$ and taking a derivative of δF with respect to ξ at state x and dividing it by $V(x)$, we have, after letting $y \to x$, $\frac{1}{V(x)}\frac{\partial \delta F}{\partial \xi}\bigg|_{x,\xi'} = \tau(x)$ (Eq. (5.8a)). And $\frac{1}{V(x)}\frac{\partial \delta W}{\partial \xi}\bigg|_{x,\xi'} = \frac{1}{V(x)}\frac{\partial \delta W}{\partial \eta}\bigg|_{X,\eta'}\frac{\partial \eta}{\partial \xi} = \tau(X)$ from Eq. (5.19) after using Eqs. (5.10-5.11). Therefore,

$$\frac{1}{V(x)}\frac{\partial \delta f}{\partial \xi}\bigg|_{x,\xi'} = \frac{1}{V(x)}\frac{\partial(\delta F - \delta W)}{\partial \xi}\bigg|_{x,\xi'} = \frac{1}{V(x)}\left[\frac{\partial \delta F}{\partial \xi} - \frac{\partial \delta W}{\partial \xi}\right]\bigg|_{x,\xi'} = \tau(x) - \tau(X). \quad (5.20a)$$

Then we use the technique, $\frac{\partial}{\partial \xi} = \frac{\partial \eta}{\partial \xi}\frac{\partial}{\partial \eta}$, combined with Eqs. (5.13) and (5.20a), and get that,

$$\frac{1}{V(X)}\frac{\partial^2 \delta f}{\partial \eta \partial \eta}\bigg|_{X,\eta'} = \frac{1}{V(X)}\frac{\partial^2(\delta F - \delta W)}{\partial \eta \partial \eta}\bigg|_{X,\eta'} = B(X), \quad (5.20b)$$

where B is expressed in Eq. (5.14).

The above relations show that the two criteria, the Polanyi-Frenkel-Orowan criterion based on stress response and the Born-Hill criterion based on energy change, are the same and one can be derived directly from another from the general expression of the free energy of the system under applied load, $f = F - W$. They represent the same physics describing the elastic stability of a solid. In other words, the ideal strength of a solid corresponds exactly to the limit of the stability criterion. In fact, the stability conditions expressed as the first order derivative (Eq. (5.20a)) and the second order derivative of f (Eq. (5.20b)) are both necessary conditions to guarantee the convexity of f [102].

In practice, Born-Hill criterion is used widely in theoretical calculations, as energy change is relatively easy to obtain, especially using first-principles or *ab initio*

methods. Since the internal energy is calculated, it is F (or the internal energy U at zero temperature) not f is obtained. Usually the calculations give the second order elastic constants C_{ijkl} from Eq. (5.7b), or higher-order elastic constants from Eqs. (5.7c) and (5.7d). To obtain elastic stiffness coefficients, one has to use Wallace relation (Eq. (4.14)). Polanyi-Frenkel-Orowan criterion, on the other hand, has an advantage practically as most experiments as well as many theoretical calculations can measure the stress-strain response function straightforwardly. However, since the applied stress (or strain) is specific, the elastic stiffness coefficient matrix obtained (Eq. (5.13)) can only have limited number of components, specific to the loading direction[16].

5.2 Elastic stability and ideal strength of gold under uniaxial stress

5.2.1 Introduction

The strength of crystalline materials is determined in general by nucleation and motion of dislocations or microcracks. If there are no such defects, the materials, so-called ideal or perfect, would fail at the limit of the so-called elastic stability. The stress at which this is achieved is called the ideal strength. It is of great interest to investigate the elastic behavior of a perfect crystal under loading because the path leading toward the instability is related to not only the ideal strength but also the atomic mechanisms of the defect formation. Such information is also very useful in the analysis of the structural response of solids, ranging from polymorphism, amorphization to fracture. Moreover, the ideal strength is connected to the strength and defect formation in nano-structured materials currently being developed, as shown in recent nanoindentation experiments where the onset of yielding on the nanoscale is suggested to be related to homogeneous

nucleation of dislocations in the small volume under the nanoindenter where stresses approach the ideal strength.[96]

The elastic stability limit is formulated traditionally following Born's original idea[5-6] that a crystal should remain stable when the change of the elastic energy with respect to the spontaneous strain exhibits convexity; Otherwise, instability would occur consequentially. The condition of convexity leads to the stability criteria in the form of a set of relations involving elastic constants appropriate to the crystal symmetry. Born's theory is, however, formulated for systems without external load. For systems under external load, it was shown[7-17] that the elastic stiffness coefficients B_{ijkl} (Eq. (5.26)) rather than elastic constants C_{ijkl} should be used in formulating the stability criteria. The onset modes at the instability derived from the stability criteria were tested for many crystalline systems using various approaches employing empirical or semi-empirical interatomic potentials such as Lennard-Jones potential,[12] Morse potential[17] or EAM potentials.[14] It is known that these inter-atomic interactions are obtained by fitting the parameters predominantly with the equilibrium properties of the material studied (i.e., under zero or infinitesimal deformation). It is, therefore, doubtful how one can apply those potentials obtained this way to simulate the materials under finite loading and still expect to obtain reliable results. *Ab initio* electronic structure calculations, on the other hand, have been performed for variously strained structures and are shown to give ideal strength of materials without resorting to doubtful extrapolations. Given recent advances in quantum theoretical methods and computers, it is possible to calculate the elastic limits with considerable accuracy, including both the theoretical stress and the detailed nature of the atomic rearrangements as the elastic limit is approached. For instance, Senoo *et al*

discussed the elastic deformation due to [100] loading of Al using the pseudopotential method.[103] Esposito *et al* dealt with the tensile strength of FCC Cu under uniaxial deformation on the basis of the *ab initio* potential, the augumented-spherical-wave (ASW), and KKR methods.[104] Sob *et al* did extensive investigation of the ideal strength of bcc iron under hydrostatic pressure, and due to [001], [111] uniaxial tension.[105] Li and Wang studied the ideal tensile strength of Al.[18] Sob *et al* worked on the tensile strength of Cu.[106] Cerny *et al.* tested the elastic stability of some magnetic crystals under hydrostatic pressure.[107]

The stability criterion based on the elastic stiffness constants[14-16] certainly provides a convenient and powerful recipe to measure stability limit. As done in these previous works, one first calculates the elastic constants and then construct the elastic stiffness coefficients as a function of the applied stress to a system, which usually under some specific load such as hydrostatic, uniaxial tensile or compressive, or shear strain. One then obtains the stability limit at the strain where a principal minor of the elastic stiffness constant matrix first becomes non-positive, or $\det\left|B_{ijkl}\right| = 0$. While along some simple loading paths such as uniaxial tension and compression the stability limit is found to relate to some shear strain modes,[18-19] under hydrostatic loading it is observed that the stability is dominated by the bulk stiffness coefficient that corresponds to void formation under expansion.[11] The possibility of bifurcations from the primary loading path or mode before the stability limit is approached was never observed in the case of hydrostatic loading. As we show below, the stability limit of Au under hydrostatic load is actually caused by shear not by volume instability as shown in the earlier work.[14] As concerned in the earlier studies, noticeably by Born[5-6] and Hill,[7-11] some perturbations, fluctuations, as

well as sample loading conditions would make the deformation path astray from the primary loading path, causing the measured stability limit different from that intended originally. As we show here, this phenomenon, which is called "stability bifurcation", plays an important rule in determining the global stability of a crystal lattice.

In this part, we present a direct investigation, using density functional theory, of the elasticity, the stress-strain relation, the stability, and the ideal strength of FCC metal Au under hydrostatic stress. Au is special in its structural stability, known experimentally to have no polymorphism under hydrostatic compression, so its original symmetry is preserved during the primary loading path under hydrostatic stress before the instability limit yet to be identified. Thus it provides a simple testing case for stability study. Therefore, the possible bifurcation along paths different from the primary loading path can be addressed relatively clearly. The additional motivation is drawn from the earlier studies made by Yip *et al* in Au[14] who performed molecular dynamics (MD) simulation using classical EAM potentials. As shown below, our results are different from theirs in that the stability limit of Au under hydrostatic expansion is dominated by shear instability, not by volumetric or bulk modulus instability. This unusual finding is a direct manifestation of the stability bifurcation.

This part is organized as follows. The stability criterion of a crystal solid is presented briefly in section 5.2.2. In this section, we review the formulation of the stress, elastic stiffness coefficients, elastic stiffness moduli, and stability criteria. In particular, we shall give a new interpretation of the stability criterion based on the elastic stiffness coefficients from the stress-strain relation in any deformed state. In section 5.2.3, we introduce our calculation models and methods and the *ab initio* DFT method. In section

5.2.4, we show our results. In section 5.2.5, we discuss our results and make comparisons with some related previous work. Finally, we will draw conclusions from this work.

5.2.2 Stability criteria of crystal solids

For a solid body subject to an external loading, the configuration of a material point in the system after elastic deformation is represented as $Y = Y(X)$, where X is the initial configuration at the equilibrium state. The deformation gradient is defined by

$$J_{ij} = \frac{\partial Y_i}{\partial X_j}, \tag{5.21}$$

where $i, j = 1,2,3,$ representing the Cartesian coordinates. Then the Lagrangian strain tensor is defined as

$$\eta = \frac{1}{2}(J^T J - I), \tag{5.22}$$

where I is the unit matrix. The internal energy is related to the Lagrangian strain through Taylor series expansion in terms of the strain tensor,[22]

$$U(X, \eta_{ij}) = U(X, 0) + V\sum_{ij} \sigma_{ij}\eta_{ij} + (1/2!)V\sum_{ijkl} C_{ijkl}\eta_{ij}\eta_{kl} + ..., \tag{5.23}$$

where

$$\sigma_{ij} = V^{-1}\left(\partial U / \partial \eta_{ij}\right)_{\eta=0} \tag{5.24}$$

$$C_{ijkl} = V^{-1}(\partial^2 U / \partial \eta_{ij}\partial \eta_{kl})_{\eta=0}, \tag{5.25}$$

and V is the volume in the configuration X. If the system is under load, the stability criterion depends on the elastic stiffness coefficients, instead of elastic constants as shown in Eq. (5.25) in Born's theoretical frame. The definition of elastic stiffness coefficients is defined as follows,

$$B_{ijkl} = C_{ijkl} + (1/2)(\delta_{ik}\tau_{jl} + \delta_{jk}\tau_{il} + \delta_{il}\tau_{jk} + \delta_{jl}\tau_{ik} - 2\delta_{kl}\tau_{ij}), \tag{5.26}$$

where τ_{ij} is the external stress, which is equal to the internal stress σ_{ij} (Eq. (5.24)) if the system remains in mechanical equilibrium. This derivation of B_{ijkl} is from the premise proposed by Hill and Milstein[7-11] that a solid can only be in stable state when the change of the internal energy δU is larger than the external work δW done to the system, or $\delta U - \delta W > 0$.

Here we give another, and physically more transparent, definition of elastic stiffness coefficients B_{ijkl} and the new interpretation of the stability criterion, which is based on the stress-strain relations in any deformed state. If a material in configuration X under stress $\sigma_{ij}(X)$ is stable, then after given a small perturbation, i.e. with a small increase of strain η_X^Y, the system will move to a new state Y with a corresponding stress $\sigma_{ij}(Y)$. The two stresses are related by a linear proportional coefficient of stress versus strain between the two states (X and Y) of the stressed system as shown by Wallace,[22]

$$\sigma_{ij}(Y) = \sigma_{ij}(X) + B_{ijkl}(\eta_X^Y)_{kl} + O[(\eta_X^Y)^2] \quad . \tag{5.27a}$$

If the material in the state X is stable, then the increment of the stress $\delta\sigma_{ij} = \sigma_{ij}(Y) - \sigma_{ij}(X)$ must remain positive to the first order in the perturbative strain η_X^Y, or

$$\delta\sigma_{ij} = \sigma_{ij}(Y) - \sigma_{ij}(X) = B_{ijkl}(\eta_X^Y)_{kl} > 0\,, \tag{5.27b}$$

for any small perturbative strain (we can assume $\eta_X^Y > 0$ without losing generality). Otherwise, the system becomes unstable. The stability criterion can be cast in the principal minor of the stiffness coefficient,

$$\det\left|B_{ijkl}\right| > 0\,. \tag{5.27c}$$

This interpretation of the stability criterion is in fact very much in the same spirit as that in the original criterion for the ideal strength of materials proposed by Frenkel[1] and Orowan[2]. We should mention in passing that the interpretation of the stability criterion this way has not been contended seriously despite its simplicity in physical meaning.

As is obvious from the definition, B_{ijkl} does not necessarily retain the symmetry relations of the original crystal since the deformed state Y can be arbitrarily far away from the initial non-deformed state[22]. Given that B_{ijkl} is in general asymmetric while $ij \leftrightarrow kl$, the symmetrized coefficient can be used,

$$\bar{B} = (1/2)(B^T + B). \tag{5.28}$$

The system becomes unstable when $\det|\bar{B}| = 0$ for the first time under the applied load. In other words, as $\bar{B}$ is a function of the deformation strain, the instability condition will lead to a set of relations among the $\bar{B}_{ij}$'s at the critical applied strain along the primary loading path.

For a cubic crystal subject to hydrostatic pressure P,

$$\tau_{ij} = -P\delta_{ij}. \tag{5.29}$$

We follow the convention that the inward pressure is positive while outward stress is negative (i.e., $P < 0$ for tension). From Eqs. (5.26) and (5.29), the elements of stiffness coefficients are

$$\begin{aligned} B_{11} &= B_{22} = B_{33} = C_{11} - P, \\ B_{12} &= B_{23} = B_{13} = C_{12} + P, \\ B_{44} &= B_{55} = B_{66} = C_{44} - P. \end{aligned} \tag{5.30}$$

Here we simplify the subscript in the tensor notion by using the Voigt notation ($11 \to 1$, $22 \to 2$, $33 \to 3$, $23 \to 4$, $31 \to 5$, and $12 \to 6$). For this special case, the stiffness

coefficients and the elastic constants have the same type of crystal symmetry. And B_{ij} possess $i \leftrightarrow j$ symmetry, so $\overline{B} = B$. Let $\det|B| \geq 0$, it turns out that there are three independent stability conditions,

$$B_{11} + 2B_{12} \geq 0, \tag{5.31}$$

$$B_{11} - B_{12} \geq 0, \tag{5.32}$$

$$B_{44} \geq 0. \tag{5.33}$$

Or

$$C_{11} + 2C_{12} + P \geq 0, \tag{5.34}$$

$$C_{11} - C_{12} - 2P \geq 0, \tag{5.35}$$

$$C_{44} - P \geq 0, \tag{5.36}$$

using the elastic constants C_{ij} in the loaded state. The bulk modulus B_T, tetragonal shear modulus G', and rhombohedral shear modulus G, are defined as the following,

$$B_T = (C_{11} + 2C_{12})/3, \tag{5.37}$$

$$G' = (C_{11} - C_{12})/2, \tag{5.38}$$

$$G = 4C_{44}. \tag{5.39}$$

These quantities are extended to the system under finite hydrostatic load, so we have the corresponding bulk and shear stiffness moduli,

$$B_T(\tau) = (B_{11} + 2B_{12})/3 = (C_{11} + 2C_{12} + P)/3, \tag{5.40}$$

$$G'(\tau) = (B_{11} - B_{12})/2 = (C_{11} - C_{12} - 2P)/2, \tag{5.41}$$

$$G(\tau) = 4B_{44} = 4(C_{44} - P). \tag{5.42}$$

In contrast to the conventional or Born's stability criteria only valid in the stress-free case, which requires that (5.37-5.39) be positive, the stability criteria in the system under load require instead (5.40-5.42) to be positive.

5.2.3 Calculation details

A. Calculation methods

To simulate hydrostatic deformation, we first calculate the properties (total energy and equilibrium lattice parameter) of a single crystal Au in the ground state. We performed the *ab initio* calculations using the Vienna *ab initio* Simulation package (VASP) developed by the Hafner Research Group at the University of Vienna. VASP uses pseudopotentials or the projector-augmented wave method (PAW) and a plane wave basis set. To obtain lattice parameter that is in better agreement with experimental value, we used the exchange-correlation energy evaluated with the generalized gradient approximation (GGA). Ultrasoft pseudopotentials were always employed to describe the electron-ion interactions. We used $18\times18\times18$ k -point mesh in our calculations following the Monkhost-Pack scheme, which as our experience shows is sufficient to reach the desired convergence in the total energy and elastic constants. We took the cutoff energy set at E_{cutoff}^{Au} = 292 eV, which are sufficiently large for the total energy to converge to the stable equilibrium state. For Au, the ground state has a face-centered cubic structure with the lattice parameter a_0=4.07 Å, which is very close to experimental measurement 4.08 Å[85] at room temperature. We will thus use 4.07 Å as the lattice parameter in our supercell, which is a face-centered cubic cell containing 4 atoms, to perform the following simulation work for deformation. The benefit to use such a supercell is that we can easily

apply specific strains on the supercell and read the values of the six components of stress tensor directly from VASP output files.

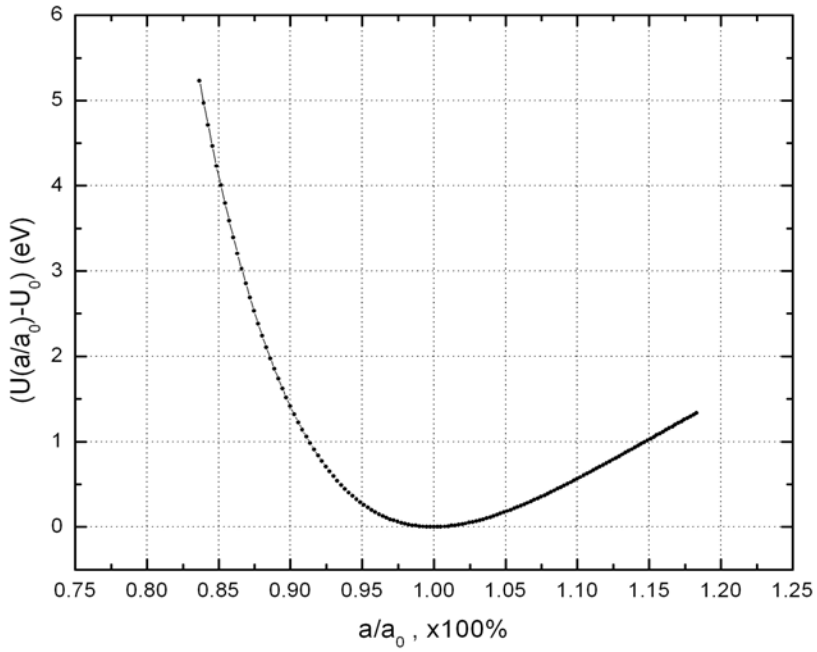

Figure 5.1 The calculated variation of elastic energy with the applied hydrostatic deformation strain. We use a/a_0 as the independent variable.

In the next step, we applied hydrostatic deformation to the crystal supercell via a strain, $\eta_{11} = \eta_{22} = \eta_{33} = \xi$, $\eta_{ij} = 0$ for $i \neq j$. We changed the value of ξ from -0.15 to $+0.15$ with a finite step size $\Delta\xi = 0.0025$. This operation is amount to changing the lattice parameter homogeneously. Let a be the lattice constant of the deformed crystal, and obviously $a / a_0 = \sqrt{1+2\xi}$ from Eqs. (5.21) and (5.22). This type of deformation is equivalent to the application of a hydrostatic stress. We then obtain the internal energy U as a function of the applied strain, or $U = U(a / a_0)$, with the first-principles calculation, as shown in figure 5.1.

B. Elastic energy and stress-strain relations

The elastic energy expanded at each arbitrary deformed configuration when the system changes from state X to state Y is,

$$U(X,\bar{\eta}) = U(X,0) + V\sum_{ij}\sigma_{ij}\bar{\eta}_{ij} + (\frac{1}{2!})V\sum_{ijkl}C_{ijkl}\bar{\eta}_{ij}\bar{\eta}_{kl} + ..., \tag{5.43}$$

where $V = a^3$, $\bar{\eta}$ is a new Lagrangian strain tensor in the deformed configuration X with lattice constant a. We can simplify the subscript in the tensors by using the Voigt notation. Eq. (5.43) can then be written as

$$V^{-1}[U(X,\bar{\eta}) - U(X,0)] = \sum_{i=1,...,6}\sigma_i\bar{\eta}_i + \frac{1}{2!}\sum_{i,j=1,...,6}c_{ij}\bar{\eta}_i\bar{\eta}_j + ... \tag{5.44}$$

Considering our face-centered cubic supercell under hydrostatic deformation, $\bar{\eta}_1 = \bar{\eta}_2 = \bar{\eta}_3 = \bar{\xi}$, $\bar{\eta}_4 = \bar{\eta}_5 = \bar{\eta}_6 = 0$, plus $\sigma_1 = \sigma_2 = \sigma_3 = \sigma$, we have

$$V^{-1}[U(X,\bar{\eta}) - U(X,0)] = 3\sigma\bar{\xi} + (\frac{3}{2}c_{11} + 3c_{12})\bar{\xi}^2 + ..., \tag{5.45}$$

And thus,

$$\sigma = \frac{1}{3V}\left(\frac{\partial U}{\partial\bar{\xi}}\right)_{\bar{\xi}=0}, \tag{5.46}$$

$$B_T = \frac{c_{11}+2c_{12}}{3} = \frac{1}{9V}\left(\frac{\partial^2 U}{\partial\bar{\xi}^2}\right)_{\bar{\xi}=0}. \tag{5.47}$$

So at each deformed configuration with lattice constant a, we select a few datum points from the $U - a/a_0$ curve nearby a/a_0 and calculate the strain value $\bar{\xi}$ for each point using X as the reference configuration. Since the elastic energy can be expressed as a polynomial of the strain parameter $\bar{\xi}$ as shown in Eqs. (5.44-5.45), when we plot the

$U-\overline{\xi}$ curve, we may obtain the internal stress (Eq. (5.46)) and elastic bulk modulus (Eq. (5.47)) through polynomial fitting mentioned above.

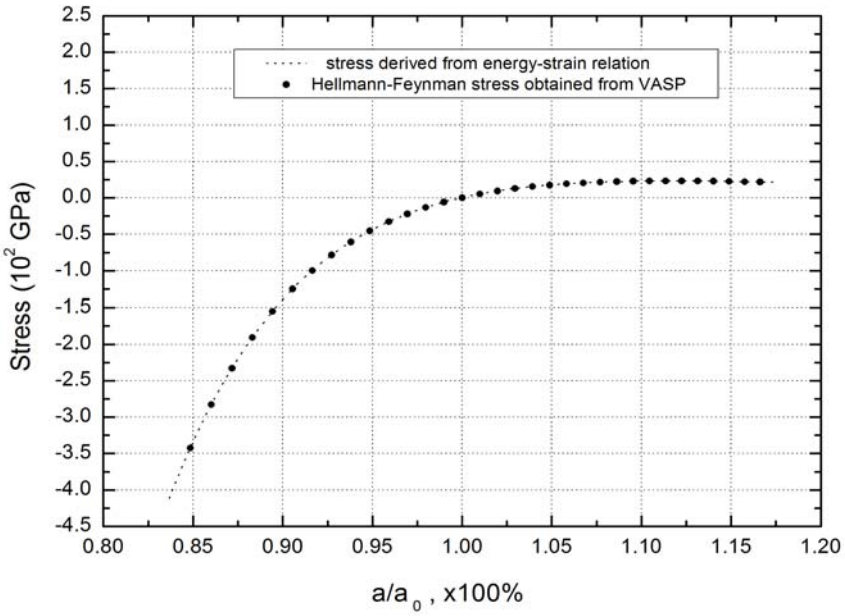

Figure 5.2 The Hellmann-Feynman stress calculated by using VASP and the stress derived from energy-strain relation. The maximum stress $\sigma_{\max} = 23.45$ GPa occurs at $a/a_0 = 1.12$.

Figure 5.2 shows the stress calculated this way. We found that it does agree very well with the Hellman-Feynman stress calculated by using VASP. As the ideal strength is conventionally defined as the maximum of the stress along the designated deformation path, from figure 5.2 it appears that the ideal strength for Au is $\sigma_{\max} = -P = 23.45$ GPa at the corresponding hydrostatic strain $a/a_0 = 1.12$. However, we will show below that this is not the true value for the ideal hydrostatic strength, because the stability limit has already been approached before this point via a shear stability bifurcation.

C. Elastic constants and elastic stiffness coefficients

As mentioned earlier, there are two ways to calculate elastic stiffness coefficients under load. One is from Eq. (5.26), to treat elastic stiffness coefficients as functions of the elastic constants and the applied stress tensor. From Eq. (5.47) via fitting of the internal energy, we have the value of $(C_{11}+2C_{12})/2$ that leads $B_T(\tau)=(C_{11}+2C_{12}+P)/3$. So we may test the stability via the so-called volumetric or bulk modulus stability condition (5.31) or (5.34), which was also called mechanical spinodal stability[14]. The other way is from Eq. (5.27b), that treats elastic stiffness coefficients as the linear expansion coefficients of $\delta\sigma-\bar{\xi}$ curve from which one can also get the value of $B_T(\tau)$.

Starting from Eqs. (5.27), we consider our face-centered cubic supercell under hydrostatic deformation ($\bar{\eta}_1=\bar{\eta}_2=\bar{\eta}_3=\bar{\xi}$, $\bar{\eta}_4=\bar{\eta}_5=\bar{\eta}_6=0$, plus $\sigma_1=\sigma_2=\sigma_3=\sigma$). We then have

$$\delta\sigma=(B_{11}+2B_{12})\bar{\xi}=3B_T(\tau)\bar{\xi} \quad . \tag{5.48}$$

So for each deformed configuration with a as the lattice constant, we take a few points from the $\sigma-a/a_0$ curve (figure 5.2) close to a/a_0, calculate the strain value $\bar{\xi}$ for each point using X as the reference configuration, and then make a linear fitting to Eq. (5.48), so we obtain the value of $B_T(\tau)$ at that reference configuration.

As shown in figure 5.3, this approach coming from the original definition of elastic stiffness coefficients (Eqs. (5.27)) does give results agreeing with those from the convexity argument by Born and Milstein *et al*. Incidentally, this agreement in our

computation provides a strong support for the capability and accuracy of the *ab initio* DFT simulation.

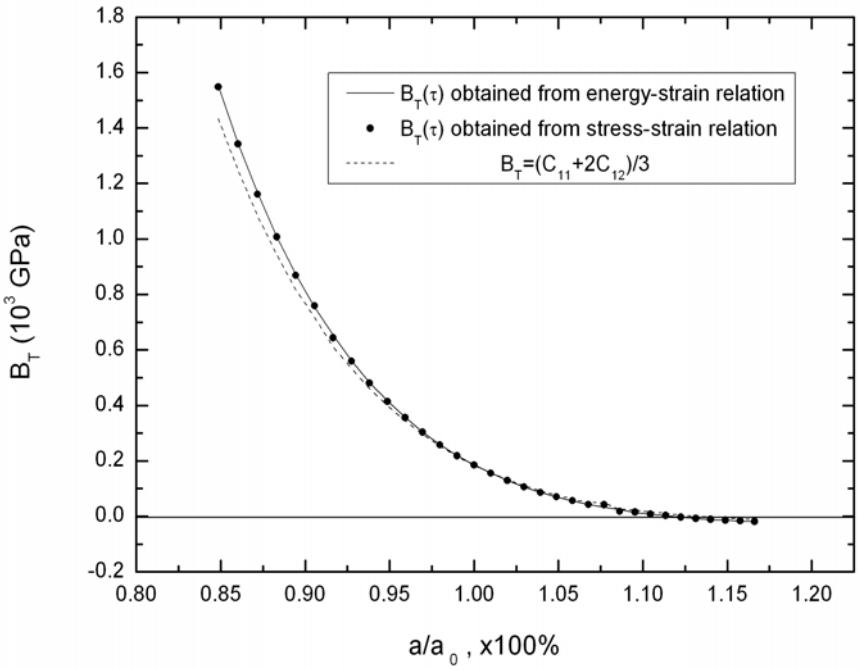

Figure 5.3 The bulk stiffness modulus is calculated using two approaches. One (smooth line) uses energy-strain relation, and the other (filled circles) uses stress-strain relation. Dashed line represents the bulk modulus defined in Eq. (5.37).

D. Shear instability and bifurcation away from the hydrostatic strain path

As mentioned in the introduction, the stability condition can be violated not through the primary loading path along which one intends to examine. For example, in experiments as well as in theory, very often one may find other stability conditions violated before the primary stability condition is, leading to the stability bifurcation. Such complication, although abundant in nature and in theoretical scenarios, has not received much attention.

For cubic crystals, other two stability paths are related to shear. To test the two shear stability conditions (5.32)-(5.33), we need to give a small perturbative shear strain $\delta\eta$ to each hydrostatically deformed configuration at the given hydrostatic strain $\bar{\xi}$. The strain $\delta\eta$ allows the system to deviate from the main hydrostatic deformation path. Then we check the elastic energy or stress change as a function of $\delta\eta$. With a set of unit lattice vectors (i.e., $[a,0,0]$, $[0,a,0]$, $[0,0,a]$ in the hydrostatically deformation sample), the perturbative deformation can be described by an appropriate Jacobian matrix J' as

$$r' = J' \cdot r, \tag{5.49}$$

where r is the position vector corresponding to the current state along the hydrostatic deformation path, and vector r' describes the perturbed state with the shear strain $\delta\eta$.

Under this combined strain state, once again there are two ways to test the stability conditions. The first one is to use the calculated $U-\delta\eta$ curves to obtain the elastic constants through polynomial fitting, which combining with the pressure at this state leads to the (shear) elastic stiffness coefficients. Then we can test if Eq. (5.35) or (5.36) is violated or not. The second way is to use Eqs. (5.27). With the given small strain $\delta\eta$, we can obtain the elastic stiffness moduli in the system under load as the linear expansion coefficients from the $\delta\sigma-\delta\eta$ curve, and then check the stability with Eqs. (5.32) and (5.33).

The stability condition as presented in Eq. (5.32) involves the tetragonal shear modulus, $G' = (C_{11}-C_{12})/2$. Its violation corresponds to a *shear instability*, which once occurs we expect the bifurcation from the hydrostatic deformation path. In order to test

this stability condition, we use the following Jacobian matrix (and corresponding strain matrix for the tetragonal shear) at each point along our hydrostatic deformation path,

$$J = \begin{pmatrix} \sqrt{1+2\xi} & 0 & 0 \\ 0 & \sqrt{1-2\xi} & 0 \\ 0 & 0 & 1 \end{pmatrix}, \qquad \delta\eta = \begin{pmatrix} \xi & 0 & 0 \\ 0 & -\xi & 0 \\ 0 & 0 & 0 \end{pmatrix},$$

where ξ is the magnitude of the shear strain. With such increments of the tetragonal deformation, the energy of the system changes according to the relation Eq. (5.44),

$$\delta U = V(C_{11} - C_{12})\xi^2 + ..., \tag{5.50}$$

where $V = a^3$ is the current volume. The tetragonal shear modulus $G' = (C_{11} - C_{12})/2.$ can be expressed as

$$G' = \frac{1}{4V}\frac{\partial^2 U}{\partial x^2}. \tag{5.51}$$

And then,

$$G'(\tau) = G' - P. \tag{5.52}$$

Or if we use a second approach employing the stress-strain relation with Eqs. (5.27), we have

$$\delta\sigma = (B_{11} - B_{12})\xi = 2G'(\tau)\xi. \tag{5.53}$$

And then we have,

$$G'(\tau) = \frac{1}{2}\frac{\partial\sigma}{\partial\xi} \tag{5.54}$$

The second shear stability corresponding to the condition in Eq. (5.33) is the rhombohedral shear instability, $G(\tau) = 4(C_{44} - P)$. To explore the bifurcation along the rhombohedral shear strain, we used the following perturbative shear strain matrix,

$$\delta\eta = \begin{pmatrix} 0 & 0 & 0 \\ 0 & 0 & \xi \\ 0 & \xi & 0 \end{pmatrix}.$$

The corresponding elastic energy change now becomes

$$\delta U = 2V\sigma_4\xi + 2VC_{44}\xi^2 + ..., \tag{5.55}$$

and the elastic constants are

$$C_{44} = \frac{1}{4V}\frac{\partial^2 U}{\partial \xi^2}, \tag{5.56}$$

$$G(\tau) = \frac{1}{V}\frac{\partial^2 U}{\partial \xi^2} - 4P. \tag{5.57}$$

Alternatively, from the stress-strain relation (Eqs. (5.27)), we have

$$\delta\sigma = 2B_{44}\xi, \tag{5.58}$$

$$G(\tau) = \frac{1}{2}\frac{\partial \sigma}{\partial \xi}. \tag{5.59}$$

5.2.4 Results

Table 5.1 summarizes the elastic stiffness coefficients B_{11}, B_{12}, B_{44} and their derivatives with respect to pressure calculated in this work using DFT. The obtained zero-pressure values of B_{ij}'s agree well with the previous theoretical calculation using *ab initio* full-potential linear muffin-tin-orbital (FP-LMTO) method.[108] Our results show better agreement with low-temperature experimental data than the room-temperature data[91, 109-110]. Under compression Au exhibits stability in the entire range of applied strain (strain up to a/a_0 =0.83 and pressure up to 412 GPa). Under expansion Au exhibits much complex stability behavior which is presented below.

Table 5.1 Zero-pressure elastic stiffness coefficients B_{ij} (in GPa), their pressure derivatives and elastic modulus B_T, G' and G (in GPa).

B_{11}	$\partial B_{11}/\partial P$	B_{12}	$\partial B_{12}/\partial P$	B_{44}	$\partial B_{44}/\partial P$	B_T	G'	G	Reference
202.1	6.34	174.2	5.34	37.9	1.74	183.5	14.0	151.6	This work
201.3	5.97	176.1	5.38	36.9	1.43	184.5	12.6	147.6	Ref. 108
192.2	7.01	162.8	6.14	42.0	1.79	172.6	14.7	168.0	Ref. 109 (RT)
192.9	5.71	163.8	4.95	41.5	1.52	167.2	14.6	166.0	Ref. 91 (RT)
200.4	6.49	169.5	5.66	44.5	1.79	179.8	15.5	178.0	Ref. 110 (79K)

The bulk stiffness modulus $B_T(\tau)$ obtained from the two different approaches, one from $U-\overline{\xi}$ relation while the other from $\sigma-\overline{\xi}$ relation, are nearly identical, so are the shear stiffness modulus $G'(\tau)$ and $G(\tau)$ as shown in figure 5.3-5.5. Figure 5.3 shows that the hydrostatic or volume strain stability condition (Eq. (5.31)) is violated at the point $a/a_0 = 1.12$ where the bulk modulus vanishes. B_T and $B_T(\tau)$ reach zero almost at the same strain, $a/a_0 = 1.12$. On the other hand, the tetragonal shear stability condition (Eq. (5.32)) is not violated until $a/a_0 = 1.09$ as shown in figure 5.4. Looking at the rhombohedral shear stability condition (Eq. (5.33)), we see that the rhombohedral shear stiffness modulus $G(\tau)$ disappears at a much smaller value of $a/a_0 = 1.06$ as shown in figure 5.5. So our *ab initio* calculations gave the following sequence in terms of applied

hydrostatic strains where the corresponding instability conditions are violated for Au under hydrostatic expansion: rhombohedral shear stability limit is reached at $a/a_0 = 1.06$, tetragonal shear stability limit at $a/a_0 = 1.09$, and the hydrostatic stability limit at $a/a_0 = 1.12$. According to the stability criterion, the system should become unstable at the smallest value of applied strain that corresponds to the first violation of the stability conditions. For Au subject to hydrostatic expansion, therefore, we show that it is at $a/a_0 = 1.06$, and the instability is dominated by rhombohedral shear. The corresponding ideal strength of Au under hydrostatic expansion is found to be 19.2 GPa.

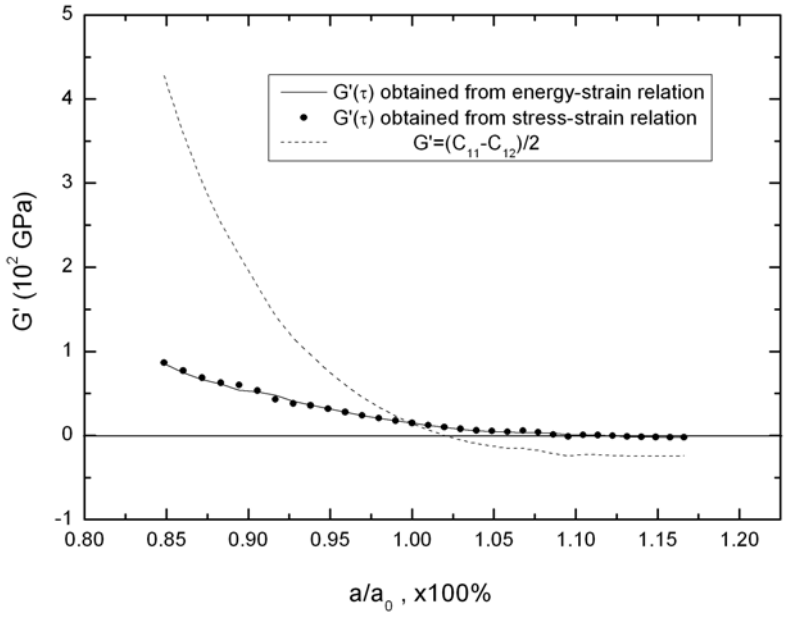

Figure 5.4 The tetragonal shear stiffness modulus calculated using two approaches. One (smooth line) is using energy-strain relation, and the other (filled circles) is from stress-strain relation. Dashed line represents the modulus defined in Eq. (5.38).

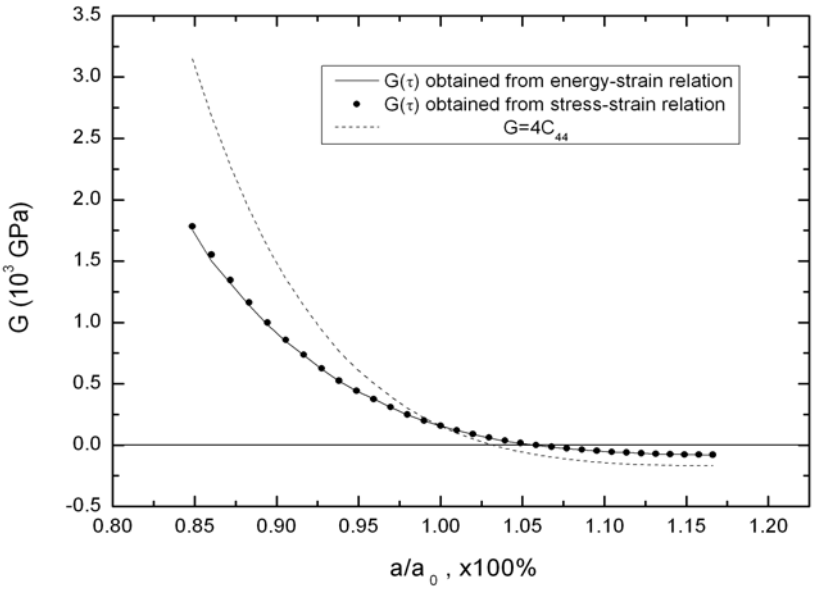

Figure 5.5 The rhombohedral shear stiffness modulus calculated using two approaches. One (smooth line) is from energy-strain relation, and the other (filled circles) is from stress-strain relation. Dashed line represents the modulus defined in Eq. (5.39).

As mentioned in the introduction, the instability for systems like Au was expected to occur along the primary loading path of hydrostatic expansion[14]. However, our results show that the occurrence of the shear instability at $a/a_0 = 1.06$ precedes and intervenes the volumetric instability that occurs at $a/a_0 = 1.12$. This preemptive effect represents clearly a stability bifurcation deviating from the primary loading path. To illustrate this point further, we plot the shear stress-strain relations in figure 5.6 for the system subject to the rhombohedral shear strain η_4 at given hydrostatic expansion. The stress-strain relations show that, when $a/a_0 < 1.06$, the slope of this $\sigma_4 - \eta_4/2$ curve at the initial point is positive, i.e. $B_{44} > 0$, when $a/a_0 \geq 1.06$, the slope becomes negative, i.e. $B_{44} \leq 0$. As shown in figure 5.2, the slope of the volumetric stress-strain curve along the

hydrostatic strain direction, or the bulk stiffness constant B_T , is still positive at $a/a_0 = 1.06,$ and only becomes zero at $a/a_0 = 1.12$. Note that the negative stress-strain relation at small strain, which corresponds to unstable state, is predicted from the calculation when the finite strain is imposed to the system. In reality, of course, such scenario may not be seen as a possible change of structure could occur precipitously.

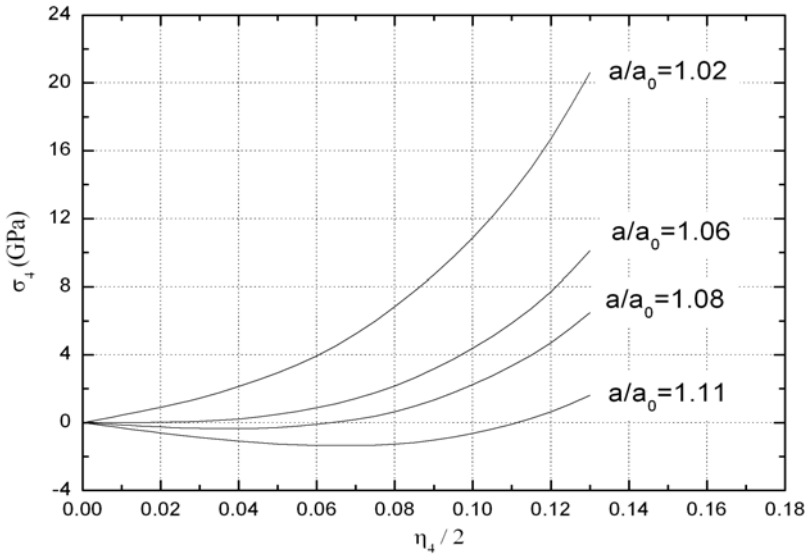

Figure 5.6 At each configuration with hydrostatic expansion, we give a perturbation of rhombohedral shear strain η_4 and calculate the stress-strain relation for the system. The slope of the curve is the rhombohedral shear stiffness modulus B_{44} which becomes negative at $a/a_0 \sim 1.06$.

5.2.5 Discussion

The stability limits for Au was investigated earlier by Yip *et al* using classical molecular dynamics simulation[14]. In their work, the bulk stiffness modulus disappears first with volume expansion at around $a/a_0 = 1.06$ that was followed by void formation. The tetragonal shear stiffness modulus remains larger than zero until $a/a_0 = 1.09$ and the rhombohedral shear stiffness modulus is nonzero until $a/a_0 = 1.08$. The results led them

to conclude the instability is caused by volumetric instability, or along the primary loading path. The difference between the MD and the current DFT calculation could originate from several causes. Firstly, since a semiempirical interatomic potential was used in the MD simulation, certain differences should be expected as compared with *ab initio* calculations, especially when dealing with large deformation strains (6-12%) which may not be adequately considered when fitting the potential. Secondly, since the MD work was performed at elevated temperatures (200~1200 K), one would expect that elastic constants as well as the elastic stiffness constants are different. Consequently, the softening of these constants at high temperature should lead to smaller critical strains corresponding to the instability points (Eqs, (5.32) and (5.33)) than those at zero temperature as seen in our DFT calculation. However, as known that the bulk modulus decrease versus temperature rise is in general much slower than the shear moduli for most metals including Au[110], one would still expect to see shear instability intervene before the volumetric instability, as the shear moduli are already much smaller than the bulk modulus in the first place. Thirdly, the stability limits in the MD results were obtained from extrapolations from the datum points away from the critical points, as known that the increasing thermal fluctuation makes the MD simulation less reliable close to those points[33] In contrast, in the DFT calculation, we can push the calculation very close to and even beyond the instability points. Finally, it is worth noting that the small sample size used in the DFT calculation may limit the void formation which was identified as the hallmark of instability in the MD work. But this limitation is irrelevant in the elastic stability modeling since we are only focus on approaching the stability limit from one side of the phase, not how the new phase (i.e. void) forms.

Besides these technical reasons, we believe that some of these differences are rooted in the fundamental interpretation of structure or lattice stability. As pioneered by Born, the elastic instability of a lattice is governed by the vanishing of the convexity of the elastic energy as the function of varying strain. The first application of this theory was to melting of crystals[5-6] where vanishing of the shear modulus at the onset of liquid phase formation was thought to be a direct indication of the elastic instability. Under applied stress, Born's convexity argument should still hold but with a few modifications by Hill and Milstein[7-8]. As argued by Born and later Hill, the presence of many fluctuations and secondary processes accompanying the primary deformation strain, including sample loading conditions and rotations, could lead to the instabilities different from that expected from the primary deformation path. In the hydrostatic expansion of Au, as we clearly demonstrated, it is the shear instability that precedes the volume or bulk instability. This bifurcation process, as we identified here, must be treated carefully when identifying the instability points and subsequently the formation of new structures or defects.

Moreover, we should note that the bifurcation observed along the rhombohedral shear direction simply tells us that the atoms in the system at the instability point are going to be engaged in displacement along the rhombohedral shear directions, thus breaking the original crystal symmetry. For the same reason, the atomic displacement is not necessarily correlated, but rather random. This leads to local symmetry breaking that precedes the local volume expansion, eventually resulting in void formation. In other words, the so-called volumetric instability with void formation may be initiated or nucleated by the shear deformation. In order to test this mechanism directly, one may

need to use a system with the minimum dimension larger than the critical nucleation size of the void.

The calculations that we performed focus mostly on the long-wave phonon limit and zero temperature. It is possible that, before violating the rhombohedral shear stability condition, some soft phonon modes or other instability may appear in the hydrostatically deformed crystal. Actually recent studies on elastic[18] and phonon[21] instabilities of aluminum verify the suggestion that this may happen in FCC metals.

5.2.6 Conclusion

In this work, we first identified the elastic stiffness constant as coefficient of the stress-strain relation in an arbitrary deformed state. And then use it to explain the stability criterion. This type of interpretation is what Frenkel and Orowan originally proposed for judging the stability limit for solids. Using an *ab initio* calculation, we explored the elastic stability in terms of the relations between the internal energy, stress, and strains in Au subject to hydrostatic stress (tension and compression). More importantly, we introduced perturbations along non-primary loading direction. We show from the results that the stability limit of Au under hydrostatic load is governed by the rhombohedral shear perturbation-induced instability, not by volumetric instability which occurs at a delayed critical volume strain. The preemptive shear instability represents a bifurcation of the crystal instability away from the primary loading path, as originally concerned by Born and Hill.

5.3 Ideal strength of gold under hydrostatic stress

5.3.1 Introduction

The ideal strength of single crystal under various loading has been investigated extensively in the past[18-19, 27-28, 111]. Au is one of the noble metals with small elastic anisotropy and also the least number of polymorphic transitions under applied stress, making it a convenient model system to test certain theoretical ideas. On the other hand, Au is a material with many current and potential applications, for example, the one-dimensional gold nanowire with a potential for novel electronic devices[112]. Its mechanical properties are therefore of a great interests. As shown in the previous *ab initio*, first-principles calculations, and atomistic simulations[18-19, 27-28, 111], Au single crystal exhibits a few structural transitions under uniaxial tension and compression loading. Under tension, Au exhibits an fcc-to-fct transition along [100] direction; and under compression, it shows a fcc-to-bcc or bct transition. For Au nanowires, there seem to be myriad structural transformations. However, as the small size wires are starved of defects, dislocation or stacking fault, the structural transitions may just be the manifestation of the polymorphisms observed in the perfect single crystal sample under surface stress, depending on the wires' initial orientations, cross-sectional shapes, and sizes[113-120]. Although there are extensive works performed to obtain the ideal strengths and structural transformations in defect-free single crystal Au, several issues still remain and call for another, more accurate calculation. One is that the precision of the results from these calculations. The earlier work used semi-empirical embedded atom method (EAM) potentials[27-28]. Although some of these potentials are quite sophisticated, as they are fitted to the second- and third-order elastic moduli, at a large strain, usually larger than 10%, the effects of the potentials still needs to be checked independently by other methods[93]. *Ab initio* electronic structure calculations, on the other hand, do not possess the

shortcoming of those semi-empirical methods, and have been performed for various strained structures and are shown to give accurate results on ideal strength of materials[18-20, 121-124]. However, few have been performed for Au, although calculations for other fcc metals are abundant. For example, Li *et al* studied the ideal tensile strength of Al[18]. Cerny *et al* worked on the ideal tensile strength of Cu[19]. The second issue is the calculation and formulations of elastic stability criterion and the elastic stiffness constants used in previous works that may leads to different answers. For example, Li *et al* did not use the symmetrized elastic stiffness coefficients. In addition, how they calculated each independent component of elastic constants at any given stress state to test the stability conditions is not clear. And the Young's modulus calculated by Cerny *et al* may only be valid in small deformation while the strain corresponding to stability limit is much larger.

In this part, we employ an *ab initio* calculation based on density functional theory to investigate the ideal strength of Au under uniaxial stress along the [100] direction. We organize this part as follows. In next section, we briefly review the stability criterion of a cubic crystal under external loading. In section 5.3.3, we introduce our calculation models and methods. In section 5.3.4, we show our results, and give discussions and comparisons with the previous works. Finally, we will draw conclusions from this work.

5.3.2 Stability of crystal solids under external stress

Although there are quite a few versions of the elastic stability criteria to judge whether or not a crystalline solid becomes unstable, from which we could obtain the ideal strength, we shall use the one derived from the stress-strain relation at any arbitrary deformed state[20]. Consider that a material in configuration X under stress $\tau_{ij}(X)$ is

undergoing a small displacement, i.e., with a small value of η_X^Y, the system will move to a new state Y with a corresponding stress $\tau_{ij}(Y)$. The two stresses are related by a linear proportional coefficient of stress versus strain between two states of the system[22],

$$\tau_{ij}(Y) = \tau_{ij}(X) + B_{ijkl}(\eta_X^Y)_{kl} + O[(\eta_X^Y)^2] \ . \tag{5.60}$$

From equation (5.60) we know that $\delta\tau = B\eta$, so if the material at the state X is stable, the increment of the stress vector (with Voigt notation, $\delta\tau = (\delta\tau_1, \delta\tau_2, \delta\tau_3, \delta\tau_4, \delta\tau_5, \delta\tau_6)$ and $\eta = (\eta_1, \eta_2, \eta_3, \eta_4, \eta_5, \eta_6)$; both stress and strain tensors can be treated as vectors) must remain positive when projected to the direction of the perturbative strain η. Otherwise, the system becomes unstable. This criterion is what Frenkel[1] and Orowan[2] originally proposed for the ideal strength of a material. The coefficient is defined as,[22]

$$B_{ijkl} = C_{ijkl} + (1/2)(\delta_{ik}\tau_{jl} + \delta_{jk}\tau_{il} + \delta_{il}\tau_{jk} + \delta_{jl}\tau_{ik} - 2\delta_{kl}\tau_{ij}), \tag{5.61}$$

where τ_{ij} is the internal stress at (stressed) state X, and $C_{ijkl} = V^{-1}(\partial^2 U / \partial\eta_{ij}\partial\eta_{kl})_{\eta=0}$ is the elastic constants at state X. This derivation of B_{ijkl} can also be obtained directly from the stability criterion proposed by Hill and Milstein[7, 9-11] where, with a perturbative strain η, a solid can only be stable when the change of the internal energy U is larger than the external work W done to the system, or $\delta U - \delta W = \eta^T B\eta > 0$.

B_{ijkl} is in general asymmetric while $ij \leftrightarrow kl$, unless the applied stress is hydrostatic, $\tau_{ij} \propto \delta_{ij}$. The stability criterion $\eta^T B\eta > 0$ will be valid if and only if its symmetrized counterpart, $\overline{B} = (1/2)(B^T + B)$, is positive-definite, or

$$\det|\overline{B}| > 0 \ . \tag{5.62}$$

The system will become unstable when $\det|\overline{B}|=0$ for the smallest stress or strain during deformation. In other words, as $\overline{B}$ is a function of the deformation strain, the stability criterion will lead to a set of relations among the components of $\overline{B}_{ijkl}$ at the critical applied strain.

For an fcc crystal under a uniaxial stress along the [100] axis, $\tau_{ij}=\tau\delta_{i1}\delta_{j1}$, where $i,j=1,2,3$, the lattice symmetry will become tetragonal after deformation. Then the number of independent elastic stiffness coefficients increase from three to six: $\overline{B}_{11}, \overline{B}_{12}=\overline{B}_{13}, \overline{B}_{22}=\overline{B}_{33}, \overline{B}_{23}, \overline{B}_{44}, \overline{B}_{55}=\overline{B}_{66}$. Here we simplify the subscript in the tensor notion by using the Voigt notation ($11\to1$, $22\to2$, $33\to3$, $23\to4$, $31\to5$, and $12\to6$). The applied stress affects only the components of $\overline{B}$ that involve the [100] axis: $\overline{B}_{11}=C_{11}+\tau$, $\overline{B}_{12}=C_{12}-\tau/2$, $\overline{B}_{55}=C_{55}+\tau/2$, and $\overline{B}_{ij}=C_{ij}$ for all other components. The determinant of $\overline{B}$ is,

$$\det\left|\overline{B}\right|=(\overline{B}_{22}-\overline{B}_{23})\overline{B}_{44}\overline{B}_{55}^2[\overline{B}_{11}(\overline{B}_{22}+\overline{B}_{23})-2\overline{B}_{12}^2].$$

The criterion, $\det|\overline{B}|>0$, gives four stability conditions, two of which are associated with applied stress explicitly:

$$\overline{B}_{11}(\overline{B}_{22}+\overline{B}_{23})-2\overline{B}_{12}^2>0\Leftrightarrow(C_{11}+\tau)(C_{22}+C_{23})-2(C_{12}-\frac{\tau}{2})^2>0, \tag{5.63}$$

$$\overline{B}_{22}-\overline{B}_{23}>0\Leftrightarrow C_{22}-C_{23}>0, \tag{5.64}$$

$$\overline{B}_{44}>0\Leftrightarrow C_{44}>0, \tag{5.65}$$

$$\overline{B}_{55}>0\Leftrightarrow C_{55}+\frac{\tau}{2}>0. \tag{5.66}$$

Equation (5.63) is different slightly from that presented by Wang *et al*[13] and by Li *et al*[18], as they did not use symmetrized quantity $\overline{B}$. So there is a correction of the order of $C_{12}\tau$ to the last term in the equation. The Young's modulus that governs a fully relaxed stretch along [100] is

$$E_{100} = (S_{11})^{-1} = \frac{\overline{B}_{11}(\overline{B}_{22} + \overline{B}_{23}) - 2\overline{B}_{12}^2}{\overline{B}_{22} + \overline{B}_{23}}, \tag{5.67}$$

where S_{ij} is the elastic compliance tensor for tetragonal crystals. Here E_{100} in general does not equals to $\overline{B}_{11}$, the modulus for an unrelaxed stretch in the same direction.

The first condition (Eq. (5.63)) is equal to that the Young's modulus $E_{100} > 0$. The second one involves symmetry breaking (bifurcation) with tetragonal shearing deformation. In the latter case the crystal may branch away from the tetragonal path to a face-centered orthorhombic path. The last two conditions give other types of shear instabilities, and the crystal symmetry will evolve monoclinic if those conditions are violated. The ideal tensile or compressive strength is the corresponding value of the normal stress τ_1 at which any one of the above four conditions starts to be violated.

5.3.3 Calculation details

We perform the *ab initio* DFT calculations using the Vienna *ab initio* Simulation package (VASP)[84] developed by the Hafner Research Group at the University of Vienna. VASP uses pseudopotentials or the projector-augmented wave method and a plane wave basis set. To simulate the deformation under uniaxial stress, we first calculate the properties (total energy and equilibrium lattice parameter) of a single face-centered cubic crystal Au in the ground state. To obtain lattice parameter that is in better agreement with experimental value, we use the exchange-correlation energy evaluated with the local

density approximation. Ultrasoft pseudopotentials[50] are always employed to describe the electron-ion interactions. We use $18\times18\times18$ k-point mesh in our calculations following the Monkhost-Pack scheme, that is sufficient to reach the desired convergence of the total energy and elastic constants. The cutoff energy $E_{cutoff}^{Au}=292$ eV is large enough for the total energy to converge to the stable equilibrium state. For Au, the ground state has a face-centered cubic structure with the lattice parameter a_0=4.07 Å, which is very close to experimental measurement 4.08 Å[85] at room temperature. We thus use 4.07 Å as the lattice parameter in our supercell, a face-centered cubic cell containing four atoms, to perform the following simulation work for deformation.

The elastic stiffness constants and the elastic stability conditions (5.63)-(5.66) can be obtained from the variation of the internal energy per atom and the normal stress σ_1 with the Lagrangian strain η_1. Firstly, we apply a small amount of stretch, δa_1, to the supercell along the direction of the lattice parameter a_1; it becomes $a_0+\delta a_1$ and $a_1/a_0=\sqrt{1+2\eta_1}$. Then, we hold the length of a_1 while allow the other lattice parameters a_2 and a_3 perpendicular to a_1 to relax to the state with $\sigma_2=\sigma_3=0$ while maintaining $a_2=a_3$, and then record the values of internal energy U and normal stress σ_1. We change the value of δa_1 again and repeat the above procedure. Thus, we simulate a strain-controlled uniaxial loading for the crystal. Figure 5.7 and figure 5.8 give us the $\delta U-\eta_1$ and $\sigma_1-\eta_1$ relations.

The stability condition (5.63) corresponds to the requirement that E_{100} is positive. Cerny *et al*[19] used the relation $E_{100}=(1/a_2^2a_0)d^2U/d\varepsilon^2$ to get Young's modulus E_{100},

where $\varepsilon = a_1 / a_0 - 1$. Their definition of Young's modulus is an approximation with a second term $2\upsilon\sigma a_0 / a_2$ missed, where υ is the Poisson's ratio. Thus the value of Young's modulus is underestimated especially with a finite value of strain, and the related tensile instability is predicted at a lower strain value. In this work, we use the following relation,

$$E_{100} = \left(S_{11}\right)^{-1} = \left(d\zeta_1 / d\sigma_1\right)^{-1}. \tag{5.68}$$

Here ζ_1 is the local Lagrangian strain calculated under the current coordinate frame. In order to obtain $d\zeta_1 / d\sigma_1$, we need the relation, $\zeta_1 - \sigma_1$. In other words, we need to have ζ_1 at each given stress σ_1 so its derivative can be obtained. Since the calculated $\sigma_1 \sim \eta_1$ relation is discrete, to obtain $d\zeta_1 / d\sigma_1$, we use the following method: For each configuration X' with a certain value of $\eta_1^{'}$ relative to the initial state, we select a few points nearby around $\eta_1^{'}$ from the calculated $\sigma_1 \sim \eta_1$ curve and calculate the new Lagrangian strain value ζ_1 for each point using X' as the reference configuration. We make a linear fitting to obtain the value of Young's modulus E_{100} using Eq. (5.68) for configuration X'. Although tedious, the procedure gives a better result at finite strain, especially at the instability point of the crystal.

The violation of stability condition (5.64) corresponds to tetragonal shear instability. For condition (5.64), there may be a potential bifurcation from the primary deformation path, where the lattice could acquire orthorhombic symmetry. In order to test the second stability condition, the following Jacobian matrix and corresponding strain matrix were used at each point of our primary deformation path, that is, the uniaxial loading:

$$J=\begin{pmatrix}1 & 0 & 0\\ 0 & \sqrt{1+2x} & 0\\ 0 & 0 & \sqrt{1-2x}\end{pmatrix},\qquad \zeta=\begin{pmatrix}0 & 0 & 0\\ 0 & x & 0\\ 0 & 0 & -x\end{pmatrix}.$$

With such deformation, the stress-strain relation (5.60) gives

$$\delta\sigma_2=-\delta\sigma_3=(B_{22}-B_{23})x+O(x^2).$$

So, the condition specified in Eq. (5.64) can be obtained through the derivative, $B_{22}-B_{23}=\delta\sigma_2/\delta x$.

The violation of stability condition (5.65) is another shear instability related to the shear stiffness coefficient B_{44}. To obtain B_{44} we apply the perturbative Jacobian matrix and corresponding strain:

$$J=\begin{pmatrix}1 & 0 & 0\\ 0 & 1-x^2/2 & x\\ 0 & x & 1-x^2/2\end{pmatrix},\qquad \zeta=\begin{pmatrix}0 & 0 & 0\\ 0 & 0 & x\\ 0 & x & 0\end{pmatrix}$$

to each configuration along our $\sigma_1-\eta_1$ curve under uniaxial loading. We have the relation $\delta\sigma_4=2B_{44}x+O(x^2)$ and thus $B_{44}=\frac{1}{2}\frac{\delta\sigma_4}{\delta x}$.

The stability condition (5.66) can be tested using the Jacobian matrix and corresponding strain:

$$J=\begin{pmatrix}1-x^2/2 & 0 & x\\ 0 & 1 & 0\\ x & 0 & 1-x^2/2\end{pmatrix},\qquad \zeta=\begin{pmatrix}0 & 0 & x\\ 0 & 0 & 0\\ x & 0 & 0\end{pmatrix}.$$

The stress-strain relation under such deformation and the elastic stiffness modulus B_{55} can be obtained through $\delta\sigma_5=2B_{55}x+O(x^2)$, and $B_{55}=\frac{1}{2}\frac{\delta\sigma_5}{\delta x}$.

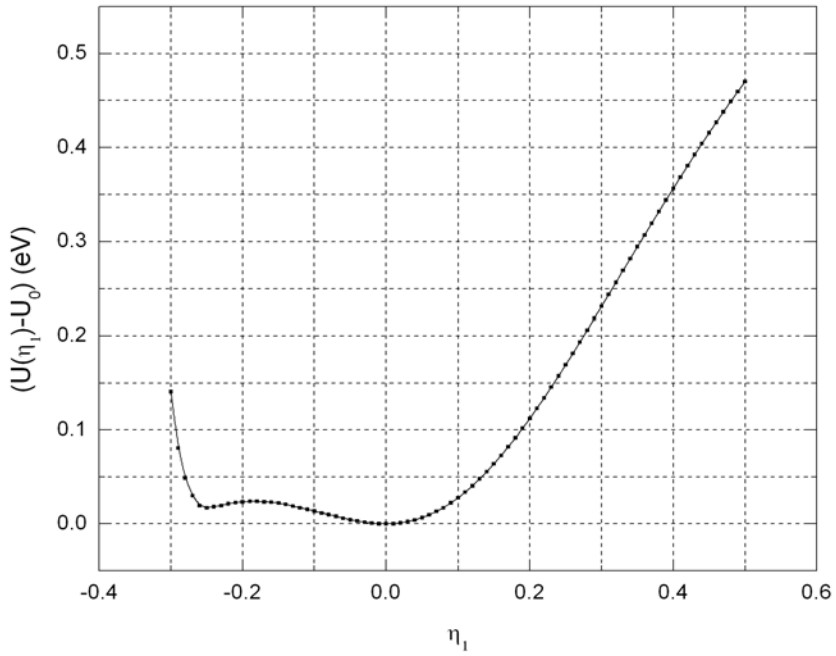

Figure 5.7 The change of the internal energy per atom as a function of strain η_1. It is shown that under compressive stress there is a metastable bct structure at $\eta_1 = -0.25$ and an unstable bcc structure at $\eta_1 = -0.19$.

5.3.4 Results and discussions

Figure 5.7 shows that the change of internal energy per atom as a function of strain during simulated uniaxial loading test along the [100] direction. The global minimum point of internal energy at the curve corresponds to $a_0 = 4.07$ Å. When the lattice parameter a_1 increases from 4.07Å, the change of internal energy per atom increases monotonically over the simulation region. When the lattice parameter a_1 decreases from 4.07Å, the change of internal energy per atom will first increase until it reaches a local maximum, where Lagrangian strain is -0.19 at $a_1 = 3.205$, then decrease

to a local minimum, where Lagrangian strain is -0.25 at $a_1 = 2.880$ Å (about the same as the result obtained by Haftel *et al*, 2.87 Å[125]), and then increase again.

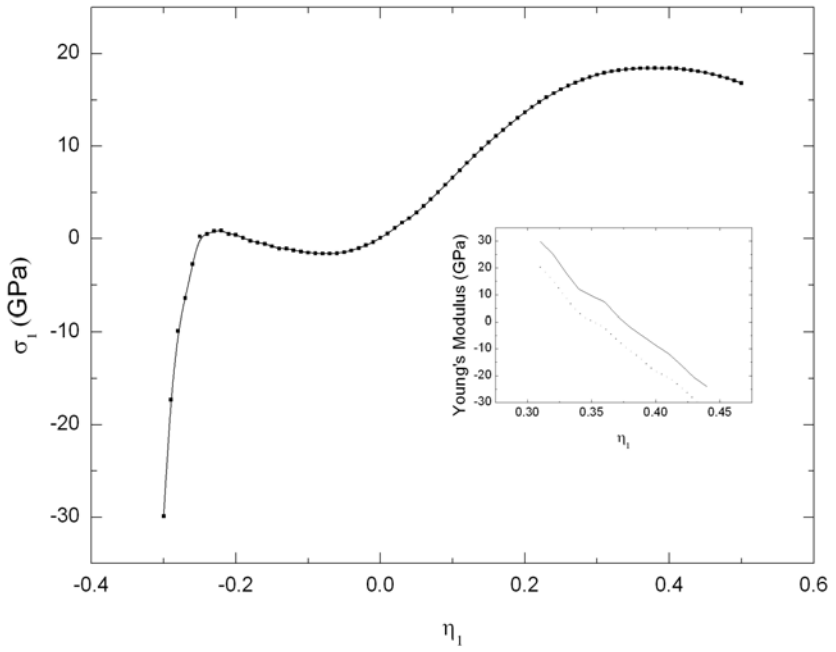

Figure 5.8 Variation of the normal stress σ_1 with strain η_1. Under compression, $\sigma_1 = 0$ where the metastable bct and unstable bcc structures should form. Under tensile elongation, σ_1 reaches its maximum value (18.44 GPa) at $\eta_1 = 0.38$ where the Young's modulus approaches zero as shown by the solid line in the inset. The dotted line in the inset is the Young's modulus calculated according to the definition from Ref. 19. It vanishes at the strain of 0.35 that corresponds to the normal stress of 18.36 GPa, lower than the maximum value of normal stress.

Figure 5.8 shows the normal stress σ_1 versus strain η_1. When the lattice parameter a_1 increases from 4.07Å, a maximum normal stress occurs at $a_1 = 5.386$ Å, and the corresponding Lagrangian strain is 0.38 and the normal stress is 18.44 GPa (theoretical fracture strength). Corresponding to the maximum stress, the Young's modulus is almost

zero as expected (see the inset of figure 5.8). Let us note that Young's modulus calculated with the definition in Ref. 19 (disregarding the term $2\upsilon\sigma a_0 / a_2$) vanishes at the strain of 0.35, that corresponds to the normal stress of 18.36 GPa, sort of lower than its maximum value. When the lattice parameter a_1 decreases from 4.07Å, the normal stress σ_1 will firstly decrease to negative values, and reach a local minimum value of -1.60 GPa at Lagrangian strain -0.07; and then it will increase to pass through zero at the

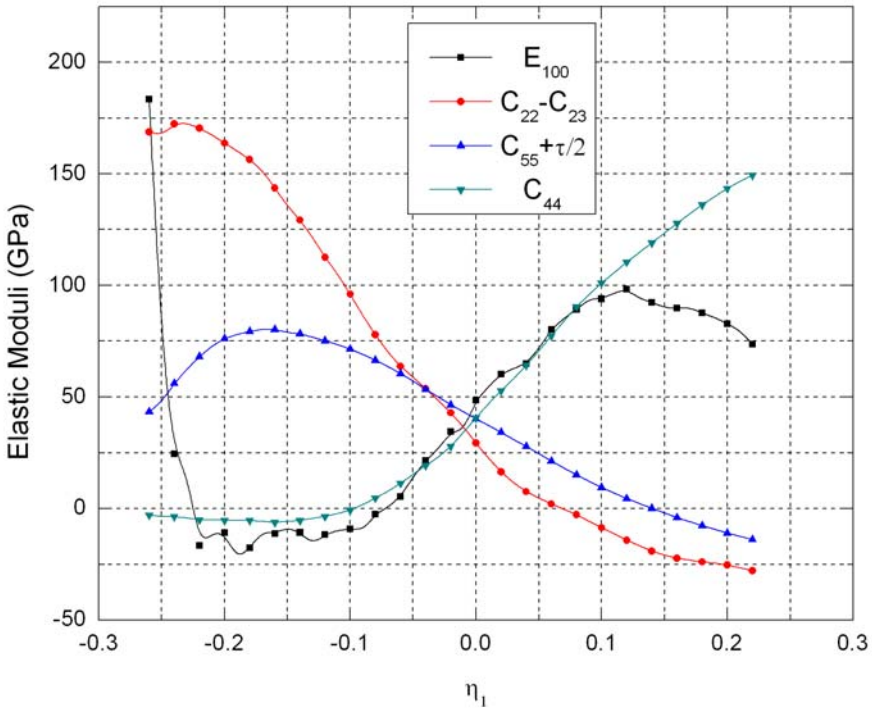

Figure 5.9 The stability conditions (Eqs. (5.63-5.66)) plotted using the elastic constants calculated from the *ab initio* method. It is shown that under compression, the Young's modulus goes to be zero first; under elongation, the tetragonal shear modulus goes to zero first. Stable region corresponding to the above stability limits is in the strain range, $\eta_1 \sim (-0.07, 0.07)$, while the corresponding ideal compressive and tensile strength are at -1.6 and 4.2 GPa respectively.

lattice parameter $a_1 = 3.205$ Å. Afterwards, the stress σ_1 will decrease again and pass through zero at $a_1 = 2.880$ Å, and then decreases with further compression. Compared with figure 5.7, we know that the two points at $\sigma_1 = 0$ correspond to a local maximum and a local minimum of the internal energy respectively.

When an fcc crystal is stretched along [100] direction, the homogeneously deformed crystal structure may be described as a bct structure throughout all processes. The fcc and bcc structures may be considered as special cases of the bct structure with $a_1 = a_2 = a_3$ and $\sqrt{2}a_1 = a_2 = a_3$, respectively. The point of $a_1 = 3.205$ Å corresponds to $a_2 / a_1 = 1.431$, that indicates a bcc crystal. Milstein *et al*[97] found the same result with a central-force Morse potential calculation. Since the bcc phase corresponds to the local maximum of the internal energy, it is unstable.

Figure 5.9 shows that under compressive or tensile stress along the [100] axis, one of the four stability conditions ((5.63)-(5.66)) would fail firstly. It is shown that when the uniaxial compressive stress is applied, the stability condition $\overline{B}_{11}(\overline{B}_{22} + \overline{B}_{23}) - 2\overline{B}_{12}^2 > 0$ would be violated first at Lagrangian stain at -0.07. Under further compression, the absolute value of σ_1 would decrease rather than increase. When a tensile stress is applied, instead of E_{100} approaches zero first, the stability condition $\overline{B}_{22} - \overline{B}_{23} > 0$ would fail first at Lagrangian strain at 0.07. The corresponding stress σ_1 at the two instabilities is -1.6 and 4.2 GPa, which give us the ideal compressive and tensile strength. The corresponding stable phase region defined by the Lagrangian strains is thus from -0.07 to 0.07. The occurrence of the shear instability at $\eta_1 = 0.07$ when condition in Eq. (5.64) is violated precedes the theoretical fracture strength at $\eta_1 = 0.38$ where Young's modulus

approaches zero. This is the so-called bifurcation deviated from the primary deformation path along the uniaxial stress. This phenomenon was also seen by Milstein *et al* with EAM potential[27]. In their work, they show that the theoretical fracture strength is 22.5 GPa, where axial stretch $\lambda_\alpha = 1.207$; the stability condition $\overline{B}_{22} - \overline{B}_{23} \geq 0$ is violated at $\lambda_\alpha = 1.102$, with $\sigma_1 = 10.0$ GPa. Here the stretch λ_α is defined as its length in the current state divided by its initial length: $\lambda_\alpha = a_1 / a_0 = \sqrt{1+2\eta_1}$. Their results of ideal tensile strength and theoretical fracture strength are both larger than ours. As mentioned before, their EAM model was formulated to reproduce empirical values. However, according to our experience[93], at such a large strain range which is beyond 0.10, the fourth-order elastic moduli would make contributions and must be taken into account in the fitting of the potentials. Zhang *et al*[28] employed a modified analytic EAM (MAEAM) model to investigate the same problem. They showed that the ideal strength is -2.21 GPa in compression and 6.31 GPa in tension, and the stable region in strain ($a_1 / a_0 - 1$) is from -9.83 to 7.87%. Their results are in better correspondence with our *ab initio* calculation results. Recently Cerny *et al*[126] presented a new way to estimate uniaxial tensile strength on the basis of theoretical shear strength calculations. Their work shows that the ideal tensile strength is 5.8 GPa from the rigid-planes approach, and 3.6 GPa from the relaxed-planes approach.

5.3.5 Conclusion

In this work we employ *ab initio* calculation based on density functional theory to investigate the elastic stability of face-centered cubic crystal gold under uniaxial stress along the [100] axis. We treat the elastic stiffness moduli as the linear coefficients of stress-strain relations, which gives a new interpretation of the stability criterion as

Frenkel and Orowan originally proposed to judge the stability limit for solids. With this criterion, we show that the stability limit, of the perfect Au crystal under tensile stress is related to the vanishing of tetragonal shear stiffness coefficient as predicted in the previous work, but with a smaller value in the ideal tensile strength, 4.2 GPa, at a less Lagrangian tensile strain of ~0.07. The potential bifurcation from the primary loading path is also shown. The stable region is found in the range from -1.6 GPa to 4.2 GPa in the ideal strength, or from -0.07 to 0.07 in the Lagrangian strain. These results are inline with those predicted from atomistic calculations using semi-empirical potentials more qualitatively than quantitatively to point out that more accurate fitting procedure is needed in the potentials used.

CHAPTER SIX

NONLINEAR THEORETICAL FORMULATION OF ELASTIC STABILITY CRITERION OF CRYSTAL SOLIDS

6.1 Introduction

Born formulated the elastic stability criterion in the context of thermal melting of a crystal[5, 94]. Born's criterion states that to ensure a crystalline solid in a stable state, the determinant of the second-order elastic constant tensor must be non-negative, $|C| > 0$. This says that given a strain η such as in thermal melting, the variation of the internal energy of system must remain positive and convex if the system is in a stable state. Furth[95] quickly realized that the Born criterion also sets the limit of the strength of a perfect crystal subject to external stress that causes a deformation strain. Thus $|C| \to 0$ would be the elastic stability condition at temperature below melting point when the crystal is under external stress. Since the Born criterion is formulated for crystalline solids in stress-free state, Furth's generalization is clearly invalid as the elastic constants at finite deformation depend on applied stress[22]. Born's criterion for crystals in deformed state should be replaced by the stress-dependent elastic constants. The general expression for the elastic constants under arbitrary applied stress was derived by Wallace[22] in the context of formulating equations of elastic wave propagation in stressed crystals; he called it *elastic stiffness constant*,

$$B_{ijkl} = C_{ijkl} + (1/2)(\delta_{ik}\tau_{jl} + \delta_{jk}\tau_{il} + \delta_{il}\tau_{jk} + \delta_{jl}\tau_{ik} - 2\delta_{kl}\tau_{ij}) \quad (6.1)$$

Here $C_{ijkl} = \rho \partial^2 F / \partial \eta_{ij} \partial \eta_{kl}$ is the elastic constant, and ρ is the density of the material in a deformed state. The Born stability criterion then becomes

$$\left| B \right| > 0 . \tag{6.2}$$

Eq. (6.2) reduces to the original Born criterion at zero applied stress ($\tau = 0$), $B = C$.

In chapter five, we showed that the general stability criterion shown in Eq. (6.2) is related to the one proposed much earlier by Polanyi, Frenkel, and Orowan[1-2, 98, 127] for predicting the ideal strength of a crystal. The connection is through the relation

$$\tau_{ij}(x) = \tau_{ij}(X) + B_{ijkl}\eta_{kl} + O[(\eta_{kl})^2], \tag{6.3}$$

where $\tau_{ij}(x)$ is the stress at a current deformed state x away from a reference state X , $\tau_{ij}(X)$ is the stress at state X , and η is the Lagrangian strain from state X to state x . If x is sufficiently close to X , the stability criterion is set by

$$\partial \tau_{ij} / \partial \eta_{kl} \to 0 \tag{6.4}$$

which is the Frenkel-Orowan criterion.

Using mainly the generalized Born criterion, Eq. (6.2), a large number of theoretical and computational work has been performed[31], to investigate the elastic stability problems associated with phase transition, ideal strength, and crystal defect formation, etc. Continuum model with finite element method[25], atomistic simulation with embedded atom method (EAM)[27-28], and *ab initio* quantum mechanic simulation[18-20, 29] have been employed extensively in various calculations. All these models however require a tremendous amount of computational resources, among which the largest fraction is on calculation of the second order elastic constants C_{ijkl}'s in each deformed state. For *ab initio* calculation, the total energy needs to be calculated and used later to

obtain C_{ijkl}'s; for atomistic simulation, C_{ijkl}'s can be obtained using either analytical expression or fluctuation formula. For the latter case, a large amount of computation resource is needed to guarantee the convergence of fluctuations so that reliable results can be acquired[33-34]. In addition, the elastic stability criterion as expressed in Eq. (6.2), though simple, often encapsulates the physical mechanisms underlying the stability limit. For example, anharmonic effects present in a crystal under applied stress play an important role in softening the material, leading to elastic instability. By focusing on only the second order elastic constants C_{ijkl}'s, this and other effects often manifested in higher order elastic constants are often masked.

In this work, we present a general theoretical framework of elastic stability criterion using higher order elastic constants. In finite deformation theory, both the stress and the second order elastic constants in a stressed state can be expressed in a series expansion in terms of the deformation strain with the expansion coefficients being the elastic constants of higher orders from a reference state. Choosing the reference state as the zero stress state, we obtain the stability criterion as expressed in Eq. (6.2) in terms of the second and higher order elastic constants at zero stress states. Many of these zero stress elastic constants are now available either from experiments or theoretical calculations, making it extremely desirable, and possible, to use the nonlinear formulation analytically to predict stability and ideal strength of crystalline materials without resorting to extensive computation.

This chapter is organized as follows. In section 6.2, we present a unified theory for stress, elastic constant, and elastic stiffness coefficient. We express the elastic stability criterion and the nonlinear formulation using higher order elastic constants. Instances of

the stability criterion for cubic crystals under hydrostatic and uniaxial stress will be given. In section 6.3, we present the methods to test the new theoretical formulations of stability conditions with high order elastic constants of the materials under zero stress. In section 6.4, we give the results obtained from several crystal systems whose higher order elastic constants are available. They include the stability region expressed by the strain limits, ideal strength or stress, and possible bifurcation mode of cubic crystal metals, such as Au, Al, and Cu. Available results from our *ab initio* calculation and other theoretical work are also shown for comparison. In section 6.5, we discuss the new method and its applications, along with the limitations, mostly from the view of the quality of the input data. Finally, in section 6.6, we draw conclusions from this work.

6.2 Theory

6.2.1 Finite deformation theory of stress and elastic constant

Suppose a material point in configuration X under stress $\sigma_{ij}(X)$ is undergoing a small displacement, i.e., with a strain η, to a new state x with a corresponding stress $\sigma_{ij}(x)$. We assume, without loss of generality, that the displacement could be arbitrary and infinitesimal as needed. The corresponding change of the Helmholtz free energy $F(x,T)=F(\eta,T)$ at state x from $F(X,T)=F(0,T)$ at sate X is expressed as

$$F(\eta,T)=F(0,T)+\left.\frac{\partial F}{\partial \eta}\right|_{X,\eta'}\eta+\frac{1}{2!}\left.\frac{\partial^2 F}{\partial\eta\partial\eta}\right|_{X,\eta'}\eta\eta+\frac{1}{3!}\left.\frac{\partial^3 F}{\partial\eta\partial\eta\partial\eta}\right|_{X,\eta'}\eta\eta\eta+\frac{1}{4!}\left.\frac{\partial^4 F}{\partial\eta\partial\eta\partial\eta\partial\eta}\right|_{X,\eta'}\eta\eta\eta\eta+\ldots, \tag{6.5}$$

correct to the fourth power in η with the understanding that all derivatives appearing in Eq. (6.5) are done at state X with all other strains η' held constant. The corresponding stress, the second- and third-order isothermal elastic constants at state X are then

$$\tau(X) = \frac{1}{V(X)} \frac{\partial F}{\partial \eta}\bigg|_{X,\eta'}, \tag{6.6a}$$

$$C(X) = \frac{1}{V(X)} \frac{\partial^2 F}{\partial \eta \partial \eta}\bigg|_{X,\eta'}, \tag{6.6b}$$

$$c(X) = \frac{1}{V(X)} \frac{\partial^3 F}{\partial \eta \partial \eta \partial \eta}\bigg|_{X,\eta'}, \tag{6.6c}$$

$$\tilde{c}(X) = \frac{1}{V(X)} \frac{\partial^4 F}{\partial \eta \partial \eta \partial \eta \partial \eta}\bigg|_{X,\eta'}, \tag{6.6d}$$

where $V(X)$ is the volume of the system at X. To avoid overcrowded notations, we shall not use indices for vectors and tensors unless necessary. Summation convention is automatically assumed. Following the same scheme, we can obtain the corresponding stress, the second- and third-order isothermal elastic constants at state x,

$$\tau(x) = \frac{1}{V(x)} \frac{\partial F}{\partial \xi}\bigg|_{x,\xi'}, \tag{6.7a}$$

$$C(x) = \frac{1}{V(x)} \frac{\partial^2 F}{\partial \xi \partial \xi}\bigg|_{x,\xi'}, \tag{6.7b}$$

$$c(x) = \frac{1}{V(x)} \frac{\partial^3 F}{\partial \xi \partial \xi \partial \xi}\bigg|_{x,\xi'}, \tag{6.7c}$$

where $V(x)$ is the volume of the system at state x, and ξ is a Lagrangian strain from state x to state y. Therefore, we can simply take a derivative of Eq. (6.5) with respect to ξ at state x, so we have, after dividing by $V(x)$ on both sides,

$$\tau(x)=\frac{1}{V(x)}\frac{\partial F}{\partial \xi}\bigg|_{x,\eta'}=\frac{V(X)}{V(x)}\frac{\partial \eta}{\partial \xi}\left[\tau(X)+C(X)\eta+\frac{1}{2!}c(X)\eta\eta+\frac{1}{3!}\tilde{c}(X)\eta\eta\eta+...\right]. \quad (6.8a)$$

Following the same scheme, we can systematically obtain the second and higher order elastic constants at state x in relation to those at state X,

$$C(x)=\frac{1}{V(x)}\frac{\partial^2 F}{\partial \xi\partial \xi}\bigg|_{x,\eta'}=\frac{V(X)}{V(x)}\frac{\partial \eta}{\partial \xi}\left[C(X)+c(X)\eta+\frac{1}{2!}\tilde{c}(X)\eta\eta+...\right], \quad (6.8b)$$

$$c(x)=\frac{1}{V(x)}\frac{\partial^3 F}{\partial \xi\partial \xi\partial \xi}\bigg|_{x,\eta'}=\frac{V(X)}{V(x)}\frac{\partial \eta}{\partial \xi}\left[c(X)+\tilde{c}(X)\eta+...\right], \quad (6.8c)$$

and so forth. As we show below, these relations enable us to formulate the nonlinear theory of elastic stability criterion.

6.2.2 Elastic stability of crystal solids under external stress

If the material at the state X is stable, given a small increment of strain η (with Voigt notation, a strain tensor is treated as a vector, $\eta=(\eta_1,\eta_2,\eta_3,\eta_4,\eta_5,\eta_6)$), the increment of the corresponding stress must remain positive along the direction of the perturbative strain η. Otherwise, the system at state X is unstable. This criterion, as we showed, is what Polanyi, Frenkel, and Orowan[1-2, 98, 127] originally proposed for estimating the ideal strength of a material where $\partial\tau_{ij}/\partial\eta_{kl}\to 0$. The elastic response coefficient defined as in Eq. (6.1) involves τ, the external stress at state X, or the Cauchy stress when the system is in equilibrium, and $C_{ijkl}=V^{-1}(\partial^2 U/\partial\eta_{ij}\partial\eta_{kl})_{\eta=0}$, the elastic constants at state X. This stability criterion can also be obtained from the stability criterion proposed by Hill and Milstein[7-11]. They showed that, with a perturbative strain η, a solid can be stable only if the variation of the internal energy or free energy F is larger than

the external work W done to the system, or $\delta(F-W)=\eta^T B\eta>0$. Both Polanyi-Frenkel-Orowan and Hill-Milstein models lead to the criterion, $|B|>0$.

Based on its definition, B_{ijkl} is in general asymmetric while $ij \leftrightarrow kl$, unless the applied stress is hydrostatic, $\tau_{ij} \propto \delta_{ij}$. The stability criterion $\delta(F-W)=\eta^T B\eta>0$ will be true only if the symmetrized counterpart of B, $\overline{B}=(B^T+B)/2$, is positive-definite, or $|\overline{B}|>0$. Specifically, for a cubic crystal subject to hydrostatic pressure P, $\tau_{ij}=-P\delta_{ij}$ and $\overline{B}=B$, due to preservation of the lattice symmetry. We follow the convention that the inward pressure is positive while outward pressure is negative (i.e., $P<0$ for tension). The stability conditions are,

$$B_T(\tau)=(B_{11}+2B_{12})/3=(C_{11}+2C_{12}+P)/3>0, \tag{6.9}$$

$$G'(\tau)=(B_{11}-B_{12})/2=(C_{11}-C_{12}-2P)/2>0, \tag{6.10}$$

$$G(\tau)=4B_{44}=4(C_{44}-P)>0. \tag{6.11}$$

Here we express the bulk stiffness modulus $B_T(\tau)$, tetragonal shear stiffness modulus $G'(\tau)$, and rhombohedral shear stiffness modulus $G(\tau)$ explicitly.

For a cubic crystal solid under a uniaxial stress along the [100] axis, $\tau_{ij}=\tau\delta_{i1}\delta_{j1}$, where $i, j=1,2,3$, the lattice symmetry will become tetragonal after deformation. The criterion, $|\overline{B}|>0$, gives four stability conditions, two of which are associated with applied stress explicitly[16]:

$$\overline{B}_{11}(\overline{B}_{22}+\overline{B}_{23})-2\overline{B}_{12}^2>0 \Leftrightarrow (C_{11}+\tau)(C_{22}+C_{23})-2(C_{12}-\frac{\tau}{2})^2>0, \tag{6.12}$$

$$\overline{B}_{22}-\overline{B}_{23}>0 \Leftrightarrow C_{22}-C_{23}>0, \tag{6.13}$$

$$\overline{B}_{44} > 0 \Leftrightarrow C_{44} > 0, \tag{6.14}$$

$$\overline{B}_{55} > 0 \Leftrightarrow C_{55} + \frac{\tau}{2} > 0. \tag{6.15}$$

Here, Voigt notation is applied. The first condition in Eq. (6.12) equals that of the Young's modulus, $E_{100} > 0$. The Young's modulus that governs a fully relaxed stretch along [100] direction is

$$E_{100} = (S_{11})^{-1} = \frac{\overline{B}_{11}(\overline{B}_{22} + \overline{B}_{23}) - 2\overline{B}_{12}^2}{\overline{B}_{22} + \overline{B}_{23}}, \tag{6.16}$$

where S_{ij} is the elastic compliance tensor for tetragonal crystals.

The ideal tensile or compressive strength of the crystal is the corresponding value of the normal stress τ at which any one of the above four conditions (Eq. (6.12-6.16)) starts to fail. This is slightly different from the Polanyi-Frenkel-Orowan criterion for theoretical strength mentioned above if the strain corresponding to the violation of the stability condition is not along the primary loading path, such as along the stretch along [100] direction. This phenomenon is called stability bifurcation[7-11, 20, 29]. The corresponding strain along the primary loading path where any one of the above four stability conditions is violated sets the strain limit for the materials.

6.2.3 Nonlinear theoretical formulation of elastic stability criterion

As mentioned in the Introduction, the necessary ingredient in acquiring the elastic stability criterion expressed in Eq. (6.2) is the second order elastic constants C_{ijkl} at the initial state. In any calculation, for each small increment of deformation strain, one must calculate C_{ijkl}, either from the total energy in *ab initio* calculation or fluctuations in atomistic simulation. This procedure demands a huge computing resource. Realizing the

relations expressed explicitly in Eq. (6.8) between the stress and elastic constants at any deformed state x and those at a reference state X, we can significantly simplify the procedure for acquiring the elastic stability criterion by using the reference at zero stress state or natural state as often called in mechanics where $\tau(X)=0$. We could express stress and elastic constants at any arbitrary stressed state x as the function of the deformation strain and the stress and elastic constants at the natural state. Considering only symmetric strain from X to x, use relations $a_{ij}=a_{ji}=\frac{\partial x_i}{\partial X_j}, \frac{\partial \eta_{ij}}{\partial \xi_{kl}}=a_{ki}a_{lj}$, the stress in Eq. (6.8) becomes

$$\tau_{ij}=(V_0/V)\sum_{kl}a_{ik}a_{jl}[\tau(0)_{ij}+\sum_{mn}C(0)_{klmn}\eta_{mn} + \frac{1}{2}\sum_{mnpq}C(0)_{klmnpq}\eta_{mn}\eta_{pq}+\frac{1}{6}\sum_{mnpqrs}C(0)_{klmnpqrs}\eta_{mn}\eta_{pq}\eta_{rs}+...], \quad (6.17)$$

where V_0, $\tau(0)_{ij}$, $C(0)_{klmn}$, $C(0)_{klmnpq}$, etc., represent the volumes, stress, the second-, the third-, and the fourth-order elastic constants at zero stress state, respectively, and V is the volume at the current state x. Similarly, following Eq. (6.8b), we can write the second-order elastic constants C_{ijkl} at state x,

$$C_{ijkl}=(V_0/V)a_{im}a_{jn}a_{kp}a_{lq}\left(C(0)_{mnpq}+C(0)_{mnpqrs}\eta_{rs}+\frac{1}{2}C(0)_{mnpqrstu}\eta_{rs}\eta_{tu}+...\right). \quad (6.18)$$

Explicitly for example, after using the relations, $J=\det|a|=\frac{V(x)}{V(X)}\approx 1+\eta_{ii}+...$ and $a_{ij}\approx\delta_{ij}+\eta_{ij}-\frac{1}{2}\eta_{ki}\eta_{kj}+...$, Eq. (6.17) becomes Eq. (6.3) but with more terms, and the second order elastic constants in Eq. (6.18) become

$$C_{ijkl} = C(0)_{ijkl} + \left[-C(0)_{ijkl}\eta_{mm} + C(0)_{ijkm}\eta_{lm} + C(0)_{ijml}\eta_{km} + C(0)_{imkl}\eta_{jm} + C(0)_{mjkl}\eta_{im} \right] + C(0)_{ijklmn}\eta_{mn} + \cdots \quad (6.19)$$

Now, we have a general expression for τ_{ij} and C_{ijkl} evaluated at any deformed state x, in terms of the second-, third-, fourth-order and higher order elastic constants evaluated at the zero stress state. If we know these elastic constants, either from experiment or theoretical calculations, we could express the elastic stability conditions, as expressed in Eqs. (6.9-6.11) or Eqs. (6.12-6.15), analytically as the function of only the deformation strain η. This new formulation based on the finite deformation theory (section 6.2.1) gives significant relief in computing the elastic stability condition; and at the same time it offers valuable insights into how the nonlinear effects such as anharmonicity contribute to crystal stability. In the following, we shall present detailed formulation for implementing this approach in cubic crystals.

6.3 Calculation details

Previously we performed *ab initio* calculations with the density functional theory to investigate the elastic stability of face-centered cubic crystal Au under hydrostatic and uniaxial stresses[20, 29]. The calculation consists of three parts: (1) equilibrate the system and then subject the system in equilibrium with deformation by applying a homogeneous deformation strain according to the loading mode; (2) obtain the elastic constants, stresses, and other relevant properties such as volume at each of the deformed state; and (3) from the elastic constants, obtain the elastic stiffness constants and thus the stability criteria (Eq. (6.2)). One can obtain the stability condition using the stress-strain relations (Eq. (6.3)) too. In the case of hydrostatic loading, due to the preservation of the symmetry,

the procedure is simple. We apply hydrostatic deformation to a crystal supercell via a strain, $\eta_{11} = \eta_{22} = \eta_{33} = \xi$, $\eta_{ij} = 0$ for $i \neq j$, which is done by changing the lattice parameter a homogeneously, or $a / a_0 = \sqrt{1 + 2\xi}$. We then obtain the pressure-volume strain relation and the internal energy U as a function of the applied strain, or $U = U(a / a_0)$, from which we obtain the elastic constants. For uniaxial loading, the procedure is much involved. To simulate deformation along [100] axis, for example, we first apply a specific incremental strain, η_1, along [100] axis to a crystal supercell. Then we hold the supercell in [100] direction but allow it to relax along the other two perpendicular directions, [010] and [001]. When the stress components σ_2 and σ_3 along these two directions disappear as required by Poisson contraction, we measure the value of η_2 and η_3 and obtain a new supercell, which is now under the non-vanishing stress along only [100] axis. Due to the tetragonal crystal symmetry and relaxation, $\sigma_2 = \sigma_3 = 0$, the total energy of the system is a function of only η_1. From the total energy of the deformed supercell at each η_1, we calculate the elastic constants and test those stability conditions Eqs. (6.12-6.15). The process is very tedious and time consuming. Next, we present the analytical model using the nonlinear formulation to express the stability conditions for cubic crystal under hydrostatic and uniaxial loading respectively.

6.3.1 Cubic crystals under hydrostatic stress

Under hydrostatic loading on a cubic crystal, the pressure on the system is $\sigma'_{ij} = -P\delta_{ij}$ and the deformation strain is $\eta_1 = \eta_2 = \eta_3$. Using Eqs. (6.17) and (6.18), we have the pressure and elastic constants for the deformed system,

$$P = -\frac{1}{3}tr(\sigma') = -\sigma_1' = \frac{-1}{\sqrt{1+2\eta_1}}[(C_{11}+2C_{12})\eta_1 + (\frac{1}{2}C_{111}+3C_{112}+C_{123})\eta_1^2 + (\frac{1}{6}C_{1111}+\frac{4}{3}C_{1112}+C_{1122}+2C_{1123})\eta_1^3] + ..., \quad (6.20)$$

correct to the third order in Lagrangian strain, and

$$C_{11}' = \sqrt{1+2\eta_1}[C_{11}+(C_{111}+2C_{112})\eta_1 + (\frac{1}{2}C_{1111} + 2C_{1112}+C_{1122}+C_{1123})\eta_1^2], \quad (6.21a)$$

$$C_{12}' = \sqrt{1+2\eta_1}[C_{12}+(2C_{112}+C_{123})\eta_1 + (C_{1112}+C_{1122} + \frac{5}{2}C_{1123})\eta_1^2], \quad (6.21b)$$

and

$$C_{44}' = \sqrt{1+2\eta_1}[C_{44}+(C_{144}+2C_{155})\eta_1 + (\frac{1}{2}C_{1144}+C_{1155}+2C_{1255} + C_{1266})\eta_1^2]. \quad (6.21c)$$

correct to the second power in Lagrangian strain. Using these relations, we can test the stability conditions expressed in Eqs. (6.9-6.11).

6.3.2 Cubic crystals under uniaxial stress along [100] axis

We denote the original state by X, that is corresponding to an initial state of a cubic supercell (not necessarily the natural or stress-free state), the state with applied strain η_1 by X', the state after relaxation by X'', both of the latter two states are with tetragonal symmetry. Then from X to X'', using Eq. (6.17) we have the stress

$$\sigma_1'' = \frac{1}{V''}\left(\frac{\partial U}{\partial \eta_1''}\right) = \frac{V_0}{V''}\left(\frac{1}{V_0}\frac{\partial U}{\partial \eta_1}\right)\left(\frac{\partial \eta_1''}{\partial \eta_1}\right) = \frac{\sqrt{1+2\eta_1}}{1+2\eta_2}[\sigma_1 +$$

$$C_{11}\eta_1 + C_{12}(\eta_2+\eta_3) + \frac{1}{2}C_{111}\eta_1^2 + C_{112}\eta_1(\eta_2+\eta_3) +$$

$$\frac{1}{2}C_{112}(\eta_2^2+\eta_3^2) + C_{123}\eta_2\eta_3 + \frac{1}{6}C_{1111}\eta_1^3 + \frac{1}{2}C_{1112}\eta_1^2(\eta_2+\eta_3) +$$

$$\frac{1}{6}C_{1112}(\eta_2^3+\eta_3^3) + \frac{1}{2}C_{1122}\eta_1(\eta_2^2+\eta_3^2) + C_{1123}(\eta_1\eta_2\eta_3 + \frac{1}{2}\eta_2^2\eta_3 + \frac{1}{2}\eta_2\eta_3^2)], \qquad (6.22)$$

correct to the third order of Langrangia strain, $O(\eta^3)$. We now choose state X as the natural state or stress-free, $\sigma_1 = 0$. Similarly, we may use Eq. (6.18) to have the six independent second-order elastic constants at the state X'',

$$C_{11}'' = \frac{(1+2\eta_1)^{3/2}}{(1+2\eta_2)}[C_{11} + C_{111}\eta_1 + C_{112}(\eta_2+\eta_3) + \frac{1}{2}C_{1111}\eta_1^2 +$$

$$C_{1112}\eta_1(\eta_2+\eta_3) + \frac{1}{2}C_{1122}(\eta_2^2+\eta_3^2) + C_{1123}\eta_2\eta_3], \qquad (6.23a)$$

$$C_{22}'' = \frac{(1+2\eta_2)}{(1+2\eta_1)^{1/2}}[C_{11} + C_{111}\eta_2 + C_{112}(\eta_1+\eta_3) + \frac{1}{2}C_{1111}\eta_2^2 +$$

$$C_{1112}\eta_2(\eta_1+\eta_3) + \frac{1}{2}C_{1122}(\eta_1^2+\eta_3^2) + C_{1123}\eta_1\eta_3], \qquad (6.23b)$$

$$C_{12}'' = (1+2\eta_1)^{1/2}[C_{12} + C_{112}(\eta_1+\eta_2) + C_{123}\eta_3 + \frac{1}{2}C_{1112}(\eta_1^2+\eta_2^2) +$$

$$C_{1122}\eta_1\eta_2 + C_{1123}(\eta_1\eta_3 + \eta_2\eta_3 + \frac{1}{2}\eta_3^2)], \qquad (6.23c)$$

$$C_{23}^{"} = \frac{(1+2\eta_2)}{(1+2\eta_1)^{1/2}}[C_{12} + C_{112}(\eta_2+\eta_3) + C_{123}\eta_1 + \frac{1}{2}C_{1112}(\eta_2^2+\eta_3^2) + C_{1122}\eta_2\eta_3 + \frac{1}{2}C_{1123}(\eta_1^2 + 2\eta_1\eta_2 + 2\eta_1\eta_3)], \quad (6.23d)$$

$$C_{44}^{"} = \frac{(1+2\eta_2)}{(1+2\eta_1)^{1/2}}[C_{44} + C_{144}\eta_1 + C_{155}(\eta_2+\eta_3) + \frac{1}{2}C_{1144}\eta_1^2 + \frac{1}{2}C_{1155}(\eta_3^2+\eta_2^2) + C_{1255}(\eta_1\eta_2+\eta_1\eta_3) + C_{1266}\eta_2\eta_3], \quad (6.23e)$$

and

$$C_{55}^{"} = (1+2\eta_1)^{1/2}[C_{44} + C_{144}\eta_2 + C_{155}(\eta_1+\eta_3) + \frac{1}{2}C_{1144}\eta_2^2 + \frac{1}{2}C_{1155}(\eta_3^2+\eta_1^2) + C_{1255}(\eta_1\eta_2+\eta_2\eta_3) + C_{1266}\eta_1\eta_3]. \quad (6.23f)$$

correct to the second power in Lagrangian strain. With Eqs. (6.22) and (6.23), we have the stress and elastic constants at state $X"$ all expressed in terms of η_1 and the second-, third-, and fourth-order elastic constants at state X, given the condition that $\eta_2 = \eta_3 = f(\eta_1)$ as required from $\sigma_2^{"} = \sigma_3^{"} = 0$ after relaxation from state X'. To identify the value of η_2 and η_3 for each specific η_1, we use the procedure shown in Appendix A. Therefore using the available elastic constants at zero stress, we can test the stability conditions expressed in Eqs. (6.12-6.15) for the stress and elastic constants at any deformed state $X"$.

6.4 Results

We present the results on testing the nonlinear formulation of the elastic stability conditions expressed in two different forms: one is expressed in terms of the elastic stiffness coefficients (Eq. (6.2)), and the other is the stress-strain relation (Eq. (6.3)). In

the nonlinear formulation, both the stress-strain relation and the elastic stiffness coefficients are functions of only the deformation strain. The inputs are the second-, third-, and fourth-order elastic constants from available experimental measurements. Obviously, the quality of the input data has a big effect on the stability results, especially at large strains. We shall discuss this issue in more detail in the next section. For comparison, we use the results from *ab initio* calculations and atomistic simulations, in particular those from our own DFT calculation of Au where all elastic constants up to the fourth order were available in our previous publications[93].

6.4.1 FCC Au under hydrostatic stress

Figure 6.1 gives the stress-strain curves of both analytic results and *ab initio* calculations for the crystal Au under hydrostatic stress. We have two stress-strain relations from Eq. (6.20) resulting from using two sets of data for the elastic constants in the nonlinear theory, one from the experiments[73] and the other from our recent *ab initio* calculations[93]. We can see that the analytical results agree well with that from the DFT calculation in the presented large strain range, except that the one with experimental input deviates from the other two only in the compressive regime.

Figures 6.2(a)-6.2(c) show the elastic stiffness moduli defined in Eqs. (6.9-6.11) with varying hydrostatic strain. As for the stress-strain relation, three sets of results are obtained for each stiffness coefficient from different inputs. We see that when we use the second-, third-, and fourth-order elastic constants[93] of the stress-free crystal Au from our calculation and the experiment, the results agree very well with the *ab initio* calculated stiffness coefficients. Our earlier *ab initio* calculation shows that under hydrostatic stress, the instability does not occur along the primary hydrostatic stress path; instead it happens

along the rhombohedral shear path at the volume expansion strain of 0.06[20]. The analytical results in this work show that under compression, all of the three stability conditions (Eqs. (6.9-6.11)) are obeyed within 10% strain range. In expansion, the stability conditions associated with the bulk and tetrahedral shear stiffness coefficients (Eqs. (6.9) and (6.10)) are maintained, and the rhombohedral shear stiffness condition is violated, i.e., goes to zero, first at Lagrangian strain $\eta_1 \sim 0.05$, which agrees well with our previous direct *ab initio* calculation of the stability condition[20].

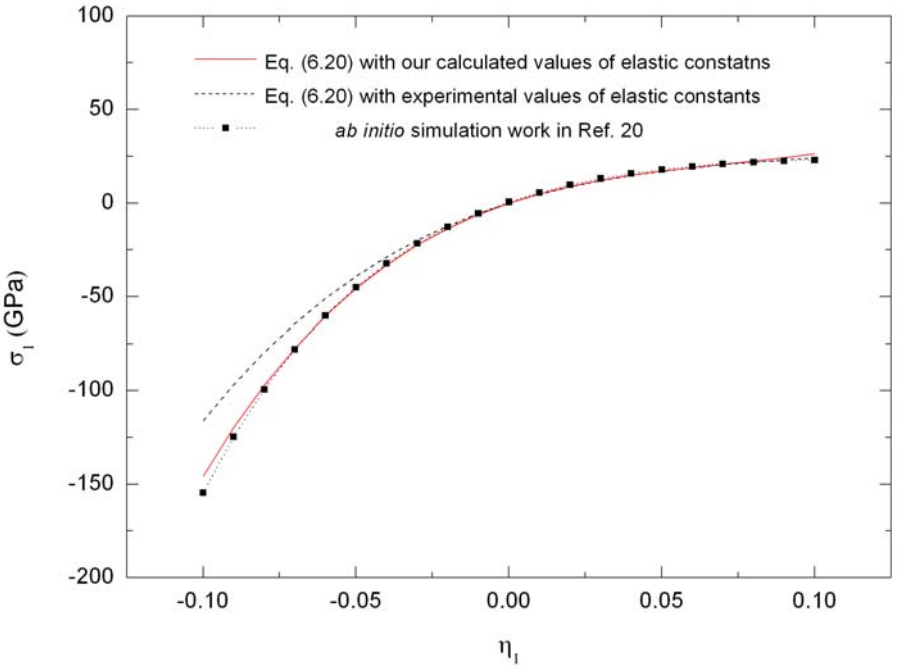

Figure 6.1 The hydrostatic stress varies with strain η_1. Two of the stress-strain curves use Eq. (6.20), with two sets of data for the elastic constants in the nonlinear theory, one from the experiments and the other from our recent *ab initio* calculations. The last line comes from our previous *ab initio* simulation [20]. The three lines agree well with each other in a finite strain range.

(a)

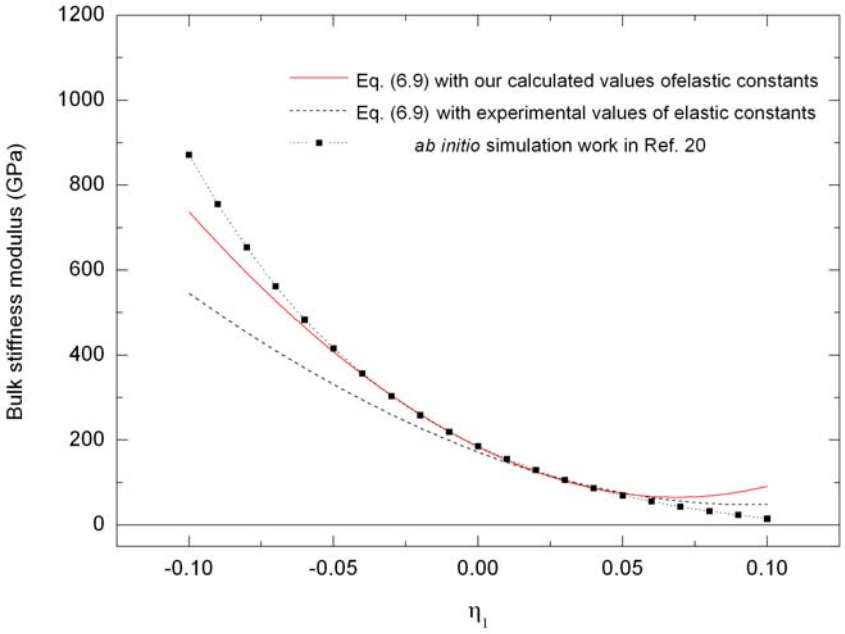
Eq. (6.9) with our calculated values ofelastic constants
Eq. (6.9) with experimental values of elastic constants
ab initio simulation work in Ref. 20
Bulk stiffness modulus (GPa)
1200
1000
800
600
400
200
0
-0.10
-0.05
0.00
0.05
0.10
η1

(b)

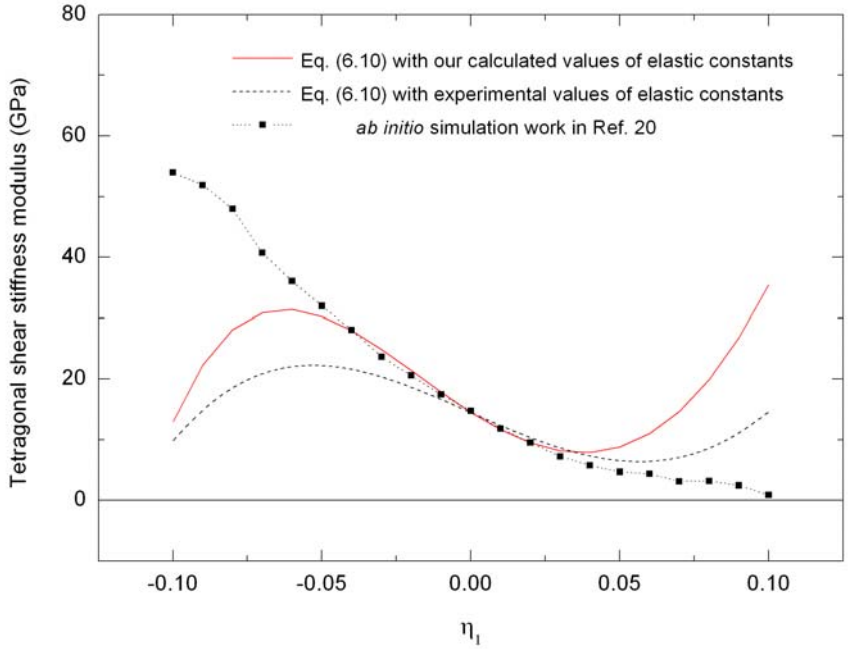
Eq. (6.10) with our calculated values of elastic constants
Eq. (6.10) with experimental values of elastic constants
ab initio simulation work in Ref. 20
Tetragonal shear stiffness modulus (GPa)
80
60
40
20
0
-0.10
-0.05
0.00
0.05
0.10
η1

(c)

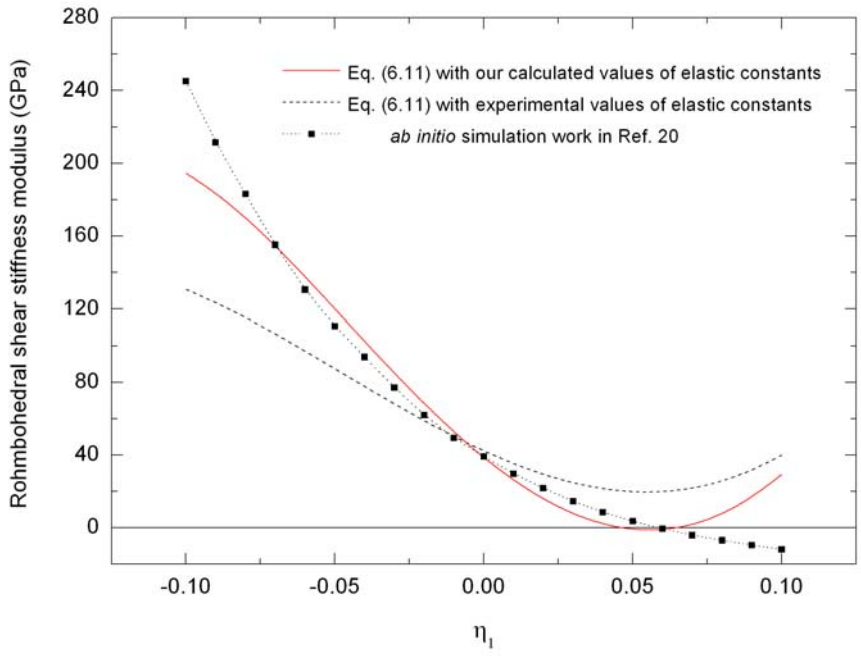

Figure 6.2 The three types of elastic moduli of Au under hydrostatic stress vary with strain η_1. Under compression, the crystal is stable. While expansion, the rhombohedral shear stiffness modulus first reaches zero at $\eta_1 \sim 0.05$.

It is interesting to notice that the rhombohedral shear stiffness condition from the analytical result using the experimental elastic constants does not show instability. Moreover, the rhombohedral shear stiffness increases at the large strain, due mainly to the use of the fourth-order elastic constants. As compared, which is different from the *ab initio* calculation where the rhombohedral shear stiffness decrease monotonically with increasing volume expansion. The rhombohedral shear, or instability bifurcation, can be obtained from the shear stress-strain relation. From the analytical stress-strain results (figure 6.1, using the input from the *ab initio* calculation) we obtain the ideal hydrostatic

strength 17.1 GPa at the shear instability, which is at 19.2 GPa from the *ab initio* calculations[20].

6.4.2 FCC Au under uniaxial stress along [100] axis

As compared with the hydrostatic case, the uniaxial loading is more complicated due to symmetry breaking. Figure 6.3 gives the uniaxial stress as a function of strain η_1 along the [100] direction for the face-centered cubic crystal Au under uniaxial stress (tension and compression). Three sets of results are presented, one is from the direct DFT calculation and the other two are from Eq. (6.22) using the elastic constants from experiments[73] and our DFT calculations[73] . The three lines agree well with each other in the range of small strains less than 0.02. Beyond this range, some differences occur. In general, the analytical result using the elastic constants calculated from the *ab initio* results agrees well with the stress-strain relation obtained directly from the same calculation; but the analytical result using the experimental data differs substantially from the *ab initio* results, which is understandable considering that the experimental data were not at zero temperature and came from different measurements and approximation[73]. Another obvious deviation among the stress-strain relations occurs at larger strains in the compression regime. The analytical result using the elastic constants from the DFT calculations shows the largest deviation from the direct *ab initio* calculation result, which is a result of keeping only a finite number of terms in the deformation energy cut off at the fourth-order. As shown later, nevertheless, the deviation in stress-strain relations does not affect the prediction of the stability conditions.

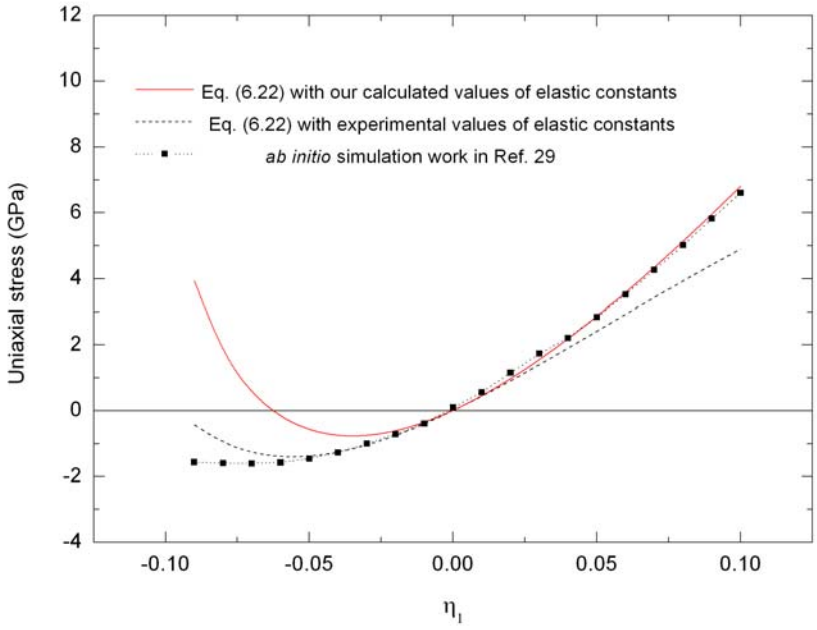

Figure 6.3 The normal stress varies with strain η_1 when fcc Au is under uniaxial stress along [100] direction. Two of the stress-strain curves come from Eq. (6.22), with two sets of data for the elastic constants in the nonlinear theory, one from the experiments and the other from our recent *ab initio* calculations. The last line comes from our previous *ab initio* simulation.

(a)

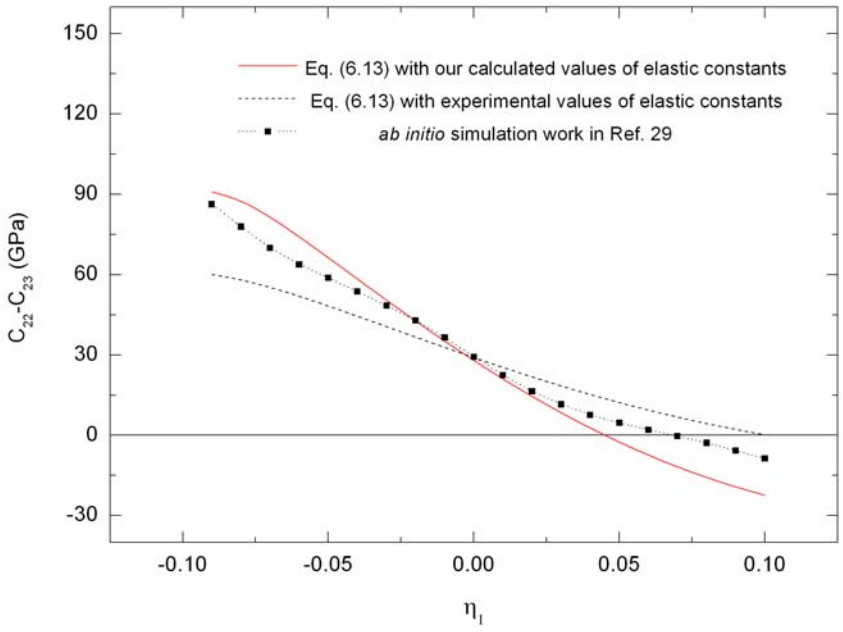
Eq. (6.13) with our calculated values of elastic constants
Eq. (6.13) with experimental values of elastic constants
ab initio simulation work in Ref. 29
C22-C23 (GPa)
η1
150
120
90
60
30
0
-30
-0.10
-0.05
0.00
0.05
0.10

(b)

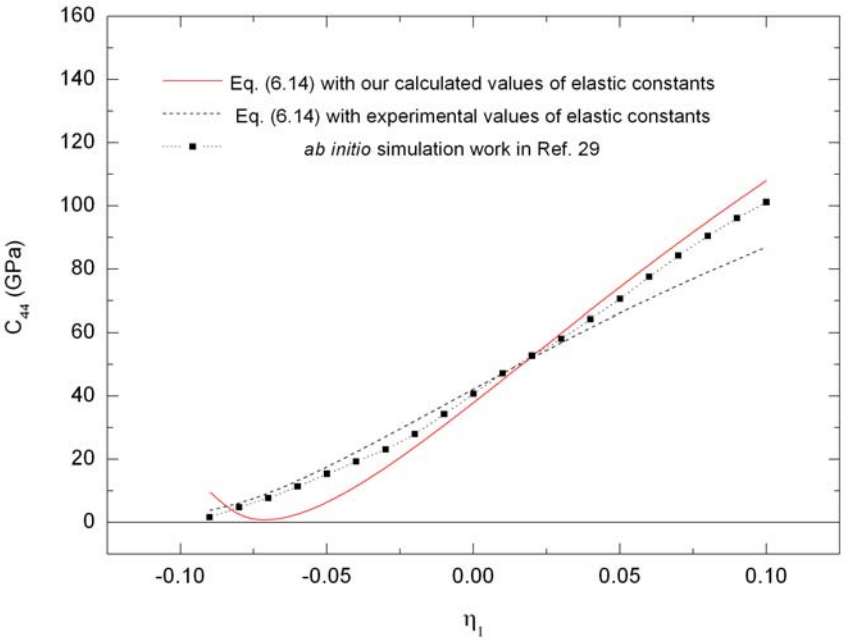
Eq. (6.14) with our calculated values of elastic constants
Eq. (6.14) with experimental values of elastic constants
ab initio simulation work in Ref. 29
C44 (GPa)
η1
160
140
120
100
80
60
40
20
0
-0.10
-0.05
0.00
0.05
0.10

(c)

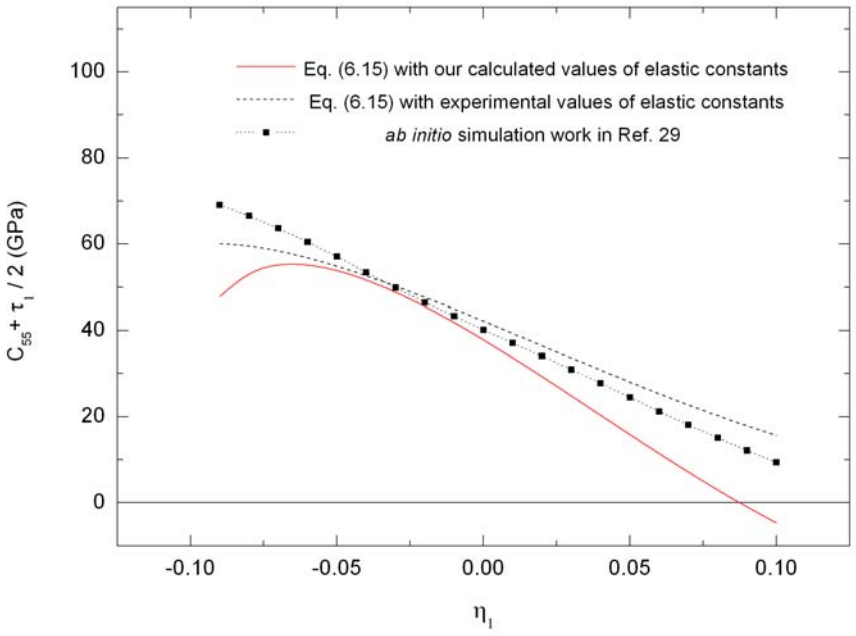
Eq. (6.15) with our calculated values of elastic constants
Eq. (6.15) with experimental values of elastic constants
ab initio simulation work in Ref. 29
C55 + τ1 / 2 (GPa)
η1
100
80
60
40
20
0
-0.10
-0.05
0.00
0.05
0.10

(d)

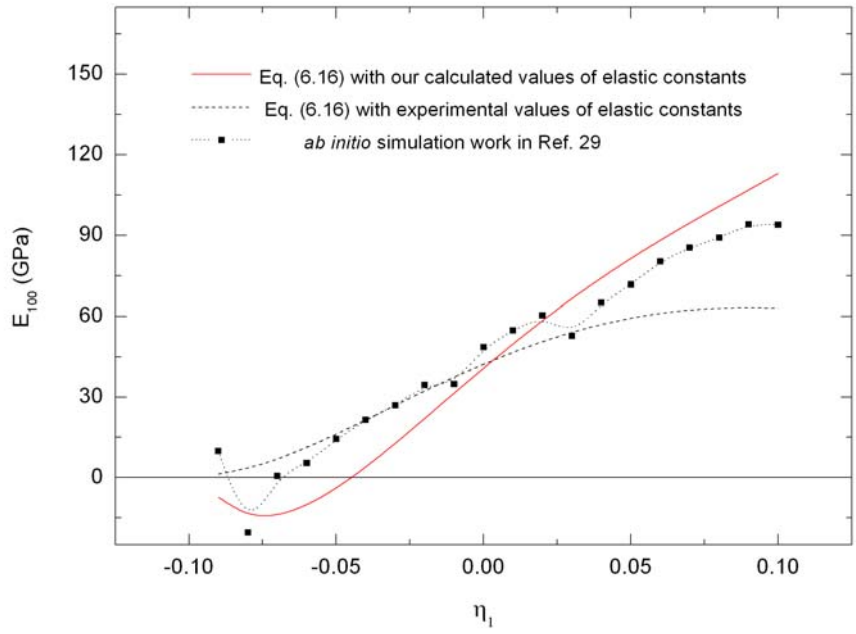
Eq. (6.16) with our calculated values of elastic constants
Eq. (6.16) with experimental values of elastic constants
ab initio simulation work in Ref. 29
E100 (GPa)
η1
150
120
90
60
30
0
-0.10
-0.05
0.00
0.05
0.10

Figure 6.4 The four types of elastic modulus of Au under uniaxial stress vary with strain η_1. Under compression, the Young's modulus first reaches zero at $\eta_1 \sim -0.045$; while under tensile stress, the tetragonal shear stiffness modulus first reach zero at $\eta_1 \sim 0.048$.

Using the relations in Eq. (6.23), we obtained the elastic constants at deformed state, from which we can obtain the stiffness coefficients (Eq. (6.1)) and thus test the stability criteria for Au under unaxiual loading (Eqs. (6.12-6.15)). Figures 6.4(a)-6.4(d) give these elastic stiffness moduli as a function of η_1. In general, the trend in each of the four moduli as functions of the uniaxial strain is captured well by the analytical results as compared with the direct ab initio calculations, although increasing deviation occurs at larger strains due to the use of the finite terms in the theory. The most salient feature is that the nonlinear theory can predict the instability and bifurcation relatively well. As shown in figure 6.4(a), under tensile stress, the stability condition involving the tetragonal shear modulus (Eq. (6.13)) is violated first. The corresponding Lagrangian strain is $\eta_1 \sim 0.048$ from the vanishing shear modulus using the elastic constants from the *ab initio* calculations and $\eta_1 \sim 0.10$ from the vanishing shear modulus using the experimental input data for elastic constants. The instability occurring not along the loading strain path but along a shear mode, or instability bifurcation, is well captured by the theory. As shown in figure 6.4(d), under compression, the stability condition governed by the Young's stiffness modulus (Eq. (6.12) or (6.16)) is violated first at the corresponding Lagrangian strains $\eta_1 \sim -0.045$ and $\eta_1 \sim -0.085$ from the vanishing Young's stiffness modulus using the inputs from the *ab initio* calculation and experiment, respectively. As a comparison, the corresponding strain limits at these two instability points from our previous *ab initio* calculation are -0.07 and 0.07[29]. From the stress-strain

curve (figure (6.3)), we can locate the ideal tensile strength of Au at 2.7 GPa at $\eta_1 \sim 0.048$ and the ideal compressive strength is 0.7 GPa at $\eta_1 \sim -0.045$. The ideal strengths at the instability points $\eta_1 \sim -0.085$ and $\eta_1 \sim 0.10$, predicted from the Young's modulus using experimental input, are much higher.

Table 6.1 The ideal strength and stable region of face-centered cubic crystal Au, Al, and Cu under uniaxial stress along [100] axis. The results from our analytic scheme, from previous *ab initio* calculation work, and from embedded atom method are listed.

	Tension $C_{11} - C_{12} = 0$		Compression $E_{[100]} = 0$	
	σ_1 (GPa)	η_1	σ_1 (GPa)	η_1
Au	2.7 [a]	0.048 [a]	-0.7 [a]	-0.045 [a]
	4.2 [b]	0.07 [b]	-1.6 [b]	-0.07 [b]
	6.31 [c]	0.079 [c]	-2.21 [c]	-0.098 [c]
	10.0 [f]	0.11 [f]	_	_
Al	6.7 [a]	0.11 [a]	-5.8 [a]	-0.09 [a]
	12.1 [d]	0.27 [d]	-5.62 [d]	-0.10 [d]
	11.1 [f]	0.25 [f]	_	_
Cu	8.2 [a]	0.09 [a]	-2.6 [a]	-0.08 [a]
	9.4 [e]	0.10 [e]	-3.5 [e]	-0.09 [e]
	9.8 [f]	0.14 [f]	_	_

[a] This work.

[b] Reference 29.
[c] Reference 28.
[d] Reference 18.
[e] Reference 19.
[f] Reference 27.

6.4.3 Other FCC crystals

The cases for Au presented above are unique in which the needed input elastic constants up to the fourth order are available from both theoretical calculations and experiment; direct *ab initio* calculations of both the hydrostatic and uniaxial deformation modes are also available for comparison[20, 29]. In a recent work, we have computed the elastic constants of several fcc metals up to the fourth order. This effort makes it possible to extend the nonlinear formulation of elastic stability to those materials, including Al and Cu. Since the detailed account of the technical approaches has been given in the last two sections, we shall summarize only the results for these fcc crystals subject to hydrostatic and uniaxial loading. Our emphasis will be on the elastic stability from the nonlinear formulation.

The ideal strength, stable region of Au, Al, Cu from this analytic scheme, from previous *ab initio* calculation work[20, 29],and from embedded atom method[27] are listed at table 6.1.

6.5 Discussion

Table 6.1 shows that our analytic model gives similar results to the ones from our *ab initio* calculations of Au. The difference may come from quite a few sources. When we calculate those second-, third-, and fourth-order elastic constants[29], we apply strains to the supercell and fit the energy-strain curves. System errors will happen during those procedures. Eqs. (6.20-6.23) are truncated to the fourth-order elastic constants under zero

stress, we utilize Eqs. (6.20-6.23) to obtain each component of the second-order elastic constants as well as the uniaxial stress at a deformed state. Then we use those values to get the elastic modulus, errors may be accumulated and amplified thereafter. Our *ab initio* work[29] employs the stress-strain relation to obtain elastic moduli, which is different with the energy-strain method we use to obtain the elastic constants. So we may find in figure 6.4 that at the original size of supercell the moduli values are not the same though they are supposed to agree with each other. Partly because of that, we cannot expect the curves from analytic method and those from *ab initio* calculations overlap completely in figure 6.4.

In figures 6.1-6.4, we also put the analytic results using experimental values of second-, third-, and fourth-order elastic constants of Au. The second-, and third-order elastic constants have been measured at room temperature using high-purity single crystals[29]. Based on those values, Hiki *et al* [29] calculated the fourth-order elastic constants with the generalized Cauchy relationship:

$$C_{1111} = 2C_{1112} = 2C_{1122} = 2C_{1155} = 2C_{1266} = 2C_{4444},$$
$$C_{1123} = C_{1144} = C_{1255} = C_{1456} = C_{4455} = 0.$$

This is a quite rough approximation. However, the fourth-order elastic constants Hiki *et al* got are the only set of data we can find from others' work since no experimental data of fourth-order elastic constants are available. When we use experimental data as well as Hiki's fourth-order elastic constants of Au, the analytic scheme gives sort of different results from those of our own *ab initio* calculated elastic constants.

Milstein[27] *et al* used an embedded atom model to perform simulation. Although their potentials are quite sophisticated, since they are fitted to the second- and third-order elastic moduli, according our experience, at such a large finite strain range which is

beyond 0.10, the fourth-order elastic moduli would make contributions and must be taken into account in the fitting of the potentials[93]. Perhaps because of that, their values of ideal tensile strength are higher, and the stable range in tension is wider than ours. Zhang *et al* [28] employed a modified analytic EAM (MAEAM) model to investigate the same problem. Their results are closer to ours. Li *et al* [18] studied the ideal strength of Al, but they did not use symmetrized elastic stiffness coefficients. In addition, how they calculate each independent component of elastic constants at any given stressed state to test the stability conditions is not clear. Cerny *et al* [19] work on the ideal strength of Cu, but the Young's modulus formulation they used may only be valid in small deformation[29]. Recently Cerny *et al* [126] presented another way to estimate uniaxial tensile strength on the basis of theoretical shear strength calculations. They claimed that the analysis of elastic stability of crystals under tensile loading would be avoided through that way. Their work shows that the ideal tensile strength is 5.8 GPa from the rigid-planes approach, and 3.6 GPa from the relaxed-planes approach.

Krenn *et al* [24] applied the transcription theory of stress and elastic constants to the nonlinear elastic behavior and ideal shear strength problems of face-centered cubic crystals Al and Cu. They used experimentally measured second- and third-order elastic constants to explain the different structural relaxation modes of the crystals Al and Cu with shear deformation. Partly due to the accuracy of experimental data, but more importantly because the limitation of third-order elastic constants, their work gives correct signs of the relaxations along x, y, and z axis, but can not agree with the relative magnitudes. At a finite strain range around 10%, the fourth-order elastic constants play an essential role in the transcription theory scheme. We test Eq. (6.20), keeping the

hydrostatic stress accurate to the second-, third-, and fourth-order elastic constants respectively, and plot the stress-strain curve in figure 6.5, compared with our previous *ab initio* simulation curve. We also test Eq. (6.21) and plot the bulk stiffness modulus with different types of accuracy varying with strain η_1 in figure 6.6. Figures 6.5 and 6.6 give us a general concept that when the analytic scheme is correct to the fourth-order elastic constants, the results will agree most with the *ab initio* simulation work.

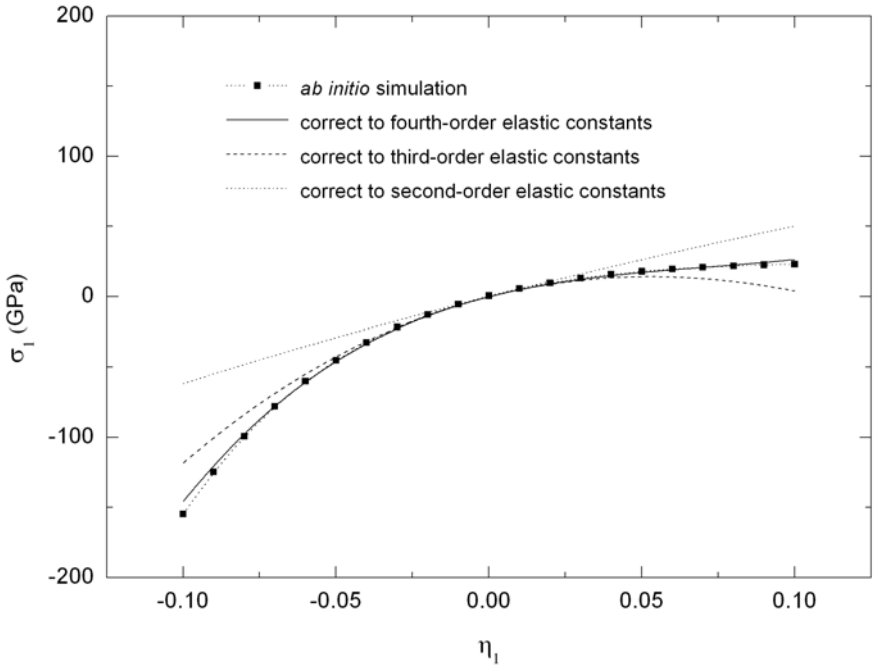

Figure 6.5 With Eq. (6.20), but keep the hydrostatic stress accurate to the second-, third-, and fourth-order elastic constants, respectively, and plot the stress-strain curves compared with our previous *ab initio* simulation result.

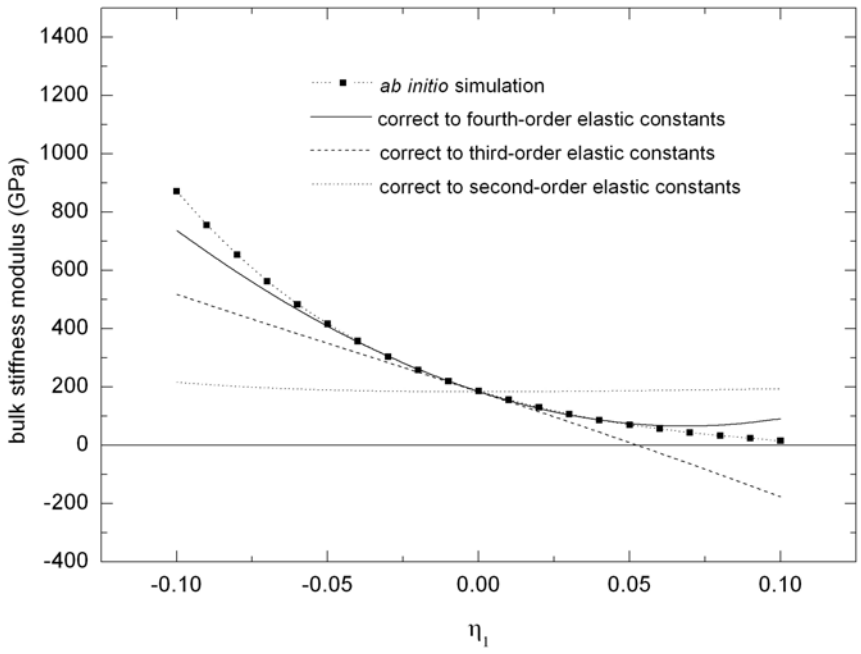

Figure 6.6 Use Eqs. (6.20-6.21), and then obtain the bulk stiffness modulus with Eq. (6.9). Control the accuracy to the second-, third-, and fourth-order elastic constants, respectively, and plot the modulus-strain curves compared with our previous *ab initio* simulation result.

6.6 Conclusion

In this work we employ a general analytic scheme to investigate the elastic stability problems of cubic crystal Au, Al, and Cu. We used the published high order elastic constants we obtained before, with Wallace transcription theory, to get the stress and elastic constant for a crystal under load. And then test the Born-Hill stability conditions. The stable region and ideal strengths we obtained are presented and are comparable to our pervious *ab initio* calculations as well as other groups' work. The analytic scheme not only shows us an application of Wallace transcription theory, but

also gives us a new way, saving computation resource, to investigate the ideal strength, bifurcation and elastic stability problems.

Appendix A:

From state X' to state X'', the internal energy as a function of strain η_i', expanded to $O(\eta'^3)$, may be written as,

$$\begin{aligned}\delta U' = &\sum_i \sigma_i'\eta_i' + \frac{1}{2}C_{11}'\eta_1'^2 + \frac{1}{2}C_{22}'(\eta_2'^2+\eta_3'^2) + C_{12}'(\eta_1'\eta_2'+\eta_3'\eta_1') + \\ &C_{23}'\eta_2'\eta_3' + \frac{1}{6}C_{111}'\eta_1'^3 + \frac{1}{6}C_{222}'(\eta_2'^3+\eta_3'^3) + \frac{1}{2}[C_{112}'\eta_1'^2(\eta_2'+\eta_3') + \\ &C_{122}'\eta_1'(\eta_2'^2+\eta_3'^2) + C_{223}'\eta_2'\eta_3'(\eta_2'+\eta_3')] + C_{123}'\eta_1'\eta_2'\eta_3',\end{aligned} \tag{A.1}$$

where σ_i', C_{ij}', and C_{ijk}' represent the stress and elastic constants at state X', and η_i' represents the Lagrangian strain from state X' to state X''. We know that $\eta_2' = \eta_3'$, $\eta_1' = 0$, and $\sigma_2' = \sigma_3'$. Let σ_i'' represent the stress at state X'', $\sigma_2'' = \sigma_3'' = 0$. With Eq. (6.22), we have

$$\sigma_2'' = \sigma_2' + C_{22}'\eta_2' + C_{23}'\eta_3' + \frac{1}{2}C_{222}'\eta_2'^2 + \frac{1}{2}C_{223}'(2\eta_2'\eta_3' + \eta_3'^2). \tag{A.2}$$

Using $\sigma_2'' = 0$, $\eta_2' = \eta_3'$,

$$0 = \sigma_2' + \left(C_{22}' + C_{23}'\right)\eta_2' + \left(\frac{1}{2}C_{222}' + \frac{3}{2}C_{223}'\right)\eta_2'^2. \tag{A.3}$$

To solve this equation, we need to know the values of σ_2', C_{22}', C_{23}', C_{222}', C_{223}'.

From state X to state X', $\eta_i = 0\,(i \neq 1)$, $\frac{V}{V'} = \frac{1}{\sqrt{1+2\eta_1}}$. Once again we use Eqs. (6.22)-(6.23), and have,

$$\sigma_2^{'} = \frac{1}{\sqrt{1+2\eta_1}}\left(C_{12}\eta_1 + \frac{1}{2}C_{112}\eta_1^2 + \frac{1}{6}C_{1112}\eta_1^3 \right), \tag{A.4}$$

$$C_{22}^{'} = \frac{1}{V'}\frac{\partial^2 U}{\partial \eta_2^{'2}} = \left(\frac{V}{V'}\right)\left(\frac{1}{V}\frac{\partial^2 U}{\partial \eta_2^2}\right) a_{22}^4 = \frac{1}{\sqrt{1+2\eta_1}}[C_{11} + C_{112}\eta_1 + \frac{1}{2}C_{1122}\eta_1^2], \tag{A.5}$$

$$C_{23}^{'} = \frac{1}{V'}\frac{\partial^2 U}{\partial \eta_2^{'}\partial \eta_3^{'}} = \left(\frac{V}{V'}\right)\left(\frac{1}{V}\frac{\partial^2 U}{\partial \eta_2 \partial \eta_3}\right) a_{22}^2 a_{33}^2 = \frac{1}{\sqrt{1+2\eta_1}}[C_{12} + C_{123}\eta_1 + \frac{1}{2}C_{1123}\eta_1^2], \tag{A.6}$$

$$C_{222}^{'} = \frac{1}{V'}\frac{\partial^3 U}{\partial \eta_2^{'3}} = \left(\frac{V}{V'}\right)\left(\frac{1}{V}\frac{\partial^2 U}{\partial \eta_2^3}\right) a_{22}^6 = \frac{1}{\sqrt{1+2\eta_1}}[C_{111} + C_{1112}\eta_1\,]. \tag{A.7}$$

$$C_{223}^{'} = \frac{1}{V'}\frac{\partial^3 U}{\partial \eta_2^{'2}\partial \eta_3^{'}} = \left(\frac{V}{V'}\right)\left(\frac{1}{V}\frac{\partial^3 U}{\partial \eta_2^2 \partial \eta_3}\right) a_{22}^4 a_{33}^2 = \frac{1}{\sqrt{1+2\eta_1}}[C_{112} + C_{1123}\eta_1\,], \tag{A.8}$$

Here all the coefficients at Eq. (A3) are expressed in terms of η_1, C_{ij} , C_{ijk} , C_{ijkl} . Then we will get a solution of η_2 from Eq. (A3) for an arbitrary value of η_1 .

CHAPTER SEVEN

TEST OF THE NONLINEAR THEORETICAL FORMULATION OF ELASTIC STABILITY TO ISOTROPIC SOLIDS

Metallic glasses (MGs) are among the most promising materials for practical applications. MGs are different from other amorphous solids made of covalent bond elements such as silicate glass and polymer glasses. A large number of MGs have non-directional metallic bonding and show considerable elasticity, high strength, and large micro-plasticity. Moreover, MGs are convenient models to be used to investigate the fundamental problems of the nature of amorphous state. As compared with crystalline materials, MGs are characterized by the following three unique attributes: no long-range translational order or symmetry, metastability, and that the bulk MGs are alloys made of multicomponents of elements. These features are expected to contribute to very different constitutive responses under external loading, and also challenge establishing the equation of state in the topological disordered materials. In the continuum mechanics, MGs are treated as isotropic media[128]. That inspired us to test the nonlinear theoretical formulation of elastic stability to MGs. Recently, Kobelev *et al*[129] experimentally evaluated the third- and fourth-order elastic moduli of metallic glass $Zr_{52.5}Ti_5Cu_{17.9}Ni_{14.6}Al_{10}$ for the first time by the linear acoustic method. They measured the dependence of the velocity of ultrasonic waves on the applied external load. Their

work enables us to use the higher order elastic constants to test the mechanical properties of metallic glass $Zr_{52.5}Ti_5Cu_{17.9}Ni_{14.6}Al_{10}$.

This chapter is organized as follows. In section 7.1, we derive the elastic stability conditions of isotropic solids. In section 7.2, we use the experimentally evaluated elastic constants to test the elastic stability of metallic glass $Zr_{52.5}Ti_5Cu_{17.9}Ni_{14.6}Al_{10}$. In section 7.3, we present a discussion.

7.1 Elastic stability conditions of isotropic solids

7.1.1 Isotropic solids under uniaxial stress

Given a cubic crystal under a stress along [100] direction, we have the following derivations as shown in figure 7.1,

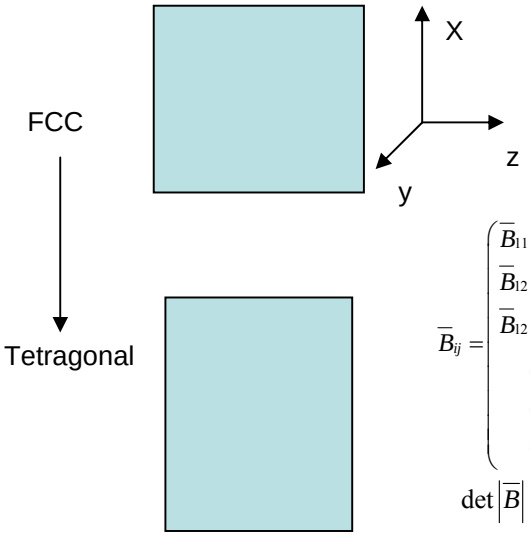

$$C_{ij} = \begin{pmatrix} C_{11} & C_{12} & C_{12} & 0 & 0 & 0 \\ C_{12} & C_{22} & C_{23} & 0 & 0 & 0 \\ C_{12} & C_{23} & C_{22} & 0 & 0 & 0 \\ 0 & 0 & 0 & C_{44} & 0 & 0 \\ 0 & 0 & 0 & 0 & C_{55} & 0 \\ 0 & 0 & 0 & 0 & 0 & C_{55} \end{pmatrix}$$

$$\bar{B}_{ij} = \begin{pmatrix} \bar{B}_{11} & \bar{B}_{12} & \bar{B}_{12} & 0 & 0 & 0 \\ \bar{B}_{12} & \bar{B}_{22} & \bar{B}_{23} & 0 & 0 & 0 \\ \bar{B}_{12} & \bar{B}_{23} & \bar{B}_{22} & 0 & 0 & 0 \\ 0 & 0 & 0 & \bar{B}_{44} & 0 & 0 \\ 0 & 0 & 0 & 0 & \bar{B}_{55} & 0 \\ 0 & 0 & 0 & 0 & 0 & \bar{B}_{55} \end{pmatrix}$$

$$\bar{B}_{11} = C_{11} + \tau,$$
$$\bar{B}_{12} = C_{12} - \frac{1}{2}\tau,$$
$$\bar{B}_{55} = C_{55} + \frac{1}{2}\tau,$$
$$\bar{B}_{ij} = C_{ij} \quad \text{(all others)}.$$

$$\det\left|\bar{B}\right| = (\bar{B}_{22} - \bar{B}_{23})\bar{B}_{44}\bar{B}_{55}^2[\bar{B}_{11}(\bar{B}_{22} + \bar{B}_{23}) - 2\bar{B}_{12}^2].$$

Figure 7.1 When a cubic crystal is deformed by a uniaxial compressive or tensile stress along [100] direction, a crystal with tetragonal symmetry results. The new elastic stiffness tensor is presented, as well as its determinant.

For an isotropic solid, the initial elastic constants are,

$$C_{ij}=\begin{pmatrix} C_{11} & C_{12} & C_{12} & 0 & 0 & 0 \\ C_{12} & C_{11} & C_{12} & 0 & 0 & 0 \\ C_{12} & C_{12} & C_{11} & 0 & 0 & 0 \\ 0 & 0 & 0 & C_{44} & 0 & 0 \\ 0 & 0 & 0 & 0 & C_{44} & 0 \\ 0 & 0 & 0 & 0 & 0 & C_{44} \end{pmatrix}, \tag{7.1}$$

where $C_{11}-C_{12}=2C_{44}$. Suppose a uniaxial stress is applied to the solid along a certain direction, then we define it as [100] direction. The solid will deform with a strain $\eta=(\eta_1,\eta_2,\eta_3,\eta_4,\eta_5,\eta_6,)$, with $\eta_2=\eta_3$, $\eta_4=\eta_5=\eta_6=0$, $(-\eta_2/\eta_1)=\sigma$, σ is Poisson ratio. Using the transcription theory of elastic constants between two coordinate frames [23], from X_0 to $X^{'}$, we have, $a_{ij}=\partial X_i^{'}/\partial X_{0j}$, and

$$\begin{aligned} \tau_{ij}^{'} &= \frac{1}{V^{'}}(\partial U/\partial \eta_{ij}^{'}) \\ &= \frac{V_0}{V^{'}}a_{im}a_{jn}\frac{1}{V_0}(\partial U/\partial \eta_{mn}) \\ &= \frac{V_0}{V^{'}}a_{im}a_{jn}(\tau_{mn}+C_{mnpq}\eta_{pq}+\frac{1}{2}C_{mnpqrs}\eta_{pq}\eta_{rs}+...), \end{aligned} \tag{7.2}$$

$$\begin{aligned} C_{ijkl}^{'} &= \frac{1}{V^{'}}(\partial^2 U/\partial \eta_{ij}^{'}\partial \eta_{kl}^{'}) \\ &= \frac{V_0}{V^{'}}a_{im}a_{jn}a_{kp}a_{lq}\frac{1}{V_0}(\partial^2 U/\partial \eta_{mn}\partial \eta_{pq}) \\ &= \frac{V_0}{V^{'}}a_{im}a_{jn}a_{kp}a_{lq}(C_{mnpq}+C_{mnpqrs}\eta_{rs}+\frac{1}{2}C_{mnpqrstu}\eta_{rs}\eta_{tu}+...). \end{aligned} \tag{7.3}$$

And then we get,

$$C_{11}^{"}=\frac{(1+2\eta_1)^{3/2}}{(1+2\eta_2)}[C_{11}+C_{111}\eta_1+C_{112}(\eta_2+\eta_3)+\frac{1}{2}C_{1111}\eta_1^2+C_{1112}\eta_1(\eta_2+\eta_3)$$
$$+\frac{1}{2}C_{1122}(\eta_2^2+\eta_3^2)+C_{1123}\eta_2\eta_3], \tag{7.4}$$

$$C_{22}^{"}=C_{33}^{"}=\frac{(1+2\eta_2)}{(1+2\eta_1)^{1/2}}[C_{11}+C_{111}\eta_2+C_{112}(\eta_1+\eta_3)+\frac{1}{2}C_{1111}\eta_2^2+C_{1112}\eta_2(\eta_1+\eta_3)$$
$$+\frac{1}{2}C_{1122}(\eta_1^2+\eta_3^2)+C_{1123}\eta_1\eta_3], \tag{7.5}$$

$$C_{12}^{"}=C_{13}^{"}=(1+2\eta_1)^{1/2}[C_{12}+C_{112}(\eta_1+\eta_2)+C_{123}\eta_3+\frac{1}{2}C_{1112}(\eta_1^2+\eta_2^2)+C_{1122}\eta_1\eta_2$$
$$+C_{1123}(\eta_1\eta_3+\eta_2\eta_3+\frac{1}{2}\eta_3^2)], \tag{7.6}$$

$$C_{23}^{"}=\frac{(1+2\eta_2)}{(1+2\eta_1)^{1/2}}[C_{12}+C_{112}(\eta_2+\eta_3)+C_{123}\eta_1+\frac{1}{2}C_{1112}(\eta_2^2+\eta_3^2)+C_{1122}\eta_2\eta_3$$
$$+\frac{1}{2}C_{1123}(\eta_1^2+2\eta_1\eta_2+2\eta_1\eta_3)], \tag{7.7}$$

$$C_{44}^{"}=(C_{22}^{"}-C_{23}^{"})/2=\frac{(1+2\eta_2)}{(1+2\eta_1)^{1/2}}[C_{44}+C_{144}\eta_1+C_{155}(\eta_2+\eta_3)+\frac{1}{2}C_{1144}\eta_1^2+$$
$$\frac{1}{2}C_{1155}(\eta_3^2+\eta_2^2)+C_{1255}(\eta_1\eta_2+\eta_1\eta_3)+C_{1266}\eta_2\eta_3], \tag{7.8}$$

$$C_{55}^{"}=C_{66}^{"}=(1+2\eta_1)^{1/2}[C_{44}+C_{144}\eta_2+C_{155}(\eta_1+\eta_3)+\frac{1}{2}C_{1144}\eta_2^2+\frac{1}{2}C_{1155}(\eta_3^2+\eta_1^2)$$
$$+C_{1255}(\eta_1\eta_2+\eta_2\eta_3)+C_{1266}\eta_1\eta_3]. \tag{7.9}$$

We have $C_{12}^{"}=C_{13}^{"}$, $C_{22}^{"}=C_{33}^{"}$, $C_{55}^{"}=C_{66}^{"}$, $C_{22}^{"}-C_{23}^{"}=2C_{44}^{"}$. So from the above derivation, the isotropic crystal will lose its original symmetry under uniaxial stress, although at the plane $y-z$, it is still isotropic.

The second-order Lamé coefficients λ, μ are frequently used for an isotropic crystal, it is known that in Eq. (7.1): $C_{11}=\lambda+2\mu$, $C_{12}=\lambda$, $C_{44}=\mu$.. Only two of C_{11}, C_{12},

and C_{44} are independent. Similarly for the higher order elastic constants, there are relations: $C_{111}=\nu_1+6\nu_2+8\nu_3$, $C_{112}=\nu_1+2\nu_2$, $C_{123}=\nu_1$, $C_{144}=\nu_2$, $C_{155}=\nu_2+2\nu_3$, $C_{456}=\nu_3$, $C_{1111}=\gamma_1+12\gamma_2+32\gamma_3+12\gamma_4$, $C_{1112}=\gamma_1+6\gamma_2+8\gamma_3$, $C_{1122}=\gamma_1+4\gamma_2+4\gamma_4$, $C_{1123}=\gamma_1+2\gamma_2$, $C_{1144}=\gamma_2+2\gamma_4$, $C_{1155}=\gamma_2+4\gamma_3+2\gamma_4$, $C_{1255}=\gamma_2+2\gamma_3$, $C_{1266}=\gamma_2+4\gamma_3$, $C_{1456}=\gamma_3$, $C_{4444}=3\gamma_4$, $C_{4455}=\gamma_4$. Here ν_1,ν_2,ν_3, and $\gamma_1,\gamma_2,\gamma_3,\gamma_4$ are third- and fourth-order Lamé coefficients, respectively. The external stress applied is $\tau_{ij}^{"}=(\tau,0,0,0,0,0)$. For the deformed solids, we use the stability criterion, let

$$\det\left|\overline{B}\right|=(\overline{B}_{22}-\overline{B}_{23})\overline{B}_{44}\overline{B}_{55}^2[\overline{B}_{11}(\overline{B}_{22}+\overline{B}_{23})-2\overline{B}_{12}^2]\geq 0,$$

and obtain three stability conditions,

$$\overline{B}_{11}(\overline{B}_{22}+\overline{B}_{23})-2\overline{B}_{12}^2\geq 0\Rightarrow(C_{11}^{"}+\tau^{"})(C_{22}^{"}+C_{23}^{"})-2(C_{12}^{"}-\frac{\tau^{"}}{2})^2\geq 0, \tag{7.10}$$

$$\overline{B}_{22}-\overline{B}_{23}\geq 0\Rightarrow C_{22}^{"}-C_{23}^{"}\geq 0, \tag{7.11}$$

$$\overline{B}_{55}\geq 0\Rightarrow C_{55}^{"}+\frac{\tau^{"}}{2}\geq 0. \tag{7.12}$$

The first one is equal to saying that, Young's modulus $E_{100}\geq 0$. Here E_{100} governs a fully relaxed stretch along [100],

$$E_{100}=\left(S_{11}\right)^{-1}=\frac{\overline{B}_{11}(\overline{B}_{22}+\overline{B}_{23})-2\overline{B}_{12}^2}{\overline{B}_{22}+\overline{B}_{23}}. \tag{7.13}$$

7.1.2 **Isotropic solids under hydrostatic stress**

Similar with the case of cubic crystal shown in figure 7.2, when an isotropic solid is subject to hydrostatic pressure P, $\tau_{ij}=-P\delta_{ij}$, we follow the convention that the inward

pressure is positive while outward pressure is negative (i.e., $P<0$ for tension), so the non-zero elements of stiffness tensor are

$$B_{11}=B_{22}=B_{33}=C_{11}-P,$$
$$B_{12}=B_{23}=B_{31}=C_{12}+P,$$
$$B_{44}=B_{55}=B_{66}=C_{44}-P.$$

All the other components of B_{ij} are zero, $C_{11}-C_{12}=2C_{44}$. The isotropic symmetry is retained. Here we simplify the subscript in the tensor notion by using the Voigt notation ($11\to1$, $22\to2$, $33\to3$, $23\to4$, $31\to5$, and $12\to6$). For this special case, the stiffness tensor and the elastic constants have the same type of crystal symmetry. And B_{ij} possess $i\leftrightarrow j$ symmetry, so $\overline{B}=B$. Let $\det|B|=0$, there are three independent stability conditions, $B_{11}+2B_{12}\geq0$, $B_{11}-B_{12}\geq0$, $B_{44}\geq0$. Or

$$C_{11}+2C_{12}+P=3\lambda+2\mu+P=3K+P\geq0, \tag{7.14}$$

$$C_{11}-C_{12}-2P=2(\mu-P)\geq0, \tag{7.15}$$

$$C_{44}-P=\mu-P\geq0, \tag{7.16}$$

using the elastic constants C_{ij} in the loaded state, where $K=\lambda+2\mu/3$ is a bulk modulus. Eq. (7.15) and Eq. (7.16) give the same results. For a free isotropic crystal, we have two independent moduli: bulk modulus K and shear modulus μ. These quantities are extended to the system under finite hydrostatic load, so we have the corresponding bulk and shear stiffness moduli:

$$K(\tau)=(B_{11}+2B_{12})/3=K+P/3, \tag{7.17}$$

$$\mu(\tau)=(B_{11}-B_{12})/2=\mu-P. \tag{7.18}$$

In contrast to the conventional or Born's stability criteria valid in only the load-free case,

which requires that K and μ be positive, the stability criteria of the isotropic system under load requires instead Eqs. (7.17-7.18) to be positive.

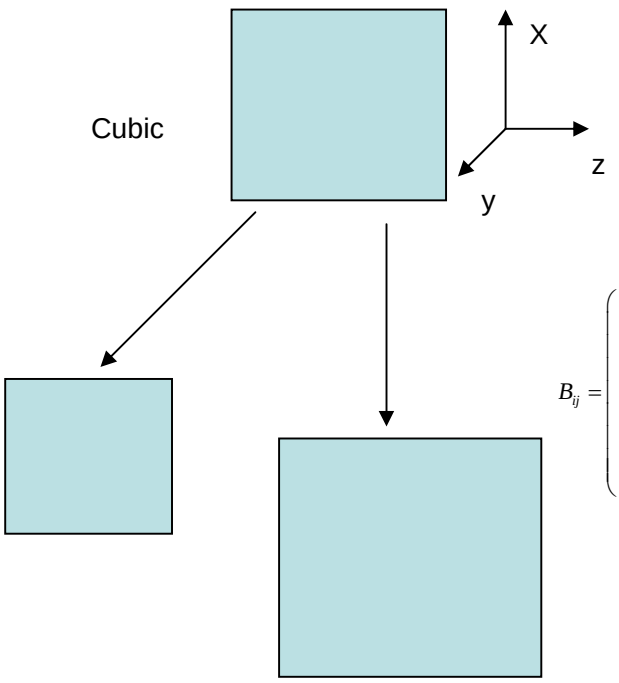

$$C_{ij} = \begin{pmatrix} C_{11} & C_{12} & C_{12} & 0 & 0 & 0 \\ C_{12} & C_{11} & C_{12} & 0 & 0 & 0 \\ C_{12} & C_{12} & C_{11} & 0 & 0 & 0 \\ 0 & 0 & 0 & C_{44} & 0 & 0 \\ 0 & 0 & 0 & 0 & C_{44} & 0 \\ 0 & 0 & 0 & 0 & 0 & C_{44} \end{pmatrix}$$

$$B_{ij} = \begin{pmatrix} B_{11} & B_{12} & B_{12} & 0 & 0 & 0 \\ B_{12} & B_{11} & B_{12} & 0 & 0 & 0 \\ B_{12} & B_{12} & B_{11} & 0 & 0 & 0 \\ 0 & 0 & 0 & B_{44} & 0 & 0 \\ 0 & 0 & 0 & 0 & B_{44} & 0 \\ 0 & 0 & 0 & 0 & 0 & B_{44} \end{pmatrix}$$

$$B_{11} = C_{11} - P,$$
$$B_{12} = C_{12} + P,$$
$$B_{44} = C_{44} - P,$$

$$\det|B| = (B_{11} - B_{12})^2 B_{44}^3 (B_{11} + 2B_{12}).$$

Figure 7.2 When a cubic crystal is compressed or expanded hydrostatically, the elastic stiffness matrix and its determinant are presented.

With Eq. (6.20) and Eq. (6.21), we use C' to represent the elastic constants at deformed state, and we may have the following relations, except that the number of independent elastic constants can be reduced according to the isotropic symmetry:

$$K(\tau) = (C_{11}^{'} + 2C_{12}^{'} + P)/3 = \{\sqrt{1+2\eta_1}[(C_{11} + 2C_{12}) + (C_{111} + 6C_{112} + 2C_{123})\eta_1 + (\frac{1}{2}C_{1111} + 4C_{1112} + 3C_{1122} + 6C_{1123})\eta_1^2] + \frac{-1}{\sqrt{1+2\eta_1}}[(C_{11} + 2C_{12})\eta_1 + (\frac{1}{2}C_{111} + 3C_{112} + C_{123})\eta_1^2 + (\frac{1}{6}C_{1111} + \frac{4}{3}C_{1112} + C_{1122} + 2C_{1123})\eta_1^3]\}/3, \quad (7.19)$$

$$\mu(\tau) = (C_{11}^{'} - C_{12}^{'} - 2P)/2 = \{\sqrt{1+2\eta_1}[(C_{11} - C_{12}) + (C_{111} - C_{123})\eta_1 + (\frac{1}{2}C_{1111} + C_{1112} - \frac{3}{2}C_{1123})\eta_1^2] + \frac{2}{\sqrt{1+2\eta_1}}[(C_{11} + 2C_{12})\eta_1 + (\frac{1}{2}C_{111} + 3C_{112} + C_{123})\eta_1^2 + (\frac{1}{6}C_{1111} + \frac{4}{3}C_{1112} + C_{1122} + 2C_{1123})\eta_1^3]\}/2. \quad (7.20)$$

7.2 High order elastic constants and the elastic stability

Kobelev *et al* [129] experimentally evaluated the second-, third-, and fourth-order elastic moduli of metallic glass $Zr_{52.5}Ti_5Cu_{17.9}Ni_{14.6}Al_{10}$. It was demonstrated that the fourth-order elastic modulus γ_4 obtained from the experiment is in qualitative agreement with the theoretical estimate made within the interstitialcy theory of condensed matter. Although their work gives only three independent values for linear combinations of fourth-order elastic moduli: $\gamma_2 + 0.033\gamma_1$, γ_3, and $\gamma_4 + 0.026\gamma_2$, we assume that the elastic modulus γ_1 is of the same order of magnitude with the others. From the relations between C_{ijkl} and γ_i, we further know that the value of γ_1 does not much affect the value of C_{ijkl}. In the following calculation work, we assume $\gamma_1 = 100$ GPa. And we select the experimental results while $\lambda^T = \lambda^S$, ignoring the effect of experimental errors. Using the

relations between Lamé coefficients and elastic constants, we have: $C_{11} = 155.7$, $C_{12} = 92.7$, $C_{44} = 31.5$, $C_{111} = -1339$, $C_{112} = -498$, $C_{123} = -218$, $C_{144} = -140$, $C_{155} = -210$, $C_{456} = -35$, $C_{1111} = 7760$, $C_{1112} = 2156$, $C_{1122} = -992$, $C_{1123} = 324$, $C_{1144} = -658$, $C_{1155} = 934$, $C_{1255} = 458$, $C_{1266} = 1254$, $C_{1456} = 398$, $C_{4444} = -480$, $C_{4455} = -160$, unit is GPa. With the same techniques we used in chapter six, we test the elastic stability conditions of Eqs. (7.10-7.12), the results are shown in figure 7.3. Also we test the stability conditions of Eqs. (7.14) and (7.15), and the results are shown in figure 7.4.

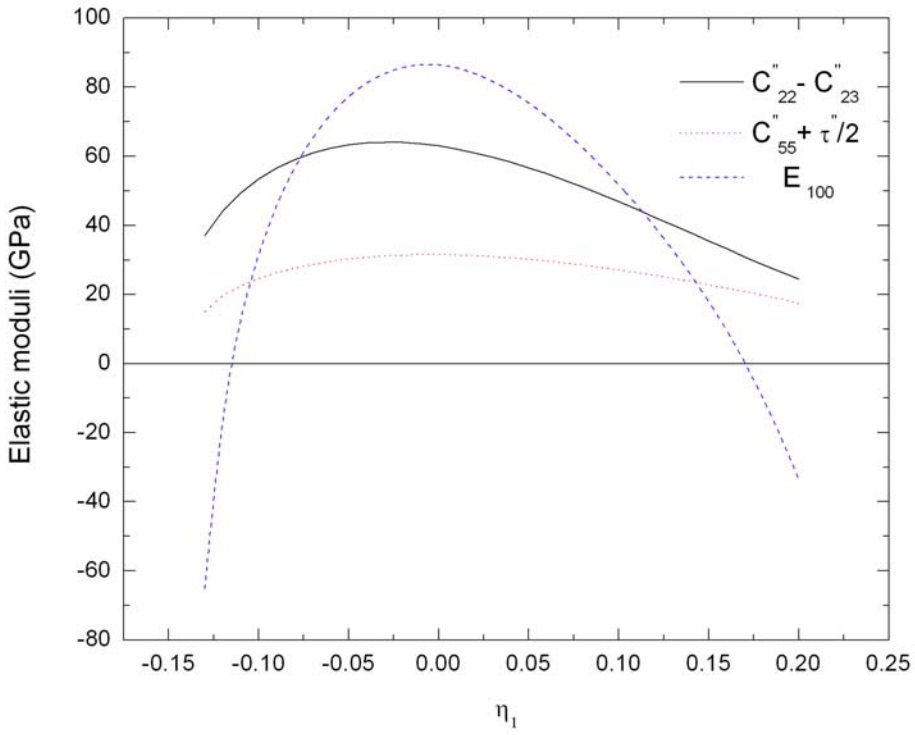

Figure 7.3 The stability conditions of Eqs. (7.10-7.12) are tested. Among the three elastic moduli, Young's modulus is the first one to reach zero, in both uniaxially compressive and tensile cases, at strain -0.12 and 0.17, respectively.

7.3 Discussion

From figures 7.3&7.4, the metallic glass $Zr_{52.5}Ti_5Cu_{17.9}Ni_{14.6}Al_{10}$ will lose the elastic stability at a quite large strain. So far as we know, MGs has a very small elastic region, 1% or so, and will fracture catastrophically without macroscopic plasticity. MGs cannot undertake so large a deformation strain as shown in the instability points at figures 7.3&7.4. The reason may be that the topological disorder of atom distribution in MGs causes the stress field non-uniform, so that a local stress somewhere in the bulk metallic glass might be already beyond the theoretical strength, leading a local failure, while the external loading is not that large. Another reason may be that, like any metastable system, an infinite number of (metastable) states exist on the free energy landscape. As a result, many (local atomic) amorphous structures could exist or co-exist at different pressures and the transitions among these states are omnipresent, especially among those separated by small barriers. High-pressure experiments and a plate impact experiments[130-132] show the discontinuity in the equation of the state of MGs that led to the suggestion of polymorphic phase transition. A first-principles calculation of CeAl binary glass suggests that the transition is caused by the electronic structure change associated with the f electrons present in Ce[131].

Although it is not applicable to MGs, the above nonlinear theoretical formulation of elastic stability will be of interest as a model for the ideal isotropic solids.

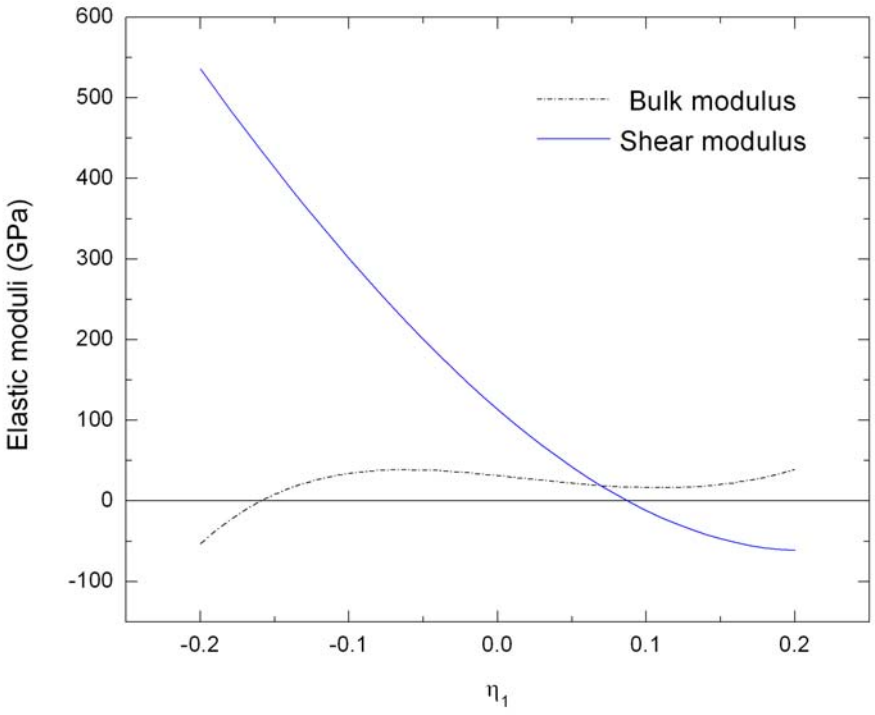

Figure 7.4 The stability conditions of Eqs. (7.14-7.15) are tested. Under hydrostatic compression, bulk modulus reach zero firstly at strain -0.16, while in case of hydrostatic tension, shear modulus reach zero first at strain 0.09.

REFERENCES

1. J. Frenkel, Z. Phys. **37**, 572 (1926).

2. E. Orowan, Rep. Prog. Phys. **12**, 183 (1948).

3. A. Considere, *Ann. ponts et chaussees* **9**, 574 (1885).

4. *The inhomogeneity of plastic deformation*. (American society for metals, 1973).

5. M. Born, Proc. Cambridge Philos. Soc. **36**, 160 (1940).

6. M. Born and K. Huang, *Dynamical Theory of Cystal Lattices*. (Clarendon, Oxford, 1956).

7. R. Hill, Math. Proc. Camb. Phil. Soc. **77** (JAN), 225-240 (1975).

8. R. Hill and F. Milstein, Phys. Rev. B **15**, 3087-3096 (1977).

9. F. Milstein and R. Hill, J. Mech. and Phys. of Solids **25**, 457-477 (1977).

10. F. Milstein and R. Hill, J. Mech. and Phys. of Solids **26**, 213-239 (1978).

11. F. Milstein and R. Hill, J. Mech. and Phys. of Solids **27**, 255 (1979).

12. F. Milstein, *Mechanics of Solids*. (Pergamon, Oxford, 1982).

13. J. H. Wang, S. Yip, S. R. Phillpot and D. Wolf, Phys. Rev. Lett. **71**, 4182-4185 (1993).

14. J. H. Wang, J. Li, S. Yip, S. Phillpot and D. Wolf, Phys. Rev. B **52**, 12627-12635 (1995).

15. Z. Zhou and B. Joos, Phys. Rev. B **54**, 3841-3850 (1996).

16. J. W. Morris and C. R. Krenn, Phil. Mag. A **80**, 2827-2840 (2000).

17. H. Djohari, F. Milstein and D. Maroudas, Appl. Phys. lett. **90**, 161910 (2007).

18. W. X. Li and T. C. Wang, J. Phys.: Condens. Matter **10**, 9889-9904 (1998).

19. M. Cerny, M. Sob, J. Pokluda and P. Sandera, J. Phys.: Condens. Matter **16** 1045 (2004).

20. H. Wang and M. Li, J. Phys.: Condens. matter **21**, 455401 (2009).

21. D. M. Clatterbuck, C. R. Krenn, M. L. Cohen and J. W. Morris, Phys. Rev. Lett. **91**, 135501 (2003).

22. D. C. Wallace, *Thermodynamics of Crystals*. (Dover Publications, 1998).

23. D. C. Wallace, Phys. Rev. **162**, 776 (1967).

24. C. Krenn, D. Roundy, J. Morris and M. Cohen, Mat. Sci. Eng. A **317**, 44 (2001).

25. X. Liu, Z. Liu, X. You, J. Nie and Z. Zhuang, Chin. Phys. Lett. **26**, 026103 (2009).

26. P. Sandera and J. Pokluda, Metall. Mat. **32**, 180 (1994).

27. F. Milstein and S. Chantasiriwan, Phys. Rev. B **58** (10), 6006-6018 (1998).

28. J. Zhang, Y. Yang and K. Xu, Can. J. Phys. **86**, 935 (2008).

29. H. Wang and M. Li, J. Phys.: Condens. matter **accepted** (2010).

30. J. Pokluda, M. Cerny, P. Sandera and M. Sob, Journal of computer-aided Materials design **11**, 1 (2004).

31. M. Sob, M. Friak, D. Legut and V. Vitek, Mat. Sci. Eng. A **148**, 387 (2004).

32. S. Ogata, Y. Umeno and M. Kohyama, Modelling Simul. Mater. Sci. Eng. **17**, 013001 (2009).

33. J. R. Ray, Comput. Phys. Rep. **8**, 109 (1988).

34. M. Li and W. L. Johnson, Physical Review B **46**, 5237 (1992).

35. M. Born and J. R. Oppenheimer, *Ann. Physik* **84**, 457 (1927).

36. L. H. Thomas, Proc. Cambridge Phil. Roy. Soc. **23**, 542 (1927).

37. E. Fermi, Rend. Accad. Naz. Lincei **6**, 602 (1927).

38. P. Hohenberg and W. Kohn, Phys. Rev. **136**, B864 (1964).

39. J. Callaway and N. H. March, Solid State Phys. **38**, 135 (1984).

40. W. Kohn and L. J. Sham, Phys. Rev. **140**, A1133 (1965).

41. C. Lee, W. Yang and R. G. Parr, Phys. Rev. B **37**, 785 (1988).

42. J. P. Perdew and Y. Wang, Phys. Rev. B **45**, 13244 (1992).

43. N. W. Ashcroft and N. D. Mermin, *Solid State Physics*. (Saunders College Publishing, 1976).

44. M. C. Payne, M. P. Teter, D. C. Allan, T. A. Arias and J. D. Joannopoulos, Rev. of Mod. Phys. **64**, 1045 (1992).

45. N. W. Ashcroft, Phys. Lett. **23**, 48 (1966).

46. I. V. Abarenkov and V. Heine, Phil. Mag. **11**, 387 (1965).

47. W. C. Herring, Phys. Rev. **57**, 1169 (1940).

48. W. C. Herring and A. G. Hill, Phys. Rev. **58**, 132 (1940).

49. D. R. Hamann, M. Schluter and C. Chiang, Phys. Rev. Lett. **43**, 1494 (1979).

50. D. Vanderbilt, Phys. Rev. B **41**, 7892-7895 (1990).

51. K. Laasonen, R. Car, C. Lee and D. Vanderbilt, Phys. Rev. B **43**, 6796 (1991).

52. P. E. Blochl, Phys. Rev. B **50**, 17953 (1994).

53. F. Birch, Phys. Rev. **71**, 809 (1947).

54. F. Murnaghan, *Finite Deformation of an Elastic Solid*. (Wiley, New York, 1951).

55. S. Bhagavantam, *Crystal Symmetry and Physical Properties*. (Academic, New York, 1966).

56. R. Thurston and K. Brugger, Phys. Rev. **133**, A1604 (1964).

57. K. Brugger, Phys. Rev. **133**, A1611 (1964).

58. P. B. Ghate, J. Appl. Phys. **35**, 337 (1964).

59. J. M. Ziman, *Electrons and Phonons*. (Clarendon, Oxford, 1960).

60. B. P. Barua and S. K. Sinha, J. Appl. Phys. **42**, 3967 (1978).

61. S. Chantasiriwan and F. Milstein, Phys. Rev. B **58**, 5996 (1998).

62. R. Kato and J. Hama, J. Phys.: Condens. Matter **6**, 7617 (1994).

63. S. P. Lepkowski and J. A. Majewski, solid State Commun. **131**, 763 (2004).

64. S. P. Lepkowski, J. A. Majewski and G. Jurczak, Phys. Rev. B **72**, 245201 (2005).

65. K. Shimada, T. Sota, K. Suzuki and H. Okumura, Jpn. J. Appl. Phys., Part 2 **37**, L1421 (1998).

66. G. Bester, X. Wu, D. Vanderbilt and A. Zunger, Phys. Rev. Lett. **96**, 187602 (2006).

67. H. F. Tiersten, J. Acoust. Soc. Am. **57**, 667 (1975).

68. J. S. Yang, Acta Mech. **196**, 103 (2008).

69. R. N. Thurston and M. J. Shapiro, J. Acoust. Soc. Am. **41**, 1112 (1967).

70. R. Fowles, J. Geophys. Res. **72**, 5729 (1967).

71. R. A. Graham, Phys. Rev. B **6**, 4779 (1972).

72. A. N. Abd-alla, Mech. Res. Commun. **26**, 335 (1999).

73. Landolt-Bornstein, in *Second and Higher Order Elastic Constants,New Series, Group III*, edited by A. G. Every and A. K. McCurdy (Springer-Verlag, Berlin, 1992), Vol. 29A.

74. P. N. Keating, Phys. Rev. **145**, 637 (1966).

75. P. N. Keating, **149**, 674 (1966).

76. T. Cagin and J. R. Ray, Phys. Rev. B **38**, 7940 (1988).

77. T. Cagin and B. M. Pettitt, Phys. Rev. B **39**, 12484 (1989).

78. R. Srinivasan, Phys. Rev. **144**, 620 (1966).

79. O. H. Nielsen and R. M. Martin, Phys. Rev. B **32**, 3792 (1985).

80. O. H. Nielsen, Phys. Rev. B **34**, 5808 (1986).

81. J. Sorgel and U. Scherz, Eur. Phys. J. **B 5**, 45 (1998).

82. J. Zhao, J. M. Winey and Y. M. Gupta, Phys. Rev. B **75**, 094105 (2007).

83. M. Lopuszynski and J. A. Majewski, Phys. Rev. B **76**, 045202 (2007).

84. G. Kresse and J. Furthmuller, Phys. Rev. B **54**, 11169-11186 (1996).

85. *American institute of Physics handbook*. (Mc-Graw-Hill, New york, 1970).

86. C. Bercegeay and S. Bernard, Phys. Rev. B **72**, 214101 (2005).

87. K. Salama and G. A. Alers, Phys. Rev. **161**, 673 (1967).

88. H. Soma and Y. Hiki, J. Phys. Soc. Jpn. **37**, 544 (1974).

89. M. F. Rose, Phys. Status Solidi **17**, K199 (1966).

90. Y. Hiki, J. R. Thomas and A. V. Granato, Phys. Rev. **153**, 764 (1967).

91. Y. Hiki and A. V. Granato, Phys. Rev. **144**, 411 (1966).

92. G. R. Barsch, Solid State Commun. **14**, 983 (1974).

93. H. Wang and M. Li, Phys. Rev. B **79**, 224102 (2009).

94. M. Born, J. Chem. Phys. 7, 591 (1939).

95. R. Furth and M. Born, Nature **145** (3680), 741 (1940).

96. K. J. Van Vliet, J. Li, T. Zhu, S. Yip and S. Suresh, Phys. Rev. B **67**, 15 (2003).

97. F. Milstein, H. Fang and J. Marschall, PHil. Mag. A **70**, 621 (1994).

98. M. Polanyi, Z. Phys. 7, 323 (1921).

99. M. Cerny, R. Boyer, M. Sob and S. Yip, Journal of computer-aided Materials design **12**, 161 (2005).

100. B. B. Karki, G. J. Ackland and J. Crain, J. Phys.: Condens. Matter **9**, 8579 (1997).

101. S. Ogata, J. Li, N. Hirosaki, Y. Shibutani and S. Yip, Phys. Rev. B **70**, 104104 (2004).

102. D. Bertsekas, A. Nedic and A. E. Ozdaglar, *Convex Analysis and Optimization*. (Athena Scientific, 2003).

103. M. Senoo, I. Fujishiro and M. Hirano, Bulletin of the Jsme-Japan Society of Mechanical Engineers **27**, 2680-2686 (1984).

104. E. Esposito, A. E. Carlsson, D. D. Ling, H. Ehrenreich and C. D. Gelatt, Philosophical Magazine a-Physics of Condensed Matter Structure Defects and Mechanical Properties **41**, 251-259 (1980).

105. M. Friak, M. Sob and V. Vitek, Philosophical Magazine a-Physics of Condensed Matter Structure Defects and Mechanical Properties **83**, 3529-3537 (2003).

106. M. Cerny, M. Sob, J. Pokluda and P. Sandera, Journal of Physics-Condensed Matter **16** 1045 (2004).

107. M. Cerny, Materials Science and Engineering a-Structural Materials Properties Microstructure and Processing **462**, 432-435 (2007).

108. T. Tsuchiya and K. Kawamura, J. Chem. Phys. **116**, 2121 (2002).

109. W. B. Daniels and C. S. Smith, Phys. Rev. **111**, 713 (1958).

110. S. N. Biswas, P. Vantklooster and N. J. Trappeniers, Physica B & C **103**, 235 (1981).

111. M. Durandurdu, Phys. Rev. B **76**, 024102 (2007).

112. V. Rodrigues, T. Fuhrer and D. Ugarte, Phys. Rev. Lett. **85**, 4124-4127 (2000).

113. A. Hasmy and E. Medina, Phys. Rev. Lett. **88**, 4 (2002).

114. Y. Kondo, Q. Ru and K. Takayanagi, Phys. Rev. Lett. **82**, 751-754 (1999).

115. Y. Kondo and K. Takayanagi, Phys. Rev. Lett. **79**, 3455-3458 (1997).

116. Y. Kondo and K. Takayanagi, Science **289**, 606-608 (2000).

117. E. Tosatti, S. Prestipino, S. Kostlmeier, A. Dal Corso and F. D. Di Tolla, Science **291**, 288-290 (2001).

118. O. Gulseren, F. Ercolessi and E. Tosatti, Phys. Rev. Lett. **80**, 3775-3778 (1998).

119. J. K. Diao, K. Gall and M. L. Dunn, Nat. Mater. **2**, 656-660 (2003).

120. J. K. Diao, K. Gall and M. L. Dunn, Phys. Rev. B **70** (7), 9 (2004).

121. M. Jahnatek, M. Krajci and J. Hafner, Physical Review B **76**, 014110 (2007).

122. Y. L. Liu, Y. Zhang, H. B. Zhou, G. H. Lu and M. Kohyama, J. Phys.: Condens. matter **20**, 335216 (2008).

123. H. B. Zhou, Y. Zhang, Y. L. Liu, M. Kohyama, P. G. Yin and G. H. Lu, J. Phys.: Condens. matter **21**, 175407 (2009).

124. S. Ogata, J. Li and S. Yip, Science **298**, 807-811 (2002).

125. M. I. Haftel and K. Gall, Phys. Rev. B **74**, 035420 (2006).

126. M. Cerny and J. Pokluda, J. Phys.: Condens. matter **21**, 145406 (2009).

127. E. Orowan, Rep. Prog. Phys. **12** (185) (1949).

128. M. Zhao and M. Li, Journal of Materials Research **24**, 2688 (2009).

129. N. P. Kobelev, E. L. Kolyvanov and V. A. Khonik, Physics. of the Solid State **49**, 1209 (2007).

130. M. Martin, T. Sekine, T. Kobayashi, L. Kecskes and N. N. Thadhani, Metall. Mat. Trans. **38A**, 2689 (2007).

131. H. W. Sheng, H. Z. Liu, Y. Q. Cheng, J. Wen, P. L. Lee, W. K. Luo and S. D. Shastri, Nat. Mat. **6**, 192 (2007).

132. Q. S. Zeng, Y. C. Li, C. M. Feng, P. Liermann, M. Somayazulu, G. Y. Shen, H. K. Mao, R. Yang, J. Liu, T. D. Hu and J. Z. Jiang, Proc. National Acad. Sci. U. S. A. **104**, 13565 (2007).

VITA

Hao Wang was born in Huanggang City, Hubei Province, China on December 2nd, 1977. He inherited the interest in science and literature from his father, while in the meantime his interest in some things such as cooking was annihilated by his father. He was enrolled in Huanggang Middle School in 1992. That is one of the most famous high schools in China, with a great reputation in training winners in the International Olympic Games of Mathematics and Physics. He left his hometown in 1995 to start his college life at Lanzhou University, where he obtained his B.S. and M.S. in 1999 and in 2002, respectively. Thereafter he was enrolled in the Ph.D. program at Georgia Institute of Technology.